

Universidad Autónoma de Madrid

Facultad de Ciencias

Departamento de Física Teórica

Aspects of Phenomenology and Cosmology in Hidden Sector Extensions of the Standard Model.

Jose Miguel No Redondo,

Madrid, Junio 2009.

Contents

Introduction and Overview.	5
Introducción (Español).	9
I Aspects of Cosmology in Hidden Sector Extensions of the SM.	13
1 Introduction.	15
1.1 The Model.	17
1.1.1 Zero Temperature Effective Potential.	17
1.1.2 Finite Temperature Effective Potential.	19
1.1.3 Impact of Two-Loop Corrections in the Analysis.	20
2 The EWPT in Hidden Sector Extensions of the SM.	23
2.1 Fate of the False Vacuum in Field Theory.	23
2.1.1 False Vacuum Decay I: Zero Temperature.	23
2.1.2 False Vacuum Decay II: Finite Temperature.	26
2.2 Dynamics of 1st Order Phase Transitions in Field Theory.	28
2.2.1 Dynamics of the Phase Transition: 1st Order vs 2nd Order.	28
2.2.2 1st Order Phase Transition: Bubble Nucleation Temperature T_n	31
2.2.3 1st Order Phase Transition: Evolution of the Phase Transition. . . .	33
2.3 The Electroweak Phase Transition in a Singlet Scalar Extension of the SM. .	35
3 Hidden Sector Scalars as Possible Candidates for Dark Matter.	43
II Phenomenology of Conformal Hidden Sectors: Unparticles.	51
4 Introduction	53
4.1 The Unparticle Idea.	53
4.2 Stephanov Deconstruction.	55
5 Higgs-Unparticle Interplay.	57
5.1 Higgs Portal to Unparticles.	57
5.1.1 Electroweak Symmetry Breaking and the IR Problem.	58
5.1.2 Solving the IR Problem.	59
5.1.3 Constrains on $\mathcal{M}_{\mathcal{U}}$ and $\Lambda_{\mathcal{U}}$	60
5.2 Plasmon Scenario.	61
5.2.1 Curing the IR Problem (Deconstructed Unparticle Self-interactions). .	61

5.2.2	Higgs-Unparticle Mixing and Plasmon Resonances from Unparticles. .	63
5.2.3	Spectral Function Analysis.	66
5.3	Phantom Higgs Scenario.	70
5.3.1	Curing the IR Problem.	70
5.3.2	Effect of Unparticles on Electroweak Symmetry Breaking.	71
5.3.3	Phantom Higgs from Higgs-Unparticle Mixing.	72
5.3.4	Spectral Function Analysis.	76
6	Unparticle Decays.	79
6.1	Introduction.	79
6.2	Simple Model of Unparticle Decays.	80
6.2.1	Pole Analysis.	80
6.2.2	Spectral Function Analysis.	83
	Summary and Conclusions.	87
	Cosmological Aspects of Hidden Sectors.	87
	Unparticles Coupled to the Higgs.	88
	Resumen y Conclusiones.	91
	Cosmología y Sectores Ocultos.	91
	Unpartículas Acopladas al Higgs.	92
III	Appendices.	95
A	Effective Potential Formalism.	97
A.1	The Effective Potential in Field Theory.	97
A.1.1	Computation of the Effective Potential.	99
A.2	The Effective Potential at 1-Loop.	100
A.3	Finite Temperature Effective Potential.	103
A.3.1	Thermal Field Theory and the Effective Potential.	103
A.3.2	Daisy Diagrams.	107
A.4	Main Two-Loop Contributions to the Zero Temperature Effective Potential of the Hidden Scalar Extension of the SM.	108
B	Approximations for $S_3(T)/T$.	111
B.1	Derivation of the approximation for $S_3(T_n)/T_n$	111
B.2	Derivation of the approximation for $S_3(T_f)/T_f$	112
C	Normalization of the Spectral Function.	115
	References.	117

Introduction and Overview.

The Standard Model (SM) [1, 2] of Electroweak and Strong interactions is one of the most successful theories ever formulated. It accounts for essentially all present accelerator experimental data, describing accurately the physics from atomic scales down to the shortest currently probed scales (about 10^{-18} m), and it provides a unified framework for describing the known elementary particles (which are divided in quarks and leptons) and three of the four known fundamental forces of Nature: the Electromagnetic, Weak and Strong interactions between these elementary particles.

Leaving aside the Strong interactions, the Standard Model of Electroweak (EW) interactions is a Gauge Theory based on the gauge group $SU(2)_L \times U(1)_Y$. However, given the fact that the W^\pm and Z gauge bosons are massive, the gauge group $SU(2)_L \times U(1)_Y$ must be spontaneously broken to the $U(1)_{EM}$ gauge group that we observe at low energies, and this gives rise to what is known as “Electroweak symmetry breaking” (EWSB).

This spontaneous symmetry breaking is implemented by means of the Higgs mechanism [3]. For the particular case of the Standard Model, the Higgs mechanism introduces a scalar doublet $H = (H^+, H^0) = (H_1 + iH_2, H_3 + iH_4)$, whose potential in the lagrangian describes the dynamics of H in such a way that H_3 acquires a vacuum expectation value (VEV), breaking the gauge symmetry $SU(2)_L \times U(1)_Y \rightarrow U(1)_{EM}$ and hence giving masses to the gauge bosons W^\pm and Z , and also to the fermions through the Yukawa couplings. This leaves just one physical scalar particle in the spectrum: the SM Higgs boson.

The precision measurements at LEP have given an extraordinary confirmation of the validity of the SM up to the electroweak scale. However, there are many hints, coming both from the theory itself (like the Hierarchy problem for the SM Higgs boson mass, or the pattern of fermion masses and mixings), and from cosmology, indicating that new physics beyond the Standard Model (BSM) should appear at or near the TeV scale.

There are various powerful reasons to suspect that this new physics might have a strong impact on the Electroweak symmetry breaking sector, the only part of the Standard Model which is not on firm experimental grounds, since the Higgs boson has not been found yet. In this respect, the Hierarchy problem strongly suggests that new physics should appear at the TeV scale in order to stabilize the Higgs boson mass. Also, $|H|^2$ is the only superrenormalizable operator in the Standard Model, so if we suppose that a new sector exists which is a singlet under the $SU(3) \times SU(2) \times U(1)$ SM gauge group (therefore called “Hidden Sector”, as opposed to the usual “Visible” SM sector¹), it is in principle plausible that this new sector

¹It should be emphasized that the idea of hidden sectors is well motivated from a theoretical perspective: in String Theory, when constructing string models that reproduce SM-like field theories at low energies, one normally gets other sectors apart from the SM-like sector, which are singlets under the SM gauge group.

is connected to the SM sector through a renormalizable coupling involving $|H|^2$; this idea is sometimes described in the literature as the “Higgs Portal” or “Hidden Valley” scenario [5, 6].

Cosmology also provides very strong hints suggesting the existence of new physics beyond the SM, that might appear naturally close to the TeV scale. First, it is believed that the asymmetry between the number of baryons and antibaryons (in general, between matter and antimatter) that we observe today in the universe is not given by initial conditions, but was generated at some epoch in the very early universe, through a process called Baryogenesis; a long time ago, Sakharov identified the three ingredients that any theory would need in order to be able to generate this asymmetry: Baryon number violation, C and CP violation, and departure from thermal equilibrium at some period [7]. Although it was not realized at first (and there are other possibilities for Baryogenesis which involve new physics at much higher scales), the Standard Model itself happens to incorporate all three ingredients, opening the possibility of having Baryogenesis at (or close to) the electroweak scale. However, it turns out that two of them exist in an insufficient amount for Baryogenesis to actually be possible in the Standard Model²; so, for Baryogenesis to take place at the electroweak scale, new BSM physics close to the TeV scale is needed in order to provide new sources of CP violation and a stronger electroweak phase transition, and hidden sector models are one possible candidate.

The existence of Dark Matter is another cosmological issue that provides strong evidence of new physics beyond the SM, since in principle there is no good candidate within the Standard Model to account for the dark matter we observe in the universe; in this respect, hidden sector extensions of the SM naturally provide dark matter candidates.

Also, very recently one special kind of “Hidden Sector” scenarios has received special attention through the so-called Unparticle scenario [8, 9], where the hidden sector coupled to the SM is conformally invariant. Since this last fact gives rise to very interesting phenomenology, there has been a lot of work on Unparticles related to cosmology, possible collider signals, and on constraints on Unparticle couplings to the SM from low energy physics (see [10] and references therein); in particular, it was shown that, being $|H|^2$ the SM gauge invariant operator with the least possible dimension, the coupling between the Higgs and Unparticles is potentially the most important for low energy phenomenology [11, 12]. A theory where the Unparticles couple to the SM through the Higgs field is a special case of the “Higgs portal” scenario, interesting on its own because of the consequences that this coupling has for both the Unparticle and the Higgs sectors.

This work can be divided in two main parts, both related to the phenomenology of hidden sectors coupled to the SM through the Higgs portal, but actually dealing with different types of scalar hidden sectors, and focusing on different aspects of these scenarios. The first part is devoted to the analysis of cosmological implications of hidden sectors, and uses a very simple extension of the SM through a coupling between the Higgs and a group of hidden scalars; we study the dynamics of the Electroweak phase transition in this case, finding the range of parameters for which the phase transition is sufficiently strong for having electroweak Baryogenesis. We also consider the possibility that the hidden scalars could account for the

²Perturbative and nonperturbative calculations indicate that the Electroweak Phase Transition (EWPT) in the SM does not provide enough departure from thermal equilibrium, and also the amount of CP violation within the SM turns out to be insufficient for generating the Baryon Asymmetry of the Universe (BAU).

dark matter of the universe, and obtain the corresponding parameter space region. In the second part we consider a conformal hidden sector coupled to the SM through the Higgs (scenario of Unparticles coupled to the Higgs), and we analyze the implications that such a scenario would have both for the Higgs sector through EWSB, and for the hidden conformal sector, through the breaking of the conformal symmetry once the Higgs field gets a VEV.

Introducción (Español).

El Modelo Estandar (SM) [1, 2] de las interacciones fuertes y electrodébiles es una de las teorías físicas mas exitosas jamás formuladas. Da cuenta de esencialmente todas las medidas experimentales llevadas a cabo en aceleradores hasta hoy, describiendo con precisión la física desde escalas atómicas hasta las escalas mas pequeñas observadas (10^{-18} m), y proporciona un marco unificado para describir las partículas elementales conocidas (divididas en quarks y leptones) y tres de las cuatro interacciones fundamentales de la naturaleza: las interacciones fuerte, débil y electromagnética.

Dejando a un lado las interacciones fuertes, el Modelo Estandar de interacciones electrodébiles (EW) es una teoría de campos gauge basada en el grupo de simetría gauge $SU(2)_L \times U(1)_Y$. Sin embargo, dado que los bosones gauge W^\pm and Z tienen masa, el grupo gauge $SU(2)_L \times U(1)_Y$ ha de romperse espontaneamente al grupo $U(1)_{EM}$ que observamos a bajas energías, dando lugar a lo que se conoce como la “ruptura de la simetría electrodébil” (EWSB).

Esta ruptura espontanea de la simetría se implementa por medio del mecanismo de Higgs [3]. Para el caso particular del Modelo Estandar, el mecanismo de Higgs introduce un doblete escalar $H = (H^+, H^0) = (H_1 + iH_2, H_3 + iH_4)$, cuyo potencial en el lagrangiano describe la dinámica de H de forma que H_3 adquiere un valor de expectación en el vacío (VEV), rompiendo la simetría gauge $SU(2)_L \times U(1)_Y \rightarrow U(1)_{EM}$ y dando masa a los bosones gauge W^\pm and Z , así como a los fermiones a través de los acoplos de Yukawa. Todo esto deja un único grado de libertad escalar físico en el espectro: el bosón de Higgs del Modelo Estandar.

Las medidas de precisión llevadas a cabo en LEP han confirmado con extraordinaria precisión la validez del Modelo Estandar hasta la escala electrodébil. Sin embargo, hay muchos indicios, provenientes tanto de la propia teoría (como el problema de las jerarquías, o el patrón de masas y mezclas de los fermiones) como de la cosmología, de que debería existir nueva física mas allá del Modelo Estandar a la escala del TeV.

Hay varias razones poderosas para sospechar que esta nueva física podría tener un gran impacto en el sector de ruptura de la simetría electrodébil, la única parte del Modelo Estandar que no esta comprobada experimentalmente, ya que el bosón de Higgs no ha sido encontrado todavía. A este respecto, el problema de las jerarquías constituye una indicación fuerte de que debería existir nueva física a la escala del TeV para estabilizar la masa del Higgs. Además $|H|^2$ es el único operador superrenormalizable en el Modelo Estandar, así que si suponemos que existe un nuevo sector, singlete bajo el grupo gauge del Modelo Estandar $SU(3) \times SU(2) \times U(1)$ (y por tanto denominado “sector oculto”, en contraposición al sector

“Visible” del SM¹), es en principio posible que este nuevo sector este conectado al Modelo Estandar a través de un acoplo renormalizable que involucre al operador $|H|^2$; esta idea se conoce en la literatura como el escenario de “Higgs Portal” o “Hidden Valley” [5, 6].

La Cosmología también proporciona razones para pensar en la existencia de nueva física mas allá del Modelo Estandar, que podría de manera natural aparecer cerca de la escala del TeV. En primer lugar, se cree que la asimetría entre el numero de bariones y antibariones (en general, entre materia y antimateria) que observamos hoy en el universo no esta dada por las condiciones iniciales, sino que fue generada dinámicamente en una cierta época durante la evolución del universo primitivo, a través de un proceso denominado Bariogénesis; a finales de los años sesenta, Sakharov identificó los tres ingredientes que toda teoría necesita para poder generar esta asimetría: violación de número bariónico, violación de C y CP, y un periodo de no-equilibrio térmico [7]. Aunque no fue puesto de manifiesto en un primer momento (y hay otras posibilidades para bariogénesis que involucran nueva física a escalas de energía mucho mas altas), el propio Modelo Estandar incorpora estas tres condiciones, lo que en principio haría posible tener bariogénesis a la escala electrodébil (o cerca de ella). Sin embargo, resulta que dos de las tres condiciones no se dan en cuantía suficiente para que el proceso sea de verdad posible en el Modelo Estandar²; por tanto, para que se pueda tener bariogénesis a la escala electrodébil, es necesaria la existencia de nueva física cerca de la escala del TeV para proporcionar nuevas fuentes de violación de CP y una transición de fase electrodébil mas fuerte, y los modelos con sectores ocultos son un candidato posible.

La existencia de Materia Oscura es otro punto que sugiere fuertemente la existencia de física mas allá del Modelo Estandar, ya que el SM no cuenta en principio con ningún candidato para dar cuenta de la materia oscura que observamos en el universo; en este sentido, las extensiones del SM mediante sectores ocultos proporcionan candidatos a materia oscura de forma natural.

Además, muy recientemente un tipo especial de modelos con sectores ocultos ha recibido una atención especial a través del llamado escenario de “Unpartículas”, en el cual el sector oculto acoplado al Modelo Estandar es invariante conforme. Ya que esta característica da lugar a fenomenología muy interesante, se han llevado a cabo numerosos estudios de las propiedades de este tipo de escenarios (de Unpartículas) en lo relativo a cosmología, a posibles señales en los aceleradores de partículas, etc (ver [10]); en particular, se mostró que, ya que $|H|^2$ es el operador escalar invariante gauge en el SM con la dimensión mas baja posible, el acoplo entre el Higgs y las Unpartículas es potencialmente el mas importante para la fenomenología de baja energía [11, 12]. Una teoría en la que las Unpartículas se acoplan al Modelo Estandar a través del Higgs es un caso especial del escenario de “Higgs portal”, interesante por sí mismo debido a las consecuencias que este acoplo tendría tanto para el sector de Unpartículas como para el sector del Higgs.

¹La posible existencia de sectores ocultos esta bien motivada desde un punto de vista teórico: en Teoría de Cuerdas, cuando se construyen modelos que tratan de obtener a baja energía teorías de campos del tipo del Modelo Estandar, aparecen de manera natural en la teoría otros sectores aparte del sector del Modelo Estandar, que son singletes bajo el grupo gauge del SM.

²Cálculos perturbativos y no perturbativos indican que la transición de fase electrodébil en el Modelo Estandar (y para masas del Higgs por encima de la cota experimental de LEP) no proporciona suficiente desviación del equilibrio térmico, y la cantidad de violación de CP en el Modelo Estandar tambien resulta insuficiente para generar la asimetría bariónica del universo.

Este trabajo puede dividirse en dos partes, ambas relacionadas con la fenomenología de sectores ocultos acoplados al Modelo Estandar a través de $|H|^2$, pero tratanto con diferentes tipos de sectores ocultos, y centrandose en distintos aspectos de estos escenarios. La primera parte esta dedicada al análisis de las implicaciones cosmológicas de los sectores ocultos, y usa una extensión del Modelo Estandar muy simple a través de un acoplo entre el Higgs y un grupo de escalares del sector oculto; estudiamos la dinámica de la transición de fase en este caso, encontrando el rango de valores de los parámetros para el que la transición de fase es suficientemente fuerte para dar lugar a bariogénesis a la escala electrodébil. Tambien consideramos la posibilidad de que los escalares del sector oculto constituyan la materia oscura del universo, y obtenemos la correspondiente región del espacio de parámetros. En la segunda parte consideramos un sector oculto invariante conforme acoplado al Modelo Estandar a través del Higgs (Unpartículas acopladas al Higgs), y analizamos las implicaciones que este escenario tendría tanto para el sector del Higgs (a través de la ruptura de la simetría electrodébil) como para el sector conforme (a través de la ruptura de la simetría conforme una vez que el Higgs toma un valor esperado).

Part I

Aspects of Cosmology in Hidden Sector Extensions of the SM.

Chapter 1

Introduction.

When dealing with the physics of the very early universe there is a strong interplay between Cosmology and Particle physics, and the latter can provide possible solutions to the numerous puzzles and open questions arising in Cosmology.

A prominent example where this is the case is Dark Matter. Over the years a wide variety of evidence has been gathered in favour of the existence of dark matter (that is, nonluminous, nonbaryonic type of matter) in the universe; apart from the numerous evidences at galactic and sub-galactic scales, which include galactic rotation curves and weak gravitational lensing of distant galaxies, the observations of the anisotropies in the Cosmic Microwave Background (CMB) together with distance measurements from Type Ia supernovae lead to a determination of the total matter density in the universe Ω_M which is about six times bigger than the estimated baryonic density Ω_B (combining the same data with measurements from light chemical element abundances)³. In this respect, many theories beyond the Standard Model provide candidates for this dark matter; hidden sector extensions of the SM naturally provide dark matter candidates, since the hidden sector fields do not share the SM gauge interactions. Lately, in view of the recent PAMELA preliminary results [14, 15], hidden sector extensions have regained attention, since they can accommodate the results from the PAMELA experiment in a rather natural way [16]. Singlet dark matter has already been extensively discussed in the literature (see e.g. [17, 18]).

Another example of the interplay between Particle Physics and Cosmology is Baryogenesis (the generation of the Baryon asymmetry that we observe today at some epoch in the very early universe). Since Sakharov first identified the ingredients any theory would need in order to give rise to Baryogenesis (baryon number violation, C and CP violation and some departure from thermal equilibrium) [7], there have been many attempts to find theories that accommodate Baryogenesis in a viable way.

The early scenarios for Baryogenesis were based on Grand Unified Theories (GUT's) [19], and in particular on the one based on the $SU(5)$ gauge group; since quarks and leptons are embedded together in multiplets of the GUT gauge group (e.g. $SU(5)$), Grand Unified Theories naturally accounted for baryon number violation, and they could also incorporate the other two necessary ingredients in an easy way. The common mechanism to achieve a

³In principle, this could be also due to a modification of General Relativity on large scales (galactic and cosmological), but this last scenario seems to be strongly disfavoured with respect to the Dark Matter hypothesis (for an extensive review on Dark Matter, see [13]).

nonzero baryon number was through out of equilibrium decays of some superheavy particle X , due to a Boltzmann suppression of the inverse-decay reactions once the temperature T dropped below the mass M_X ; assuming a CP biased (complex) coupling of X to its decay products, a baryon asymmetry could be generated in this way, and was supposed to remain constant during the subsequent evolution of the universe.

Even though GUT baryogenesis seemed to be appealingly simple, it was soon realized that this scenarios were not free of problems. The simplest Grand Unified Theories predict a relic abundance of massive stable magnetic monopoles (generated during the GUT phase transition) much larger than Ω_M , the so called “Monopole Problem”; among the possible solutions to this problem, Inflation is the most natural one, since an inflationary period would enormously dilute the density of magnetic monopoles; however, it would also dilute any previously generated baryon asymmetry.

Another problem had to do with the fact that in the Standard Model baryon number is an anomalous symmetry and therefore it is violated through nonperturbative processes; at zero temperature these processes involve quantum tunneling between electroweak vacua with different baryon and lepton number [20] and are mediated by instantons, but turn out to be extremely suppressed. Kuzmin, Rubakov and Shaposhnikov showed [21] that at finite temperature baryon violating transitions can proceed through thermal fluctuations over the potential barrier between vacua, rather than quantum tunneling (these transitions would be mediated by a static gauge configuration sitting on top of the barrier, called the “Sphaleron” [22]); more explicitly, they showed that these transitions would be unsuppressed and in equilibrium for high temperatures ($10^2\text{GeV} < T < 10^{12}\text{GeV}$). Since these sphaleron transitions conserve $B - L$ but violate $B + L$ (which they rapidly wash-out), they would erase any previously generated baryon asymmetry during baryogenesis in any $B - L$ conserving Grand Unified Theory, as in $SU(5)$.

However, as already stated in [21], Sphaleron processes turned out to be both a curse and a blessing; they posed a big problem to GUT baryogenesis, but opened the possibility for achieving Baryogenesis at or near the electroweak scale, since they provided the necessary baryon number violation within the Standard Model. It was also known that C and CP were violated in the SM, and it was conjectured that the third necessary ingredient to achieve Baryogenesis at the electroweak scale (called Electroweak Baryogenesis) could also be obtained through the electroweak phase transition (at very high temperatures the electroweak symmetry is restored, so the universe is supposed to have undergone a transition from the symmetric to the broken phase at or near the electroweak scale) since it could provide the necessary departure from equilibrium, if strong enough.

Unfortunately, it was later realized that both the second and third conditions are not realized in a sufficient amount (the amount of CP violation within the SM turned out to be insufficient for generating the baryon asymmetry of the universe, and also perturbative calculations indicated that the electroweak phase transition in the SM is not strong enough), which made necessary the existence of physics beyond the SM close to the EW scale in order to achieve electroweak baryogenesis, providing new sources of CP violation and modifying the Electroweak Symmetry Breaking Sector in order to have a strong EWPT. Here is precisely where hidden sector extensions of the SM fit in the context of electroweak baryogenesis.

In these hidden sector extensions it is also relatively easy to perform an accurate analysis of the Electroweak phase transition and the washout of the baryon asymmetry, and one can extract certain model-independent results from the analysis. We will therefore consider a very simple hidden sector extension of the Standard Model, that serves as a benchmark theory from which to derive model independent results that then can be used when dealing with more complicated hidden sectors, and also in other scenarios beyond the Standard Model.

1.1 The Model.

We extend the Standard Model by adding a set of N real scalar singlets S_i coupled to the SM Higgs doublet field H . We assume there are no linear or cubic terms in the hidden-sector scalar fields S_i (this can be enforced by some global symmetry, e.g. $O(N)$). So, the tree-level scalar potential is:

$$V = \mu^2 H^\dagger H + \lambda (H^\dagger H)^2 + \sum_i \left(\frac{1}{2} m_{S_i}^2 + \zeta_i^2 H^\dagger H \right) S_i^2 + \lambda_S \sum_i S_i^4 \quad (1.1)$$

We also assume that the squared masses of the hidden scalars are semi-positive definite ($m_{S_i}^2 \geq 0$), so that this global symmetry remains unbroken and no quartic terms are necessary to stabilize the potential. Then, since we are not interested in giving a VEV to the singlets, we will set $\lambda_S = 0$.

1.1.1 Zero Temperature Effective Potential.

If the hidden-sector scalar fields don't acquire a VEV, in obtaining the Effective Potential of the theory we can just look at the Higgs field direction, so the Effective Potential just involves the Higgs field. All the details concerning the Effective Potential formalism and the actual calculation of the Effective Potential can be found in Appendix A; in this chapter we will use the main results from that appendix.

In the presence of a background Higgs field, $\langle H^0 \rangle = h/\sqrt{2}$, the 1-loop Effective Potential in Landau gauge and \overline{MS} renormalization scheme is given by:

$$V_{eff}^{1-loop}(h) = \frac{m^2}{2} h^2 + \frac{\lambda}{4} h^4 + \sum_a \frac{N_a M_a^4(h)}{64\pi^2} \left[\log \left(\frac{M_a^2(h)}{Q^2} \right) - C_a \right] \quad (1.2)$$

The relevant contributions to the Effective Potential for the Higgs in the Landau gauge come from the gauge bosons (Z^0 and W^\pm), top quark, Higgs boson, Goldstone bosons (G^0 and G^\pm) and hidden-sector scalar fields; the contribution from the rest of fields (all quarks and leptons except from the top) can be safely neglected, since their couplings to the Higgs field are tiny compared to the ones from the previous fields. Then, the subscript a runs through $a = \{Z, W, t, H, G, S_i\}$, with $N_a = \{3, 6, -12, 1, 3, N_S\}$, while $C_a = 5/6$ for gauge bosons and $3/2$ for fermions and scalars.

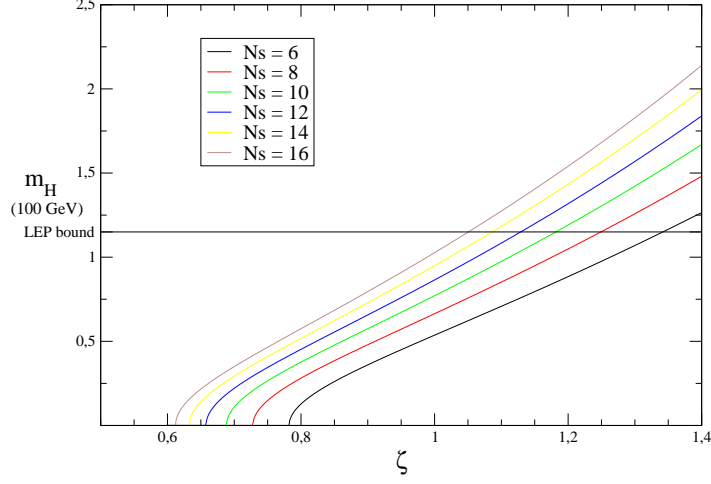


Figure 1.1: Higgs mass as a function of the Higgs-scalar coupling ζ in the conformal case, for various choices of the number of hidden scalar species N_S . The horizontal line represents the LEP lower bound on the Higgs mass: $m_H \geq 114.4$ GeV.

In order to obtain the field-dependent squared masses $M_a^2(h)$ for the various fields, one has simply to read off the quadratic terms for the fields in a background field configuration $\langle H^0 \rangle = h/\sqrt{2}$ for the Higgs. We obtain:

$$\begin{aligned}
 M_H^2(h) &= m^2 + 3\lambda h^2 & M_G^2(h) &= m^2 + \lambda h^2 \\
 M_W^2(h) &= \frac{1}{4}g^2 h^2 & M_Z^2(h) &= \frac{1}{4}(g^2 + g'^2)h^2 \\
 M_t^2(h) &= \frac{1}{2}y_t^2 h^2 & M_{S_i}^2(h) &= m_{S_i}^2 + \zeta_i^2 h^2
 \end{aligned}$$

Here g and g' denote the SM gauge couplings and y_t the top quark Yukawa coupling. The case with classical conformal invariance (i.e. $m^2 = 0$ and $m_{S_i}^2 = 0$) is particularly interesting. In this situation all masses are proportional to the Higgs vacuum expectation value (VEV) and no dimensionful parameters enter into the tree level potential. However, conformal invariance is broken by loop corrections as can be seen in (1.2) by the appearance of the renormalization scale Q . In this way a mass scale is introduced via dimensional transmutation [25]. The correct VEV follows from the minimization condition, which in the classically conformal case translates into:

$$\lambda = - \sum_a \frac{N_a M_a^4(v)}{16\pi^2 v^4} \left[\log \left(\frac{M_a^2(v)}{Q^2} \right) - C_a + \frac{1}{2} \right] \quad (1.3)$$

where $v \simeq 246$ GeV is the Higgs VEV of the SM. We can then write (1.2) as:

$$V_{eff}^{1-loop}(h) = \sum_a \frac{N_a M_a^4(h)}{64\pi^2} \left[\log \left(\frac{h^2}{v^2} \right) - \frac{1}{2} \right] = \frac{m_H^2}{8v^2} h^4 \left[\log \left(\frac{h^2}{v^2} \right) - \frac{1}{2} \right] \quad (1.4)$$

where m_H is the 1-loop Higgs mass, given by:

$$m_H^2 = \left. \frac{\partial^2}{\partial h^2} V_{eff}^{1-loop}(h) \right|_{h=v} = \sum_a \frac{N_a M_a^4(v)}{8\pi^2 v^2} \quad (1.5)$$

One can see that the occurrence of a sizable number of hidden-sector scalars, rather strongly coupled to the Higgs field, can lead to a Higgs mass above the LEP bound (see fig. 1.1), even if the theory is classically conformally invariant⁴ [26, 27].

Finally, the hidden sector scalars will also influence the cubic Higgs self-coupling, deviating it from its SM value; taking only into account the top and hidden-sector scalar contributions, one obtains:

$$\frac{\partial_\phi^3 V}{\partial_\phi^3 V^{\text{SM}}} - 1 = \frac{\sum_i \zeta_i^4}{12\pi^2 M_H^2/v^2 - 3y_t^4} \quad (1.6)$$

In [40] the claim was made that a strong phase transition often would lead to a deviation of the cubic Higgs coupling from its SM value, so that by measuring the cubic Higgs self-coupling one could indirectly obtain information about the nature of the electroweak phase transition. For the present model, this claim will be analyzed in section 2.3.

1.1.2 Finite Temperature Effective Potential.

When the system is in contact with a hot thermal reservoir, such as in the early universe, the usual Effective Potential must be modified in order to include the interactions between the Higgs and the thermal plasma [28].

In order to properly study the electroweak phase transition of the model, we consider the 1-loop Effective Potential at finite temperature⁵ including the resummed Daisy-diagrams (see Appendix A for details). The corresponding contributions are given by:

$$\begin{aligned} V_{eff}^{1-loop}(h, T) = & \frac{m^2}{2} h^2 + \frac{\lambda}{4} h^4 + \sum_a \frac{N_a M_a^4(h)}{64\pi^2} \left[\log \left(\frac{M_a^2(h)}{Q^2} \right) - C_a \right] + \\ & + \frac{T^4}{2\pi^2} \sum_{a \in \text{bosons}} N_a \int_0^\infty dk k^2 \log \left(1 - e^{-\sqrt{k^2 + M_a^2(\Phi)}/T} \right) + \\ & + \frac{T^4}{2\pi^2} \sum_{a \in \text{fermions}} N_a \int_0^\infty dk k^2 \log \left(1 + e^{-\sqrt{k^2 + M_a^2(\Phi)}/T} \right) + \\ & + \frac{T}{12\pi} \sum_{a \in \text{bosons}} \overline{N}_a \left\{ M_a^3(h) - [M_a^2(h) + \Pi_a(T)]^{3/2} \right\} \end{aligned} \quad (1.7)$$

⁴In this case the 1-loop Higgs mass differs significantly from its tree level value $m_H^2 = 3\lambda v^2$. Similarly the Goldstone boson is massless at 1-loop, as opposed to the tree level result $m_G^2 = \lambda v^2$. This discrepancy between the tree-level and 1-loop masses does also appear in the non-conformal case.

⁵Strictly speaking, it is the Free Energy of the system.

Here $\Pi_\alpha(T)$ are the thermal (Debye) masses of the different bosonic species. They can be obtained applying the techniques from [29], and turn out to be:

$$\Pi_G(T) = \Pi_H(T) = \left(\frac{1}{6}(3g^2 + g'^2) + \frac{1}{4}y_t^2 + \frac{1}{2}\lambda + \frac{1}{12}\sum_i \zeta_i^2 \right) T^2 \quad (1.8)$$

$$\Pi_{S_i}(T) = \frac{1}{3}\zeta_i^2 T^2 \quad \Pi_W(T) = \Pi_Z(T) = \frac{11}{6}g^2 T^2 \quad (1.9)$$

Besides, in the resummed Daisy diagrams only the longitudinal polarizations of the gauge bosons contribute, and so $\overline{N}_a = \{1, 2, 1, 3, N_S\}$ for $a = \{Z, W, H, G, S_i\}$.

1.1.3 Impact of Two-Loop Corrections in the Analysis.

Given the fact that the dramatic impact on electroweak symmetry breaking we find⁶ is due to a large ($\mathcal{O}(10)$) number of scalars with sizable couplings to the Higgs, one might worry about the stability of the results when higher-loop corrections to the potential are included. It is relatively easy to obtain the dominant two-loop radiative corrections to the Higgs potential (those that depend on the top Yukawa coupling y_t and ζ) borrowing well known results from the MSSM [31].

In order to properly use the MSSM result, keeping just the y_t^2 and ζ^2 couplings, one has to isolate the stops-R contribution, turning off all their interactions except $\delta V_{MSSM}^0 = y_t^2 |\tilde{t}_R|^2 |H_2|^2 \rightarrow 2 \zeta_i^2 S_i^2 |H|^2$ (see Appendix A.5 for details). In fig. (1.2) we show that these two-loop effects do not modify the structure of the potential in a qualitative way.

⁶As is the fact that the conformal case can give a Higgs mass above the LEP experimental limit [26], as opposed to the SM case [25, 30]

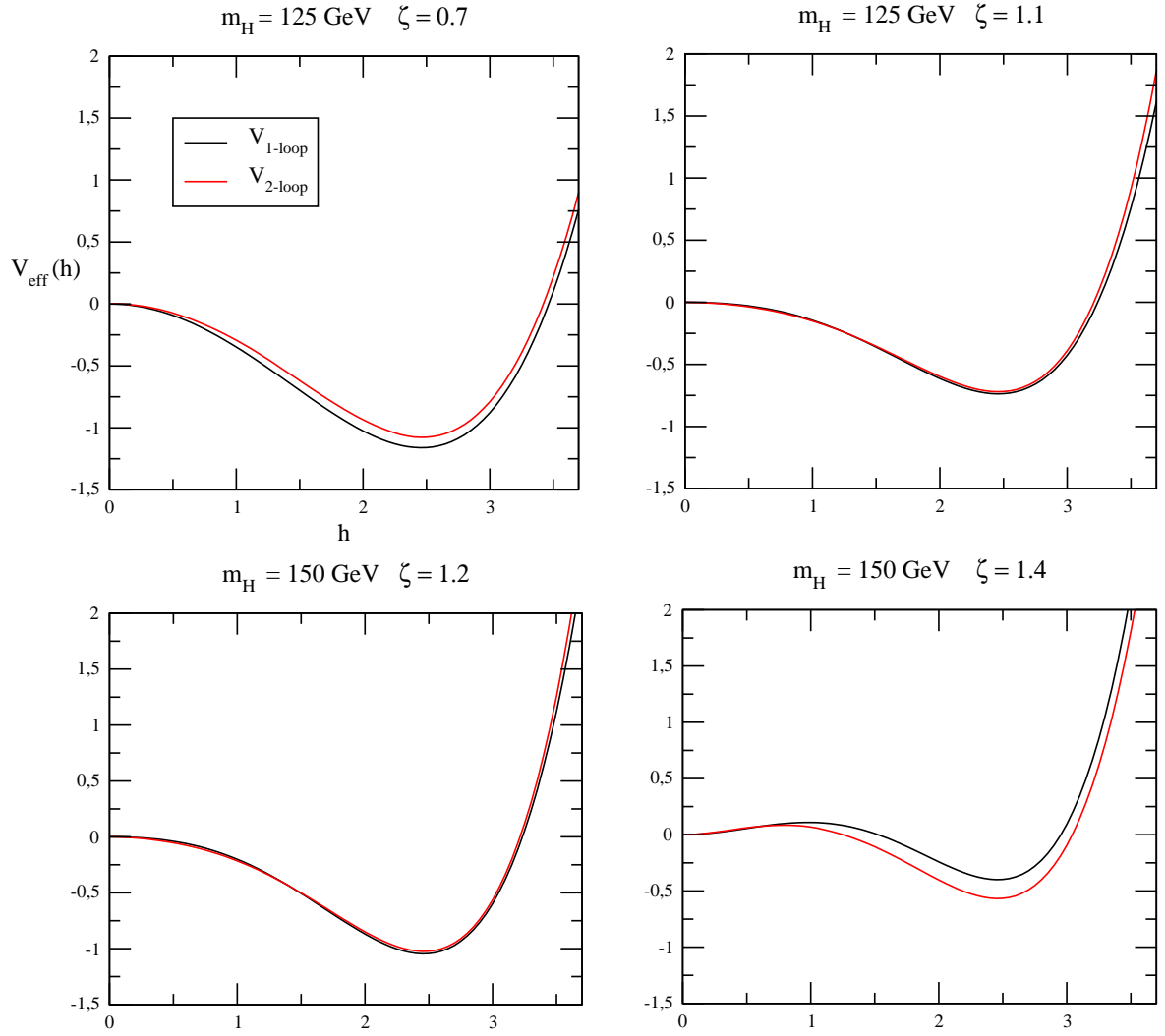


Figure 1.2: Comparison between the 1-loop (black) and 2-loop (red) Zero Temperature Effective Potentials for various choices of the Higgs mass m_H and the coupling ζ ; the qualitative structure of V_{eff} is not modified by the inclusion of the dominant 2-loop corrections.

Chapter 2

The EWPT in Hidden Sector Extensions of the SM.

2.1 Fate of the False Vacuum in Field Theory.

2.1.1 False Vacuum Decay I: Zero Temperature.

Consider a Quantum Field Theory (at zero temperature) for a field φ , and suppose a potential $V(\varphi)$ with two minima, one at $\varphi = 0$ (for simplicity, we will take the potential V such that $V(\varphi = 0) = 0$) and a deeper one at $\varphi = v \neq 0$ (see fig. 2.1). The vacuum $\varphi = 0$ would in principle be stable, but it is rendered unstable by quantum effects (by barrier penetration); it is therefore a false (metastable) vacuum.

The qualitative features of the decay process of the unstable vacuum are relatively simple. Quantum fluctuations are constantly causing bubbles of the true vacuum ($\varphi = v$) to materialize in a sea of false vacuum ($\varphi = 0$). When a bubble forms, if it is too small, the gain in volume energy does not compensate the loss in surface energy (since the volume energy scales like R^3 , being R the bubble radius, and the surface energy scales like R^2), and the bubble shrinks then to nothing. However, as bigger bubbles materialize, they will reach a critical size for which the volume energy compensates the surface energy and it is favorable for the bubble to grow; once bubbles of this type form, they expand converting false vacuum to true, and eventually filling up all space. In order to obtain a more quantitative insight on the process, one has to compute the decay probability per unit time per unit volume Γ of the unstable vacuum, which is given by [32, 33]:

$$\Gamma = \left\{ \frac{S_4^2}{4\pi^2} \left[\frac{\det'(-\square + V''(\varphi_s))}{\det(-\square + V''(0))} \right]^{-\frac{1}{2}} e^{-S_4} \right\} \times [1 + \mathcal{O}(\hbar)] \quad (2.1)$$

Here, $\det'(\dots)$ means that the functional determinant has to be evaluated excluding its zero eigenvalues. The coefficient S_4 is calculated to be the euclidean action S_E for a certain field configuration φ_s :

$$S_4 \equiv S_E = \int d\tau \, d^3\vec{x} \left[\frac{1}{2} \left(\frac{\partial \varphi_s}{\partial \tau} \right)^2 + \frac{1}{2} (\nabla \varphi_s)^2 + V(\varphi_s) \right] \quad (2.2)$$

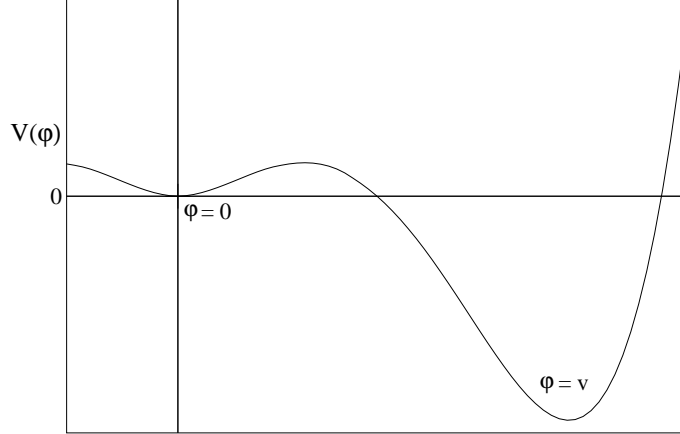


Figure 2.1: Potential $V(\varphi)$ with two nondegenerate minima.

The field configuration φ_s (called the “Bounce”) corresponds to the configuration that minimizes the euclidean action S_E (this means the barrier penetration takes place through the path of “least resistance”) satisfying the boundary conditions:

$$\left. \frac{\partial \varphi_s(\tau, \vec{x})}{\partial \tau} \right|_{\tau=0} = 0 \quad \varphi_s(\tau \rightarrow \pm\infty, \vec{x}) = 0 \quad (2.3)$$

The dependence on the euclidean (imaginary) time $\tau \equiv it$ is due to the fact that the Euclidean action is the one related to the decay rate (see [32, 33]). Also, for S_E to be finite, it is necessary that:

$$\varphi_s(\tau, |\vec{x}| \rightarrow \pm\infty) = 0 \quad (2.4)$$

This last condition is consistent with the qualitative description of the tunneling process given above: quantum fluctuations make a bubble appear somewhere, but far from this place the false vacuum persists undisturbed. The requirement of φ_s minimizing the euclidean action implies that it has to satisfy the following differential equation:

$$\left(\frac{\partial^2}{\partial \tau^2} + \nabla^2 \right) \varphi_s = \frac{dV(\varphi)}{d\varphi} \Big|_{\varphi=\varphi_s} \quad (2.5)$$

All of the above is consistent with the assumption of an $O(4)$ -invariant bounce φ_s . So, we define:

$$\rho = \left(\tau^2 + |\vec{x}|^2 \right)^{\frac{1}{2}} \quad (2.6)$$

We then assume that φ_s is a function of ρ only: $\varphi_s(\tau, \vec{x}) = \varphi_s(\rho)$; the differential equation for the $O(4)$ -invariant bounce $\varphi_s(\rho)$ becomes:

$$\frac{d^2\varphi_s}{d\rho^2} + \frac{3}{\rho} \frac{d\varphi_s}{d\rho} = \frac{dV(\varphi)}{d\varphi} \Big|_{\varphi=\varphi_s} \quad (2.7)$$

with the boundary conditions

$$\frac{\partial\varphi_s(\rho)}{\partial\rho} \Big|_{\rho=0} = 0 \quad \varphi_s(\rho \rightarrow \infty) = 0 \quad (2.8)$$

The action for the $O(4)$ -invariant bounce $\varphi_s(\rho)$ is:

$$S_4 = 2\pi^2 \int_0^\infty \rho^3 d\rho \left[\frac{1}{2} \left(\frac{\partial\varphi_s}{\partial\rho} \right)^2 + V(\varphi_s) \right] \quad (2.9)$$

It can be shown that the system always admits an $O(4)$ -invariant bounce $\varphi_s(\rho)$ (that is to say, there always exists a solution for (2.7) with the appropriate boundary conditions). The way to show it is the following: if we interpret φ as a particle position and ρ as a time, (2.7) can be viewed as the mechanical equation for a particle moving in the inverted potential $-V$ and subject to a viscous damping force with a Stokes's-law coefficient inversely proportional to the time ρ ; the particle is released at rest at time zero, therefore satisfying the first boundary condition, and it is always possible to choose the initial point in such a way that the particle will come to rest at $\rho = \infty$ at $\varphi = 0$, therefore satisfying the second boundary condition [32]. Of course, the initial position will vary depending on the form of the potential (mainly on the relative energy between the two minima), but in any case it is understood that the bounce solution φ_s starts (at $\rho = 0$) close to the global minimum of the potential. Also, it is assumed that any $O(4)$ -noninvariant bounces will have higher euclidean action than the $O(4)$ -invariant bounce, so in principle we don't need to worry about them.

The last step for computing Γ is the evaluation of the determinants $\det'(-\square + V''(\varphi_s))$ and $\det(-\square + V''(0))$; it is not possible in general to obtain a closed expression for them (even with the $O(4)$ -invariance assumption), but being v the only dimensionful quantity present in the theory, they can be estimated to be:

$$\left[\frac{\det'(-\square + V''(\varphi_s))}{\det(-\square + V''(0))} \right]^{-\frac{1}{2}} \sim v^4 \quad (2.10)$$

So, the estimate for the decay probability Γ per unit time and volume of the false vacuum at zero temperature is:

$$\Gamma \simeq \left(\frac{S_4}{2\pi} \right)^2 v^4 e^{-S_4} \quad (2.11)$$

2.1.2 False Vacuum Decay II: Finite Temperature.

In turning to the description of false vacuum decay at nonzero temperature, it has to be remembered that quantum statistics for bosons (fermions) is formally equivalent to quantum field theory in euclidean space-time, periodic (antiperiodic) in the euclidean “time” coordinate τ , with period $\beta = T^{-1}$ [34]. Thus, the only modification with respect to the previous, zero temperature case, is that instead of the $O(4)$ –invariant solution one has to look for an $O(3)$ –invariant (with respect to the spatial coordinates) bounce periodic in τ with period T^{-1} [35]; also, in this case the potential $V(\varphi)$ will depend on temperature. There are two different types of bounce solutions that can be computed for the nonzero temperature case:

1. The first type of bounce φ_{s_3} is spatial $O(3)$ –invariant and τ independent. So, the τ integration from (2.2) just gives a factor T^{-1} , and we obtain for the euclidean action:

$$\begin{aligned} S_E &= \frac{S_3}{T} = \frac{1}{T} \int d^3 \vec{x} \left[\frac{1}{2} (\nabla \varphi_{s_3})^2 + V(\varphi_{s_3}) \right] \\ &= \frac{4\pi}{T} \int_0^\infty r^2 dr \left[\frac{1}{2} \left(\frac{\partial \varphi_{s_3}}{\partial r} \right)^2 + V(\varphi_{s_3}, T) \right] \end{aligned} \quad (2.12)$$

The bounce φ_{s_3} is obtained as the solution to the differential equation

$$\frac{d^2 \varphi_{s_3}}{dr^2} + \frac{2}{r} \frac{d\varphi_{s_3}}{dr} = \frac{dV(\varphi, T)}{d\varphi} \Big|_{\varphi=\varphi_{s_3}} \quad (2.13)$$

with the boundary conditions

$$\frac{\partial \varphi_{s_3}(r)}{\partial r} \Big|_{r=0} = 0 \quad \varphi_{s_3}(r \rightarrow \infty) = 0 \quad (2.14)$$

Notice that any $O(3)$ –invariant bounce periodic in τ must approach the τ –independent one in the limit of high T (since in this limit the period of the bounce, $\beta = T^{-1}$, goes to zero). Finally, the decay probability Γ per unit time per unit volume is [35]:

$$\Gamma = \left\{ T \left(\frac{S_3}{2\pi T} \right)^{\frac{3}{2}} \left[\frac{\det'(-\Delta + V''(\varphi_{s_3}, T))}{\det(-\Delta + V''(0, T))} \right]^{-\frac{1}{2}} e^{-\frac{S_3}{T}} \right\} \quad (2.15)$$

The computation of the determinants $\det'(-\Delta + V''(\varphi_{s_3}, T))$ and $\det(-\Delta + V''(0, T))$ is again very difficult in general (although it has been explicitly calculated in some cases [36]), but we can give an estimate based on dimensional grounds:

$$\left[\frac{\det'(-\Delta + V''(\varphi_{s_3}, T))}{\det(-\Delta + V''(0, T))} \right]^{-\frac{1}{2}} \sim T^3 \quad (2.16)$$

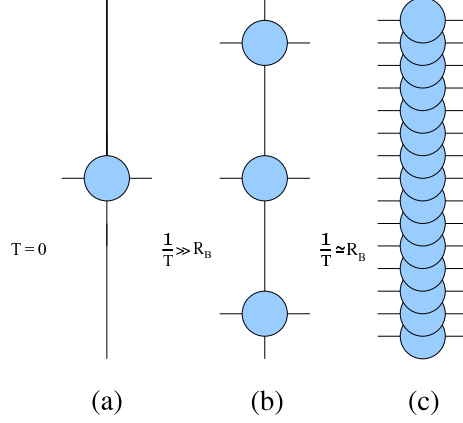


Figure 2.2: $O(4)$ -invariant approximate bounce solutions in the small T limit.

Then, the estimate for Γ in this case is:

$$\Gamma \simeq T^4 \left(\frac{S_3}{2\pi T} \right)^{\frac{3}{2}} e^{\frac{-S_3}{T}} \quad (2.17)$$

2. Suppose that R_B is the radius of the $O(4)$ -invariant bubble (bounce solution $\varphi_s(\rho)$) at zero temperature (fig. 2.2 (a)). At very low temperature $T \ll R_B^{-1}$, an $O(4)$ -invariant bounce is still a good approximation to the solution locally, and one can take the $O(3)$ -invariant, τ periodic bounce $\varphi_s(\tau, r)$ as a sum of $O(4)$ -invariant bubbles placed at a distance (in the euclidean time dimension τ) T^{-1} from one another (fig. 2.2 (b)):

$$\varphi_{s_4}(\tau, r) = \sum_n \varphi_s(\rho_n) = \sum_n \varphi_s \left(\sqrt{r^2 + (\tau + 2\pi n T^{-1})^2} \right) \quad (2.18)$$

For $T \simeq R_B^{-1}$ the bubbles $\varphi_s(\rho_n)$ start overlapping, the previous approximation breaks down, and φ_{s_4} ceases to be a good approximate bounce solution (fig. 2.2 (c)).

So, for $0 < T \leq R_B^{-1}$ one can still use the zero temperature results for the decay of the false vacuum (2.7), (2.8), (2.9) and (2.11), taking into account in this case the temperature dependence of the potential $V(\varphi, T)$. Then, it is clear that for $0 < T \leq R_B^{-1}$ there will be two competing bounce solutions, φ_{s_3} and φ_{s_4} , and the decay probability Γ will be:

$$\Gamma \simeq T^4 \left(\frac{S_3(\varphi_{s_3}, T)}{2\pi T} \right)^{\frac{3}{2}} e^{\frac{-S_3(\varphi_{s_3}, T)}{T}} + \left(\frac{S_4(\varphi_{s_4}, T)}{2\pi} \right)^2 v^4 e^{-S_4(\varphi_{s_4}, T)} \quad (2.19)$$

However, for $T \geq R_B^{-1}$ the field configuration φ_{s_4} stops being a reliable bounce solution and we are left with only one bounce solution, φ_{s_3} . The decay probability Γ is then:

$$\Gamma \simeq T^4 \left(\frac{S_3(\varphi_{s_3}, T)}{2\pi T} \right)^{\frac{3}{2}} e^{\frac{-S_3(\varphi_{s_3}, T)}{T}} \quad (2.20)$$

2.2 Dynamics of 1st Order Phase Transitions in Field Theory.

2.2.1 Dynamics of the Phase Transition: 1st Order vs 2nd Order.

Suppose a temperature dependent potential for a field φ of the form:

$$V(\varphi, T) = a(T)\varphi^2 + c(T)\varphi^4 \quad (2.21)$$

The temperature dependent coefficients $a(T)$ and $c(T)$ have certain important properties: $a(T > T_2) > 0$ and $a(T < T_2) < 0$ (symmetry restoration above a certain temperature T_2) and $c(T) > 0$ (in order to assure stability of the potential).

For $T > T_2$, the only minimum of the potential is at $\varphi = 0$, since $a(T) > 0$ and the equation for $v(T) \neq 0$ does not have real solutions:

$$\frac{\partial V(\varphi, T)}{\partial \varphi} \Big|_{\varphi=v(T)} = 0 \quad v(T) = \sqrt{-\frac{a(T)}{2c(T)}} \quad (2.22)$$

As we lower T below T_2 , the minimum at $\varphi = 0$ becomes a maximum and a new minimum develops at $v(T) \neq 0$ (see fig. 2.3); at each point in space, thermal fluctuations perturb the field at $\varphi = 0$, which then rolls classically to the new global minimum (this process is known as “spinodal decomposition”). The phase transition from $\varphi = 0$ to $\varphi = v(T) \neq 0$ is in this case of 2nd order, since the change in the order parameter of the transition, $v(T)$, is continuous at the transition point.

Now suppose that a term $b(T)\varphi^3$ is added to the previous temperature dependent potential $V(\varphi, T)$:

$$V(\varphi, T) = a(T)\varphi^2 + b(T)\varphi^3 + c(T)\varphi^4 \quad (2.23)$$

with $b(T) < 0$ (the coefficients $a(T)$ and $c(T)$ have the same properties as before); we will also assume that $a(T)$ grows faster with T than $|b(T)|$, so that for sufficiently high temperature $a(T) \gg |b(T)|$. At very high T , we have $a(T) \gg (b(T))^2$ and the only minimum of the potential is at $\varphi = 0$, since the equation for $v(T) \neq 0$ does not have real solutions:

$$\frac{\partial V(\varphi, T)}{\partial \varphi} \Big|_{\varphi=v(T)} = 0 \quad v(T) = \frac{3|b(T)|}{8c(T)} \pm \sqrt{\left(\frac{3b(T)}{8c(T)}\right)^2 - \frac{a(T)}{2c(T)}} \quad (2.24)$$

As we lower T we reach a temperature T_1 when $a(T) = 9(b(T))^2/32c(T)$, and a new extremum develops away from the origin (still $a(T) > 0$, so $\varphi = 0$ continues to be a minimum); below that temperature a new (local) minimum develops away from the origin, and this minimum $\varphi = v(T)$ is separated from $\varphi = 0$ by a potential barrier. If we continue lowering T we reach a critical temperature T_c at which both minima are degenerate, and below T_c the true minimum of the potential is $\varphi = v(T)$ and there exists the possibility of tunneling

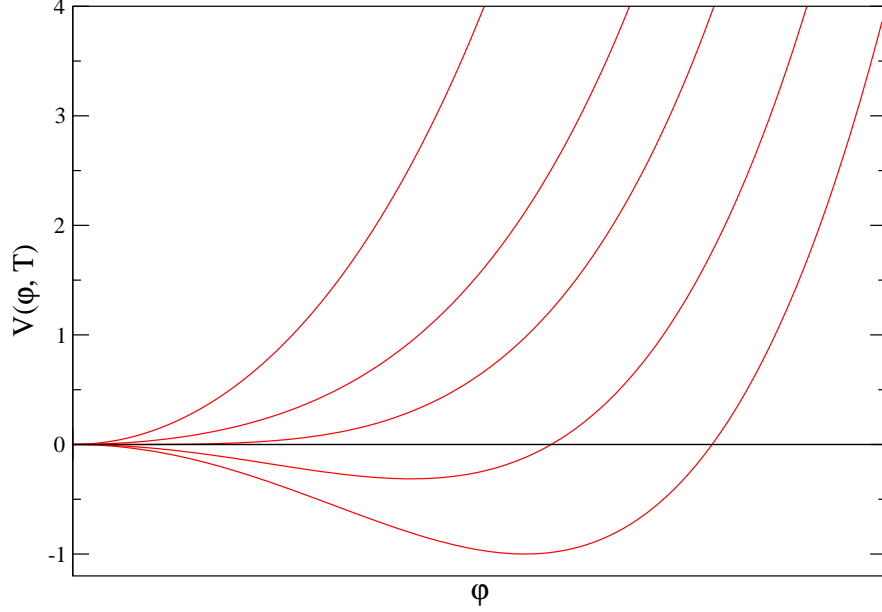


Figure 2.3: Variation of the potential from (2.21) with the temperature. It is clear that a 2nd phase transition is occurring.

between $\varphi = 0$ and $\varphi = v(T)$. As we lower the temperature further, we eventually reach $T = T_2$ and $\varphi = 0$ becomes a maximum (see fig. 2.4). In the interval $T_c > T > T_2$, bubbles of true vacuum ($\varphi = v(T)$) nucleate in a sea of false vacuum ($\varphi = 0$) in the way described in sections 2.1.1 and 2.1.2; the transition is clearly of 1st order since the process of bubble nucleation implies a discontinuous change in the order parameter at the transition point.

We can now apply the previous results to the study of the temperature behaviour of the 1-loop Finite Temperature Effective Potential $V_{eff}^{1-loop}(\varphi, T)$. The high temperature expansion of V_{eff}^{1-loop} (A.39) is precisely of the form (2.23) assuming all field dependent masses are of the form⁷ $M_a^2(\varphi) = k_a^2 \varphi^2$ and a lagrangian scalar potential for φ of the form $V(\varphi) = m^2 \varphi^2 + \lambda \varphi^4$:

$$\begin{aligned}
 V_{eff}^{1-loop}(\varphi, T) &= \left[m^2 + \frac{T^2}{48} \left(2 \sum_{a \in b} N_a k_a^2 + \sum_{a \in f} N_a k_a^2 \right) \right] \varphi^2 - \left[\frac{\pi T}{12} \sum_{a \in b} N_a k_a^3 \right] \varphi^3 \\
 &+ \left[\lambda + \frac{1}{64\pi^2} \sum_{a \in b} N_a k_a^4 \left(\log \left(\frac{T^2 a_b}{Q^2} \right) - C_a \right) - \frac{1}{64\pi^2} \sum_{a \in f} N_a k_a^4 \left(\log \left(\frac{T^2 a_f}{Q^2} \right) - C_a \right) \right] \varphi^4 \\
 &\Downarrow \\
 V_{eff}^{1-loop}(\varphi, T) &= c_2(T) \varphi^2 + c_3(T) \varphi^3 + c_4(T) \varphi^4 \tag{2.25}
 \end{aligned}$$

⁷For the case of the Effective Potential for the Higgs field in the Standard Model this would imply neglecting the contributions from both the Higgs and Goldstone bosons, whose field dependent masses are of the form $M_a^2(\varphi) = k_a^2 \varphi^2 + m_a^2$.

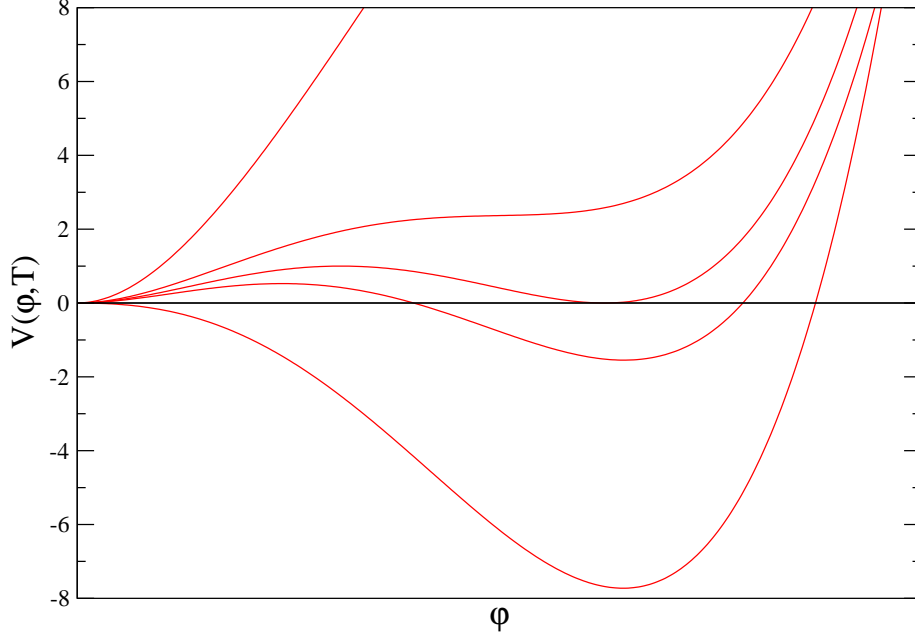


Figure 2.4: Variation of the potential from (2.23) with the temperature. It is clear that a 1st phase transition is occurring.

b (f) stands for bosons (fermions). We see then that $c_2(T)$, $c_3(T)$ and $c_4(T)$ have the properties we were imposing on the coefficients $a(T)$, $b(T)$ and $c(T)$ from (2.23) under certain conditions (for $c_2(T=0) < 0$ we need $m^2 < 0$).

The previous discussion gives a qualitative idea of how the phase transition proceeds. Also, as the order of the phase transition is controlled by the coefficient $c_3(T)$, if this coefficient is negligible compared to $c_2(T)$ and $c_4(T)$ we are approximately in the situation described by (2.21), and the phase transition will be 2nd order or very weakly 1st order, whereas if $c_3(T)$ is sizeable the transition will be 1st order. In fact, the strength of the 1st order phase transition, as measured by the quantity⁸ $v(T_c)/T_c$ is to first approximation:

$$\frac{v(T_c)}{T_c} \simeq \frac{1}{\lambda} \left[\frac{2\pi}{36} \sum_{a \in b} N_a k_a^3 \right] \quad (2.26)$$

So, it is directly proportional to the number of bosonic degrees of freedom coupled to the field φ and to the strength of these couplings (through the parameters M_a), and inversely proportional to the quartic coupling λ (which is in turn proportional to the mass squared of φ , m_φ^2). Then, a way of achieving a stronger phase transition than the Standard Model case is adding new bosonic particles to the SM, coupled to the Higgs; this is precisely what happens in the singlet scalar extension of the SM we have discussed in section 1.1.

⁸This is just an approximation, since the phase transition does not really take place at $T = T_c$, as will be discussed in sections 2.2.2 and 2.2.3.

2.2.2 1st Order Phase Transition: Bubble Nucleation Temperature T_n .

As stated in section 2.2.1, when the potential $V(\varphi, T)$ develops two different minima (at $\varphi = 0$ and $\varphi = v(T) \neq 0$), for $T < T_c$ there exists the possibility of a 1st order phase transition from $\varphi = 0$ to $\varphi = v(T)$. However, although tunneling becomes in principle possible below T_c (the $O(3)$ bounce solution exists no matter how close we are to T_c from below, and $\Gamma(T)$ is given by (2.20)⁹), for T very close to T_c (for almost degenerate vacua) the tunneling rate is still too small to start the phase transition:

$$S_3(\varphi_{S_3}, T) \rightarrow \infty \quad \text{when} \quad T \rightarrow T_c^- \quad (2.27)$$

Therefore, the temperature T_n at which the phase transition actually starts must be lower than T_c . The proper definition of T_n is obtained in the following way [37]:

The mean number of bubbles nucleated inside a Hubble volume between $t_c(T_c)$ and $t(T)$ is given by:

$$P(T) = \int_{t_c(T_c)}^{t(T)} \Gamma(\tilde{t}) V(\tilde{t}) d\tilde{t} \quad (2.28)$$

which can also be interpreted as the probability that a bubble of true vacuum nucleates in the time interval between $t_c(T_c)$ and $t(T)$, so long as $P(T) < 1$.

In the early universe, during the radiation dominated era, the horizon radius scales like $d_H = 2t$; so, taking then a Hubble volume as d_H^3 we get $V(t) = 8 t^3$. Also, in the radiation dominated era the time-temperature relation is:

$$t = \xi \frac{M_{Pl}}{T^2} \quad \xi = \left[\left(\frac{90}{32\pi^3} \right) \frac{1}{\sum g_B + \frac{7}{8} \sum g_F} \right]^{\frac{1}{2}} = \left[\left(\frac{90}{32\pi^3} \right) \frac{1}{g_{eff}} \right]^{\frac{1}{2}} \quad (2.29)$$

where $M_{Pl} = 1.22 \times 10^{19}$ GeV is the Planck mass and $g_{eff} \simeq 106.75 + N_S$ is the effective number of degrees of freedom.

Then, the mean number of bubbles becomes:

$$\begin{aligned} P(T) &= \int_{T_c}^T \frac{8\xi^3 M_{Pl}^3}{\tilde{T}^2} \left(\frac{S_3}{2\pi\tilde{T}} \right)^{\frac{3}{2}} e^{-S_3/\tilde{T}} \frac{dt}{d\tilde{T}} d\tilde{T} = \\ &= \int_T^{T_c} \frac{16\xi^4 M_{Pl}^4}{\tilde{T}^5} \left(\frac{S_3}{2\pi\tilde{T}} \right)^{\frac{3}{2}} e^{-S_3/\tilde{T}} d\tilde{T} \end{aligned} \quad (2.30)$$

⁹The use of (2.20) for $\Gamma(T)$, which involves just the $O(3)$ bounce solution instead of (2.19), which involves both the $O(3)$ and the $O(4)$ bounces, will be justified at the end of this section.

The nucleation temperature T_n is defined as the temperature for which the mean number of nucleated bubbles per Hubble volume is one¹⁰.

$$P(T_n) = 1 \implies \int_{T_n}^{T_c} \frac{16\xi^4 M_{Pl}^4}{T^5} \left(\frac{S_3}{2\pi T} \right)^{\frac{3}{2}} e^{-S_3/T} dT = 1 \quad (2.31)$$

It is also possible to obtain an approximate value for S_3/T at the onset of nucleation, $S_3(T_n)/T_n$ (see Appendix B for the details):

$$\frac{S_3(T_n)}{T_n} \simeq 140 - 148 \quad (2.32)$$

The result (2.32) is model independent, and greatly simplifies the task of determining the beginning of the phase transition.

Having defined the nucleation temperature T_n , let us remark that there is an important distinction between the case in which there is a potential barrier separating both minima even at $T = 0$ and the case when this barrier disappears for $T = T_2 > 0$ (obviously $T_2 < T_c$):

- When the potential barrier disappears for $T = T_2 > 0$, the phase transition will always take place, since:

$$S_3(T) \rightarrow 0 \quad \text{when} \quad T \rightarrow T_2^+ \quad (2.33)$$

and so the condition from (2.32) will always be fulfilled for a certain T_n with $T_c > T_n > T_2$. Moreover, since T_n will generally be much higher than the temperature $T_B \equiv R_B^{-1}$ at which the locally $O(4)$ -invariant bounce φ_{S_4} ceases to be a good approximate bounce solution (this is automatically guaranteed when $T_2 > T_B$, but it also happens in the case $T_B > T_2 > 0$), we can safely consider the $O(3)$ -invariant (τ independent) bounce as our only bounce solution when computing the false vacuum decay rate Γ , which will in turn be given by (2.20).

- When there is still a potential barrier at $T = 0$ separating both minima, it is not guaranteed that the phase transition will take place by thermal fluctuations, since now:

$$\frac{S_3(T)}{T} \rightarrow \infty \quad \text{when} \quad T \rightarrow 0 \quad (2.34)$$

Therefore the function $S_3(T)/T$ will have a minimum at a certain temperature T_m . If $S_3(T_m)/T_m < 140 - 148$ (this also implies $T_n > T_m$), then the phase transition will still occur; in this situation we still find generically $T_m > T_B$ and so the $O(3)$ -invariant bounce continues to be the only relevant bounce solution in the process of computing $\Gamma(T)$. However, for $S_3(T_m)/T_m > 140 - 148$ the function $S_3(T)/T$ never

¹⁰One important remark is that the condition $P(T_n) = 1$ does not need to be very accurate in order to obtain the correct nucleation temperature (with $P(T'_n) = \mathcal{O}(0.1 - 1)$, we obtain $T_n - T'_n \ll 1$; since we are dealing with mean numbers/probabilities, this is necessary in order to trust the definition of T_n from (2.31).

reaches the nucleation value and the phase transition cannot take place through thermal fluctuations. In this last case the temperature drops to T_B and the $O(4)$ -invariant bounce solution φ_{S_4} becomes relevant; we then have to use (2.19) for $\Gamma(T)$ below T_B (this two possibilities are shown in fig. 2.12).

2.2.3 1st Order Phase Transition: Evolution of the Phase Transition.

In order to determine the end of the phase transition, the temperature T_f at which the transition completes has to be computed. Let $f(T)$ be the fraction of space filled with true vacuum (covered by nucleated bubbles):

$$f(T) \equiv \frac{\text{Mean Number of Nucleated Bubbles} \times \text{Volume of Bubbles}}{\text{Volume of Horizon}} \quad (2.35)$$

The volume $V_{Bub}(\tilde{T}, T)$ at temperature T of a bubble nucleated at \tilde{T} is given by:

$$\begin{aligned} V_{Bub}(\tilde{T}, T) &= \frac{4\pi}{3} \left[R_B + 2v_B \xi M_{Pl} \left(\frac{1}{T^2} - \frac{1}{\tilde{T}^2} \right) \right]^3 \simeq \\ &\simeq \frac{32\pi (\xi v_B M_{Pl})^3}{3} \left(\frac{1}{T^2} - \frac{1}{\tilde{T}^2} \right)^3 \end{aligned} \quad (2.36)$$

Here, v_B is the velocity of the expanding bubble wall, and the initial bubble radius R_B can be safely neglected with respect to the size of the bubble once it starts growing. Then we get for $f(T)$:

$$\begin{aligned} f(T) &= \int_T^{T_n} \Gamma(\tilde{T}) V(\tilde{T}) V_{Bub}(\tilde{T}, T) d\tilde{T} = \\ &= \frac{64\pi v_B^3 \xi^4 M_{Pl}^4}{3 (2\pi)^{3/2}} \int_T^{T_n} \frac{1}{\tilde{T}^5} \left(\frac{S_3}{\tilde{T}} \right)^{\frac{3}{2}} e^{-S_3/\tilde{T}} \left(1 - \frac{T^2}{\tilde{T}^2} \right)^3 d\tilde{T} \end{aligned} \quad (2.37)$$

Notice that the upper limit of integration must be T_n , since for $T > T_n$ no bubble has been nucleated. There is an important subtlety concerning (2.37): once bubbles start nucleating, the available horizon volume for more bubbles to nucleate at a temperature T is no longer $V(T)$ but $V(T)(1 - f(T))$; therefore, in order to account for the overlapping of bubbles, (2.37) has to be modified to¹¹:

$$f(T) = \frac{64\pi v_B^3 \xi^4 M_{Pl}^4}{3 (2\pi)^{3/2}} \int_T^{T_n} \frac{1}{\tilde{T}^5} \left(\frac{S_3}{\tilde{T}} \right)^{\frac{3}{2}} e^{-S_3/\tilde{T}} \left(1 - \frac{T^2}{\tilde{T}^2} \right)^3 (1 - f(\tilde{T})) d\tilde{T} \quad (2.38)$$

¹¹There are other, alternative ways of defining $f(T)$ [38].

This definition also has the important feature of ensuring $f(T) \leq 1$. However, for practical purposes (2.38) is much more difficult to deal with than (2.37), and the effect of taking into account the overlapping of bubbles is negligible, so from now on we will use (2.37) as our definition of $f(T)$. The end of the phase transition is defined as:

$$f(T_f) = 1 \implies \frac{64\pi v_B^3 \xi^4 M_{Pl}^4}{3(2\pi)^{3/2}} \int_{T_f}^{T_n} \frac{1}{T^5} \left(\frac{S_3}{T}\right)^{\frac{3}{2}} e^{-S_3/T} \left(1 - \frac{T_f^2}{T^2}\right)^3 dT = 1 \quad (2.39)$$

Similarly to $S_3(T_n)/T_n$, there is also a way to obtain an approximate value for $S_3(T)/T$ at the end of the transition, $S_3(T_f)/T_f$, which for weak 1st order phase transitions is (see Appendix B):

$$\frac{S_3(T_n)}{T_n} \simeq 110 - 115 \quad (2.40)$$

This result, although not completely model independent¹², gives an approximate value for $S_3(T_f)/T_f$ (which is valid for weak transitions; the analytic result valid also for strong transitions is given by (B.10)).

In addition, there are several quantities that can be determined in order to quantify the strength of the 1st order phase transition; these are usually evaluated at the end of the phase transition, when most cosmological processes related to the phase transition (such as electroweak baryogenesis, in the case of φ being the Higgs field, or gravitational wave production) take place. The first quantity is the ratio between the field VEV and the temperature, $R \equiv v(T)/T$; as has been mentioned in the introduction, this ratio is important for baryogenesis, since for the baryon asymmetry to survive after the transition the washout effects by sphalerons have to be suppressed, and this in turn requires $v(T_f)/T_f \geq 1.0$ in the Standard Model [21]. We do not expect this bound to be much different in the present model, since the sphaleron energy is dominated by the contributions from the gauge field configurations excited in the sphaleron rather than the scalar ones [22].

The second quantity is the duration of the phase transition, which is simply given by:

$$\Delta t \equiv t_f - t_n = \xi M_{Pl} \left(\frac{1}{T_f^2} - \frac{1}{T_n^2} \right) = \frac{\xi M_{Pl}}{T_f^2} \left(1 - \frac{T_f^2}{T_n^2} \right) \quad (2.41)$$

from which we obtain the dimensionless ratio $(\Delta t)^{-1}/H$:

$$\frac{(\Delta t)^{-1}}{H(t_f)} = \frac{2}{\left(1 - \frac{T_f^2}{T_n^2}\right)} \quad (2.42)$$

¹²The bubble wall velocity v_B obviously depends on the particular model.

Another important quantity is the rate of variation of the bubble nucleation rate (bearing in mind that most of the time variation in Γ is in S_3/T), called β , which is defined as [39]:

$$\frac{S_3}{T} = \frac{S_3}{T} \Big|_{t_f} - \beta(t - t_f) + \dots \quad \beta \equiv - \frac{d(S_3/T)}{dt} \Big|_{t_f} \quad (2.43)$$

\Downarrow

$$\frac{\beta}{H(t_f)} = T_f \frac{d}{dT} \left(\frac{S_3}{T} \right) \Big|_{T_f} \simeq \frac{S_3(T_f)}{T_f} \frac{1}{\left(\frac{T_c}{T_f} - 1 \right)} \quad (2.44)$$

In the last line we have used both (2.43) and the approximation from (B.6). The parameter β^{-1} is usually used as an estimate of the duration of the phase transition [39, 27], although in practice it tends to be shorter (but of the same order of magnitude) than the actual duration of the phase transition Δt (see fig. 2.9).

The last quantity is the latent heat L liberated at the phase transition, which is the sum of two contributions; the first one is the difference in free energy between the two minima (the stable and the metastable) $\epsilon \equiv \Delta V(\varphi)$, and the second one corresponds to the entropy variation (which is nonzero for a 1st order phase transition):

$$L = \Delta V(\varphi) - T \Delta s = \left(T \frac{dV(v)}{dT} - V(v) + V(0) \right)_{T_f} \quad (2.45)$$

The latent heat is usually normalized to the energy density of the radiation in the plasma, through the dimensionless parameter α :

$$\alpha \equiv \frac{L}{\rho_{\text{rad}}} = \frac{30L}{\pi^2 g_{\text{eff}} T^4} \quad (2.46)$$

Both α and the duration of the phase transition (as parametrized by either Δt or β^{-1}) play a very important role in describing the spectrum of gravitational waves generated during a 1st order phase transition through bubble collisions [39, 27], although we will not analyze this issue here.

2.3 The Electroweak Phase Transition in a Singlet Scalar Extension of the SM.

Once we have defined the relevant quantities that characterize a 1st order phase transition, we can analyze the phase transition for the singlet scalar extension of the Standard Model defined in section 1.1, using the 1-loop finite temperature effective potential including the resummed ring diagrams (see section 1.1.2). For the numerical analysis we will take, as in [26, 27], a number of scalars $N_S = 12$ with universal couplings to the Higgs, $\zeta_i = \zeta$, and no explicit mass terms, $m_{S_i} = 0$. All the quantities are obtained as functions of ζ and for several values of the Higgs mass m_H (consistent with electroweak breaking conditions).

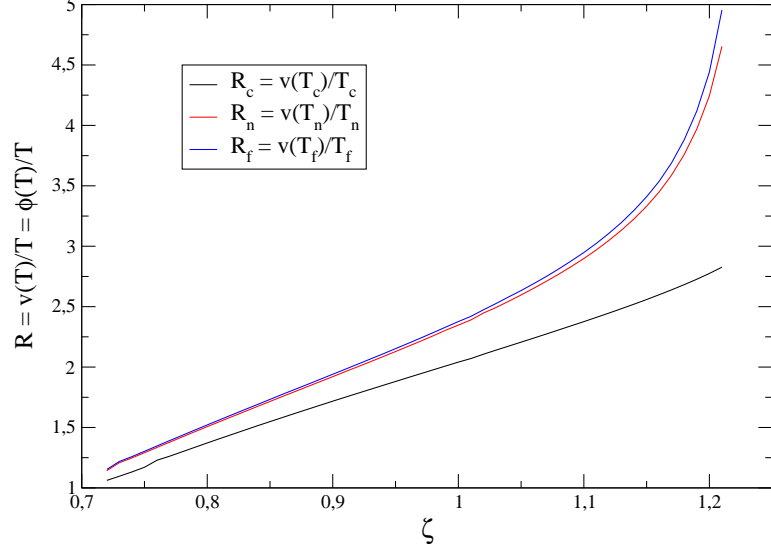


Figure 2.5: Ratio $\phi(T)/T$ at T_c , T_n and T_f as a function of ζ for $m_H = 125$ GeV.

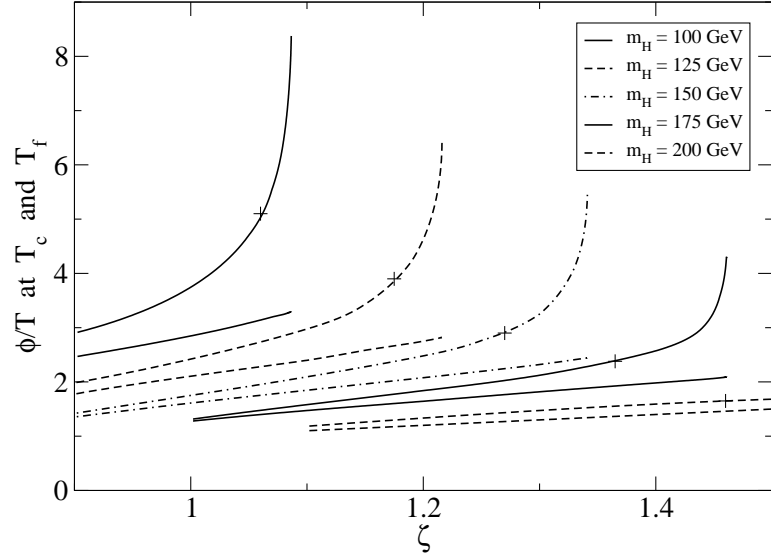


Figure 2.6: Ratio $\phi(T)/T$ at T_c (lower curve) and at T_f (upper curve) as a function of ζ for various Higgs masses m_H . The crosses mark the conformal case.

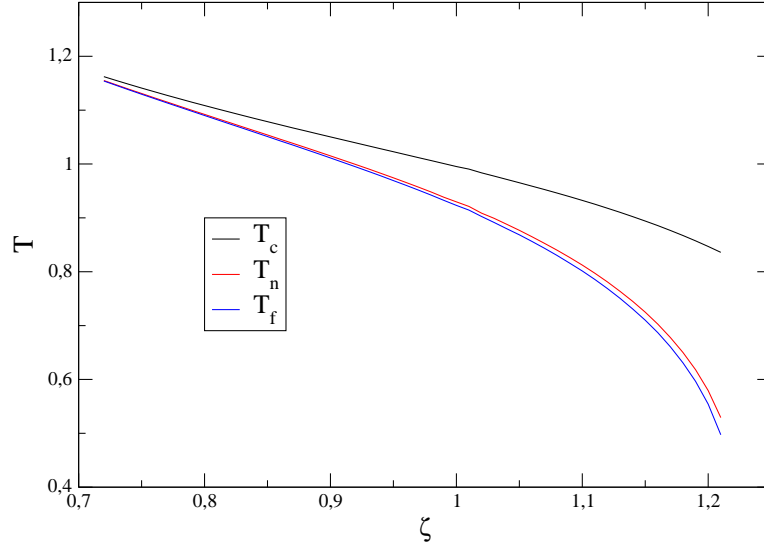


Figure 2.7: T_c , T_n and T_f as a function of ζ for $m_H = 125$ GeV.

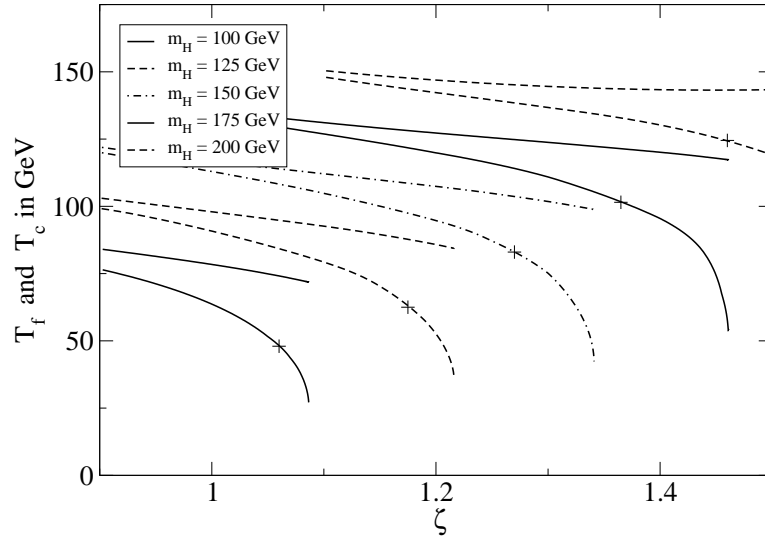


Figure 2.8: T_c (upper curve) and T_f (lower curve), as a function of ζ for various values of the Higgs mass m_H .

The strength of the phase transition at the three relevant temperatures (critical temperature for vacuum degeneracy T_c , nucleation temperature T_n and temperature at the end of the phase transition T_f), measured by $R \equiv v(T)/T = \phi(T)/T$, becomes larger as ζ increases (see fig. 2.5) and is also larger for smaller Higgs masses (see fig. 2.6). For very small values of ζ , we expect the phase transition to be SM-like and therefore of second-order or a cross-over; we mark the conformal ($m = 0$) case with a cross and we see that, even in this case, the model shows a first-order phase transition strong enough to allow for electroweak baryogenesis.

In fig. 2.7 we show the different temperatures T_c , T_n and T_f as a function of ζ for $m_H = 125$ GeV; for weak 1st order phase transitions (small ζ) we obtain $T_f \simeq T_n$ compared to T_c , and as the phase transition gets stronger both the difference between T_n and T_f and between T_c and the other two become larger; also, as the Higgs mass m_H increases, all the three temperatures get larger (see fig. 2.8). As has been already pointed out, these temperature behaviours are responsible of raising the value of the analytical approximations for $S_3(T_n)/T_n$ and $S_3(T_f)/T_f$ ((B.5) and (B.10)) as the phase transition becomes stronger; this can be explicitly seen in fig. 2.9, where it also becomes clear that the analytical approximations agree very well with the explicit numerical results from (2.31) and (2.39).

The comparison between the duration of the transition Δt and the usual estimate β^{-1} is plotted in fig. 2.10 as a function of ζ for $m_H = 125$ GeV, showing that Δt is actually larger than β^{-1} ($(\Delta t)^{-1}/H$ shorter than β/H). We also find that as the strength of the phase transition grows the duration of the transition gets larger and larger (see also fig. 2.11); this can be understood in the following way: let us label the value of ζ for the conformal case as ζ_1 ; to the right of that conformal point ($\zeta > \zeta_1$) the Higgs potential of the model has a barrier separating the symmetric and broken phases even at $T = 0$, and this barrier increases with increasing ζ , rendering tunneling less efficient and making the time of the transition larger; eventually, for too large values of ζ this barrier becomes too high and tunneling by thermal fluctuations is not efficient to trigger the electroweak phase transition (no thermal transition will occur beyond a critical value ζ_c and for $\zeta > \zeta_c$ one is stuck in the symmetric minimum).

In order to make the previous discussion clearer, we recall the discussion at the end of section 2.2.2, where we pointed out that to the left of the conformal point ($\zeta < \zeta_1$) the barrier between vacua disappears at a temperature $T_2 > 0$, and so $S_3/T \rightarrow 0$ as $T \rightarrow T_2$. However, beyond the conformal point T_2 ceases to exist, and $S_3/T \rightarrow \infty$ as $T \rightarrow 0$, so it is possible that for sufficiently high ζ the action $S_3(T)/T$ does not reach the nucleation value $S_3(T_n)/T_n$ and there is no thermal phase transition; this is shown in fig. 2.12, where we plot the typical behavior of the tunneling actions, S_3/T and S_4 , as functions of the temperature for $M_H = 125$ GeV and two choices of $\zeta > \zeta_1 \simeq 1.17$ in this case. For $\zeta = 1.2$, S_3/T gets eventually below the critical nucleation value ~ 142 (horizontal line), and the electroweak phase transition takes place. For $\zeta = 1.25$ no satisfactory transition would occur.

The last important quantity in our description of the phase transition, the latent heat (as described by α), is quickly increasing with ζ and larger for smaller m_H (see fig. 2.13).

Finally, we analyze the claim in [40] about the possible correlation between the strength of the phase transition and the deviation of the cubic Higgs self-coupling from its SM value (section 1.1). We can see from fig. 2.14 that in the present model a strong first-order phase

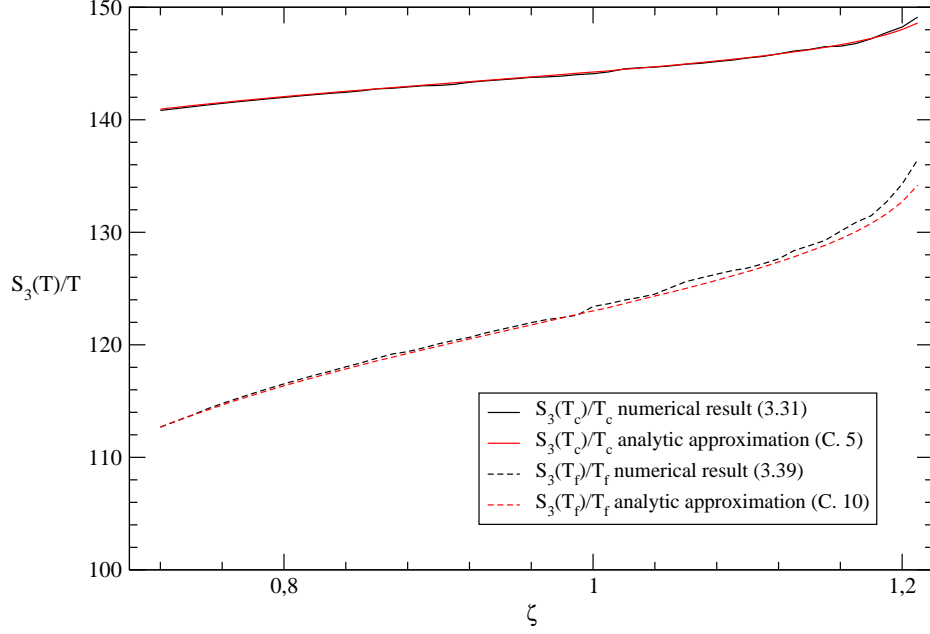


Figure 2.9: $S_3(T)/T$ at T_n and T_f as a function of ζ for $m_H = 125$ GeV.

transition does not necessarily imply a very large deviation of the cubic Higgs coupling from its SM value. Independently of the value of the Higgs mass, a phase transition that is strong enough for the suppression of sphaleron processes, $v(T)/T \geq 1.0$, is possible for deviations of the cubic coupling as small as 15% (there has been recent work that also point in this direction [41])

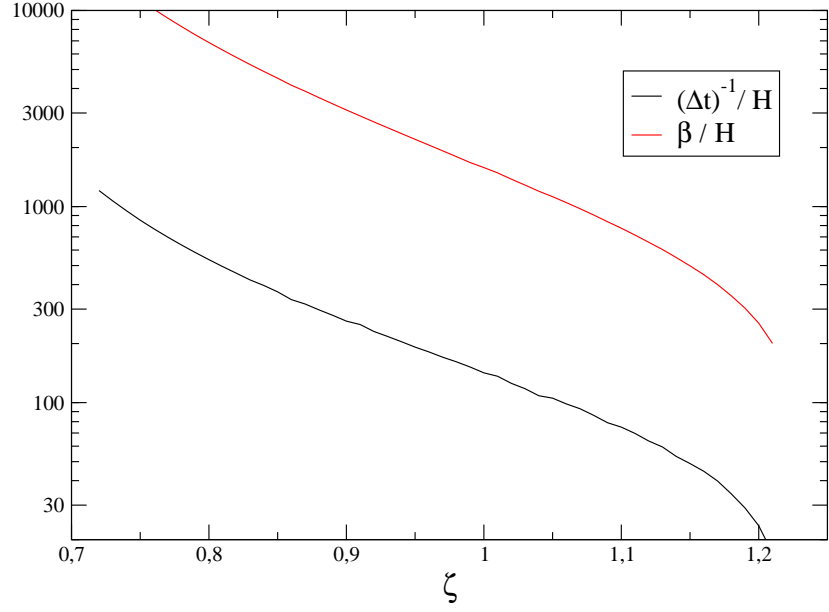


Figure 2.10: Comparison between $(\Delta t)^{-1}$ and β as a function of ζ for $m_H = 125$ GeV.

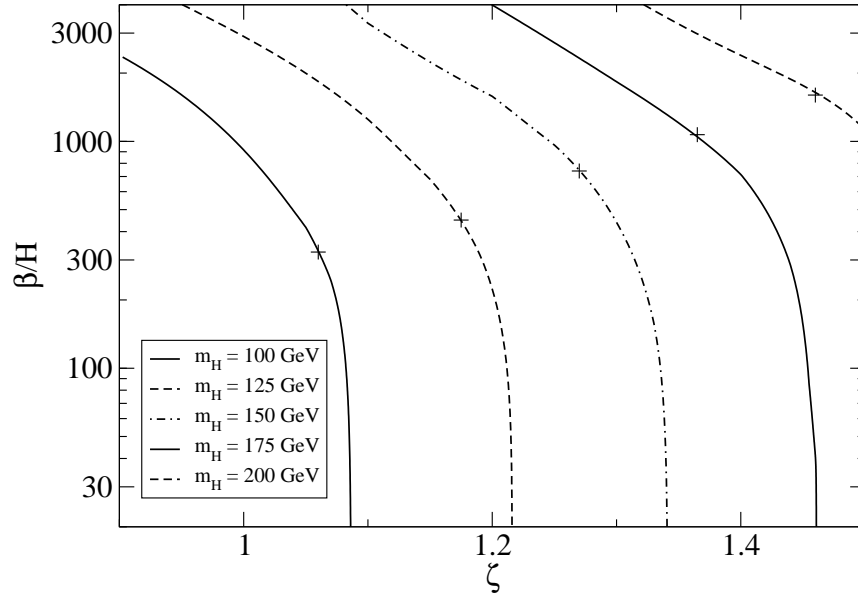


Figure 2.11: The parameter β characterizing the approximate duration of the electroweak phase transition as a function of ζ for several Higgs masses.

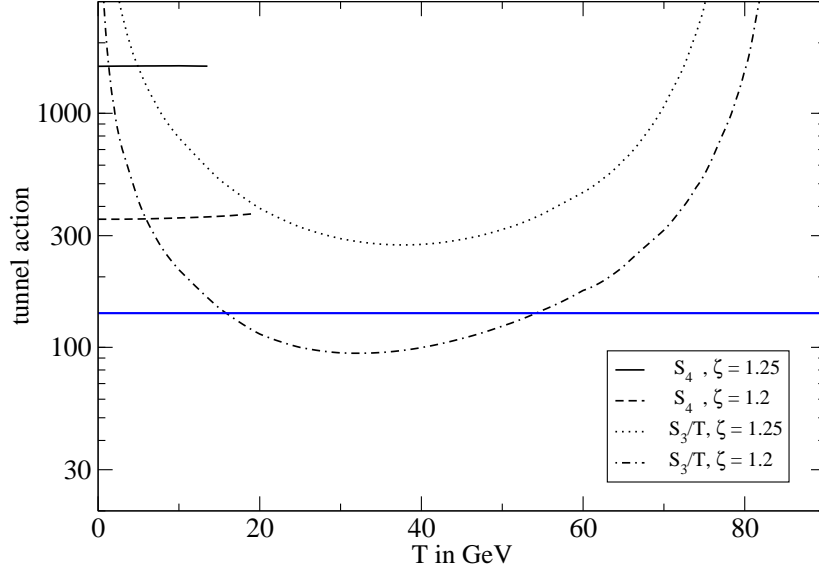


Figure 2.12: Tunneling actions, S_3/T and S_4 , as a function of temperature for $M_H = 125$ GeV and two different values of the coupling ζ as indicated. The curves for S_4 are stopped when the four-dimensional bounce ceases to be reliable.

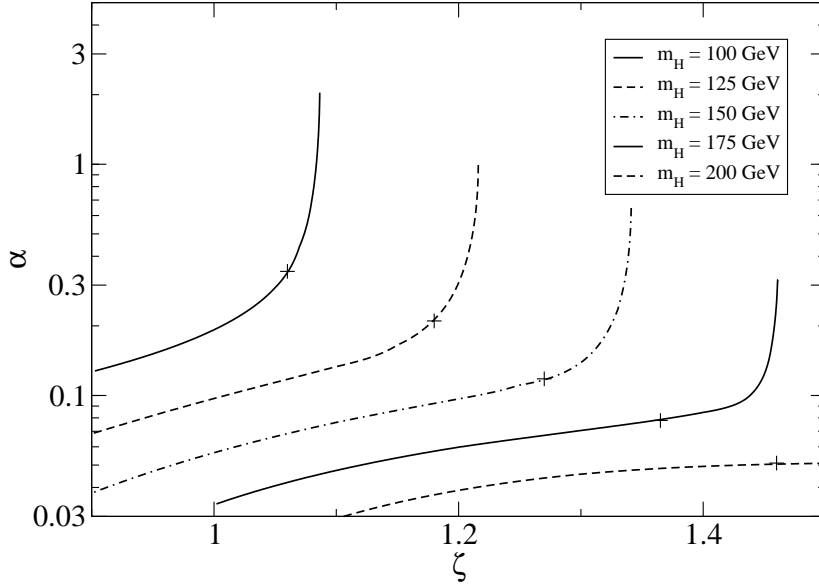


Figure 2.13: The parameter α characterizing the latent heat liberated during the electroweak phase transition as a function of ζ for several Higgs masses.

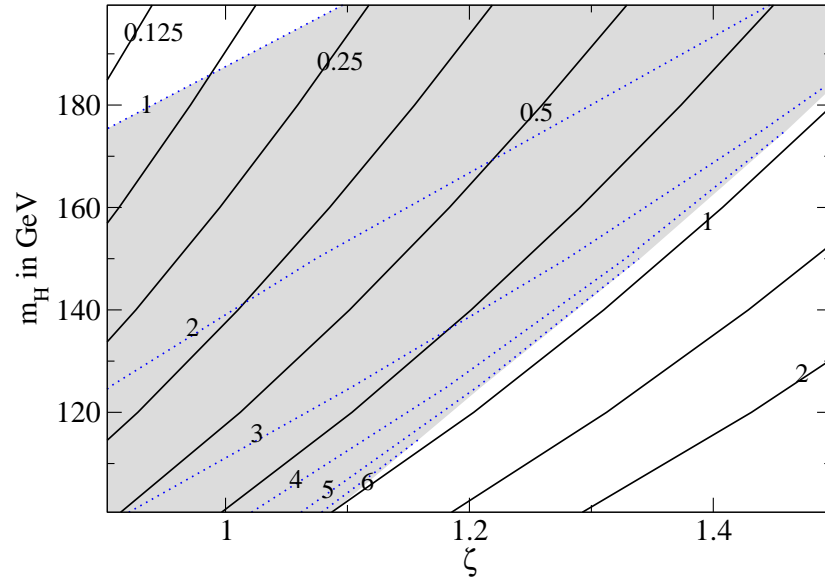


Figure 2.14: The deviation of the cubic Higgs coupling from its value in the Standard Model (solid lines). The shaded region corresponds to a strong first-order phase transition: the dotted lines are labeled by the corresponding value of $v(T_f)/T_f$.

Chapter 3

Hidden Sector Scalars as Possible Candidates for Dark Matter.

Many extensions of the Standard Model have dark matter candidates, and hidden sector extensions are no exception; any hidden sector stable particles could in principle serve as candidates for the dark matter of the universe, as discussed in the introduction. Here we investigate if the new hidden-sector scalar degrees of freedom are a viable dark matter candidate. For simplicity we consider only one scalar, as the generalization to several scalars is straightforward. We will focus on two aspects: we first analyze the possibility that the same scalar species might be responsible both for a strong phase transition and for dark matter; we then focus on the classically conformal case, in which the scalar has no explicit mass term m_s .

In order to be a viable dark matter candidate, the scalar has to be stable. This can easily be achieved by a Z_2 symmetry (or an $O(N)$ symmetry in the case of various scalar species), as in the scalar potential from (1.1), and assuming that this symmetry is not spontaneously broken. Nevertheless the scalars can still annihilate and the particle density n_s of the scalar will obey a Boltzmann equation, which can be written as [42]:

$$\frac{dn_s}{dt} + 3H n_s = - \langle \sigma_{\text{ann}} |v| \rangle \left(n_s^2 - (n_s^{EQ})^2 \right)$$

or, using the time-temperature relation in the radiation dominated era

$$\frac{dn_s}{dT} - \frac{3}{T} n_s = \left(\sqrt{\frac{45}{16\pi^3 g_{\text{eff}}(T)}} \frac{2M_{Pl}}{T^3} \right) \langle \sigma_{\text{ann}} |v| \rangle \left(n_s^2 - (n_s^{EQ})^2 \right) \quad (3.1)$$

Here n_s^{EQ} is the particle number equilibrium distribution, H is the Hubble parameter, σ_{ann} is the annihilation cross section of the scalar particles, $|v|$ is the relative velocity between them and $\langle \dots \rangle$ represents in this case a thermal average. The quantities n_s^{EQ} and H are respectively given by:

$$n_s^{EQ} = T^3 \left(\frac{M_S}{2\pi T} \right)^{3/2} e^{-\frac{M_S}{T}} \quad H^2 \simeq \frac{8\pi^3 g_{\text{eff}}(T) T^4}{90M_{Pl}^2}$$

The mass of the scalar is $M_S = m_S + \zeta^2 v^2$ and the quantity $g_{eff}(T)$ is the effective number of relativistic degrees of freedom in the plasma at a temperature T , given by:

$$g_{eff}(T) = \sum_B g_i \left(\frac{T_i}{T} \right)^4 + \frac{7}{8} \sum_F g_i \left(\frac{T_i}{T} \right)^4 \quad (3.2)$$

Here g_i is the number of degrees of freedom of each species in the plasma, and T_i are the temperatures of the different species.

When the rate of interactions of a certain species with the rest of the plasma at a certain temperature is much larger than the expansion rate of the universe at that temperature, $\Gamma_i(T) \gg H(T)$, then that species (either relativistic or not at that temperature) is in thermal equilibrium with the rest of the plasma. It can happen though that as the universe cools down, a temperature T_{dec} is reached when $\Gamma_i(T_{dec}) \simeq H(T_{dec})$; below that temperature the rate of interactions is not sufficient to maintain thermal equilibrium with the rest of particle species in the plasma, and the species is effectively decoupled from the plasma¹³ (we say that this species has been “frozen-out”). So, when $T_i > T_{dec}$ for a certain species, then $T_i = T$ (being T the temperature of the plasma).

We want to obtain the temperature T_{dec} at which the hidden sector scalars decouple from the rest of the thermal plasma; rescaling the particle density distribution functions, $F_s(T) = n_s(T)/T^3$ and $F_s^{EQ}(T) = n_s^{EQ}(T)/T^3$, Boltzmann equation transforms into:

$$\frac{dF_s}{dT} = \sqrt{\frac{45M_{Pl}^2}{4\pi^3 g_{eff}}} \langle \sigma_{ann} |v| \rangle \left(F_s^2 - (F_s^{EQ})^2 \right) \quad (3.3)$$

We now need an explicit expression for $\langle \sigma_{ann} |v| \rangle$. For a general cross section σ_{ann} it is not possible to analytically compute the integrals contained in the definition of the thermal average, and one then has to rely on an expansion of $\langle \sigma_{ann} |v| \rangle$ in powers of T/M_S [43]. For $T/M_S \ll 1$, it is a good approximation to keep just the first coefficient of the expansion, which is precisely $\sigma_{ann} |v|$.

Notice that this last approximation will yield a T -independent result for $\langle \sigma_{ann} |v| \rangle$, despite $\langle \sigma_{ann} |v| \rangle$ being a thermal average; this is so because for $T \ll M_S$ the typical accesible energies for the scalar particles are of the order of M_S , and so T does not play a role in the averaging; of course the approximation of $\langle \sigma_{ann} |v| \rangle$ being T -independent will be good only in the case $T \ll T_{EW}$ (being T_{EW} the temperature at which the electroweak phase transition takes place), because otherwise we have to take into account that the masses of the different species depend on T , and also that the different species may not have had time to thermalize after the electroweak phase transition.

¹³Once a certain species decouples from the plasma, it evolves in thermal equilibrium with herself at the decoupling temperature T_{dec} .

We then calculate the cross section from the different annihilation modes of $S + S$. The different annihilation channels (as shown in the next page) give the following contributions to $\langle \sigma_{\text{ann}} | v \rangle$ [17]:

$$S + S \rightarrow h^0 + h^0:$$

$$\frac{\zeta^4}{16\pi M_S^2} \left(1 - \frac{m_H^2}{M_S^2}\right)^{1/2} \left\{ 1 + \frac{3m_H^2}{D_h} (8M_S^2 + m_H^2) + \frac{8\zeta^2 v^2}{D_S} (m_H^2 + 2\zeta^2 v^2 - 2M_S^2) \right. \\ \left. - \left(\frac{3m_H^2}{D_h} \right) \left(\frac{8\zeta^2 v^2}{D_S} \right) [(4M_S^2 - m_H^2)(2M_S^2 - m_H^2) - m_H M_S \Gamma_H \Gamma_S] \right\}$$

$$S + S \rightarrow W^- + W^+:$$

$$\frac{\zeta^4 M_W^4}{2\pi M_S^2 D_h} \left(1 - \frac{M_W^2}{M_S^2}\right)^{1/2} \left[2 + \left(1 - \frac{2M_S^2}{M_W^2}\right)^2 \right]$$

$$S + S \rightarrow Z^0 + Z^0:$$

$$\frac{\zeta^4 M_Z^4}{4\pi M_S^2 D_h} \left(1 - \frac{M_Z^2}{M_S^2}\right)^{1/2} \left[2 + \left(1 - \frac{2M_S^2}{M_Z^2}\right)^2 \right]$$

$$S + S \rightarrow f + \bar{f}:$$

$$\sum_{\text{fermions}} \frac{N_f \zeta^4 m_f^2}{\pi D_h} \left(1 - \frac{m_f^2}{M_S^2}\right)^{3/2}$$

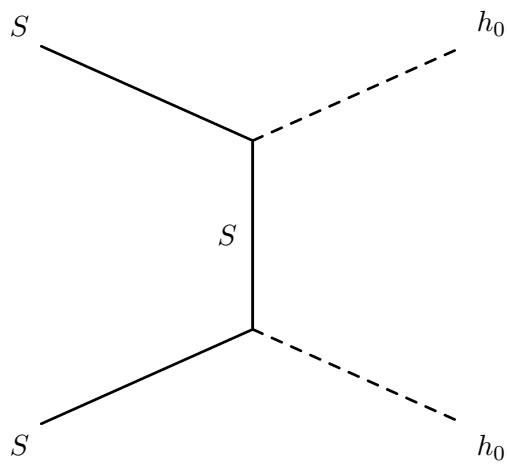
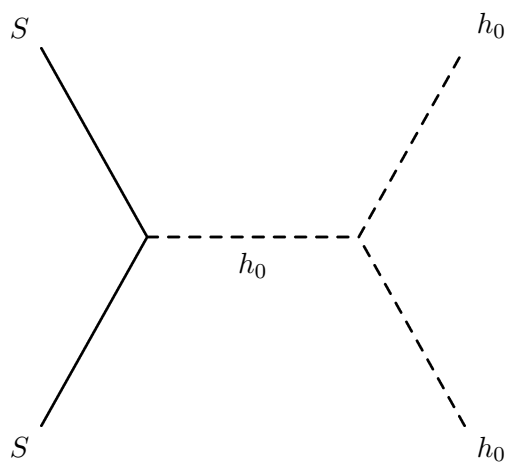
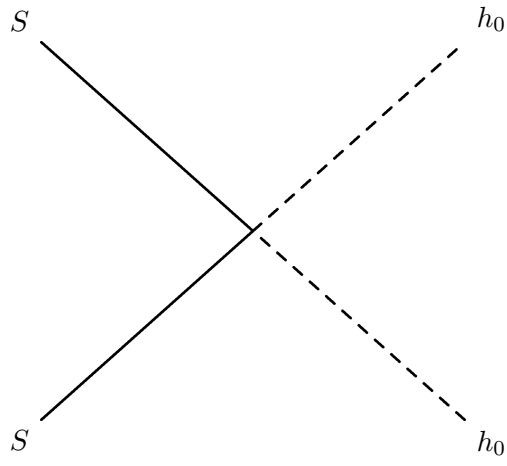
where

$$\begin{aligned} D_h &\equiv (4M_S^2 - m_H^2)^2 + m_H^2 \Gamma_H^2 \\ D_S &\equiv (2M_S^2 - m_H^2)^2 \end{aligned} \tag{3.4}$$

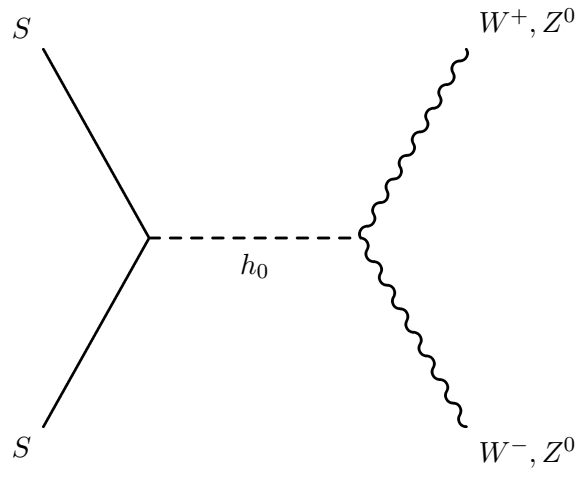
Here $\Gamma_H \approx 8 \times 10^{-5} m_H$ is the decay width of the Higgs particle in the SM, and $N_f = 1(3)$ for leptons (quarks). The formulas above are only valid for¹⁴ $M_S \geq m_a$ (with $a = \{h^0, W^\pm, Z^0, f\}$).

¹⁴Being the energies of the scalar particles of order of their rest mass M_S , the region $M_S \leq m_a$ becomes, to a good approximation, energetically forbidden.

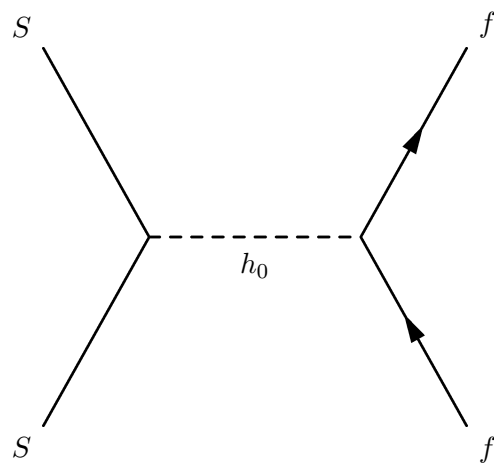
$$S + S \rightarrow h^0 + h^0$$



$$S + S \rightarrow W^- + W^+ / Z^0 + Z^0:$$



$$S + S \rightarrow f + \bar{f}:$$



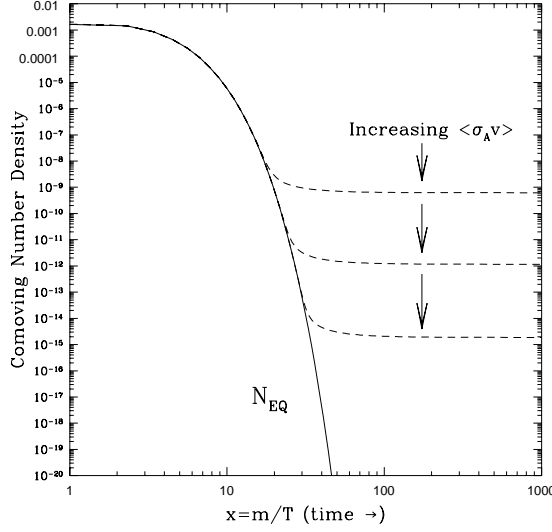


Figure 3.1: Comparison between F_s and F_s^{EQ} .

Now, in order to obtain the freeze-out temperature T_{dec} for the hidden sector scalars there are two options:

- Boltzmann equation can be solved numerically, obtaining the rescaled number particle distribution $F_s(T)$, and defining T_{dec} as the temperature for which F_s deviates from F_s^{EQ} by a certain amount (see fig. 3.1).
- There is an approximate analytical solution to Boltzmann equation, the so-called “Lee-Weinberg” solution [44]. The Lee-Weinberg solution is obtained by assuming that $F_s = F_s^{EQ}$ for $T > T_{dec}$; then, T_{dec} is defined by the condition:

$$\left| \frac{dF_s^{EQ}}{dT} \right|_{T_{dec}} = \sqrt{\frac{45M_{Pl}^2}{4\pi^3 g_{eff}}} \langle \sigma_{ann} |v| \rangle \left(F_s^{EQ}(T_{dec}) \right)^2$$

$$\Downarrow$$

$$\frac{M_S}{T_{dec}} = \log \left[\left(\frac{45M_{Pl}^2 M_S T_{dec}}{2g_{eff}} \right)^{\frac{1}{2}} \frac{\langle \sigma_{ann} |v| \rangle}{(2\pi)^3 \left(1 - \frac{3T_{dec}}{2M_S} \right)} \right] \quad (3.5)$$

One can solve this last equation for T_{dec} in an easy way (typically one finds $M_S \approx (15 - 25) T_{dec}$). In order to obtain $F_s(T)$ for $T < T_{dec}$, one solves:

$$\frac{dF_s}{dT} = \sqrt{\frac{45M_{Pl}^2}{4\pi^3 g_{eff}}} \langle \sigma_{ann} |v| \rangle F_s^2 \quad (3.6)$$

with the boundary condition $F_s(T_{dec}) = F_s^{EQ}(T_{dec})$.

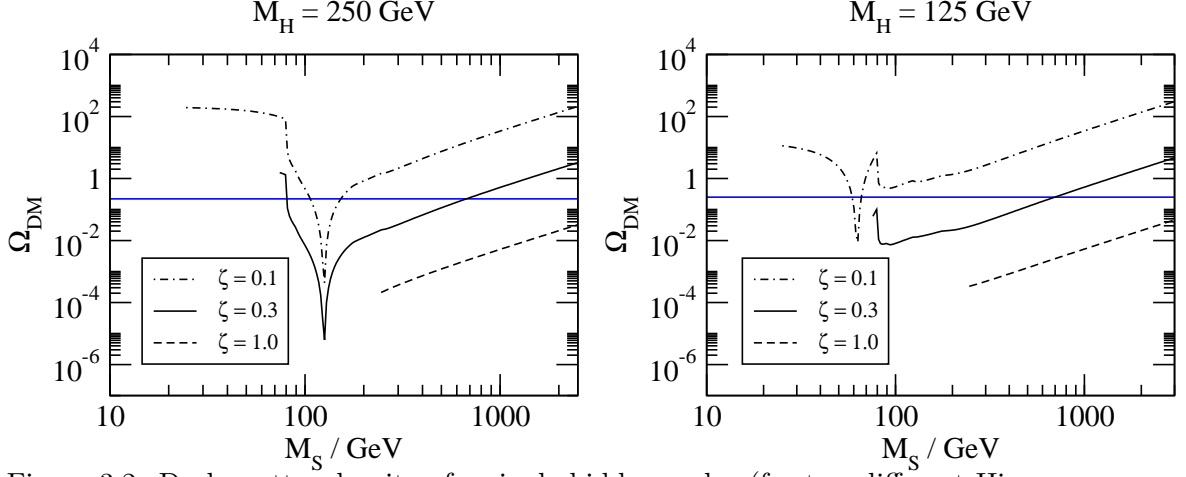


Figure 3.2: Dark matter density of a single hidden scalar (for two different Higgs masses as indicated) as a function of the scalar mass M_S and different values for its coupling to the Higgs, ζ .

Either with T_{dec} obtained by one method or the other, we can then obtain the relic mass density Ω_S of hidden sector scalar particles¹⁵ freezing out of equilibrium:

$$\Omega_{DM} = \Omega_S = \frac{\rho_S}{\rho_c} = \frac{g_{eff}(T_\gamma)}{g_{eff}(T_{dec})} \sqrt{\frac{4\pi^3 g_{eff}}{45 M_{Pl}^2}} \frac{M_S}{\langle \sigma_{ann} |v| \rangle T_\gamma T_{dec}} \left(\frac{T_\gamma}{\rho_c} \right) \frac{\left(1 - \frac{3T_{dec}}{2M_S} \right)}{\left(1 - \frac{T_{dec}}{2M_S} \right)} \quad (3.7)$$

Here $T_\gamma = 2.73$ K^o is the temperature of the Cosmic Microwave Background (CMB) today, and ρ_c is the critical energy density of the universe now:

$$\rho_c = \frac{3H_0^2}{8\pi G} \quad (3.8)$$

with H_0 the Hubble parameter today.

The dependence of Ω_{DM} on the scalar mass for fixed coupling ζ is plotted in fig. 3.2. Notice that we only plotted the dark matter density for scalar masses that are larger than ζv and hence correspond to a positive mass term m_S^2 in the Lagrangian (according to $M_S^2 = m_S^2 + \zeta^2 v^2$).

Besides a logarithmic dependence on the freeze-out temperature, the dark matter density scales for large masses as $\Omega_{DM} \propto M_S^2/\zeta^4$. Notice that for $2M_S \approx m_H$ most annihilation channels are enhanced and the scalar contribution to dark matter is suppressed. Finally, the annihilation cross-section drops considerably below the W-boson threshold, $M_S < M_W$, since if the scalar is light it mostly annihilates into bottom/anti-bottom pairs, which is suppressed

¹⁵For $N > 1$ the only difference is that now we have more scalar species and each of them contributes equally to the dark matter density, so $\Omega_S^{Tot} = N\Omega_S$.

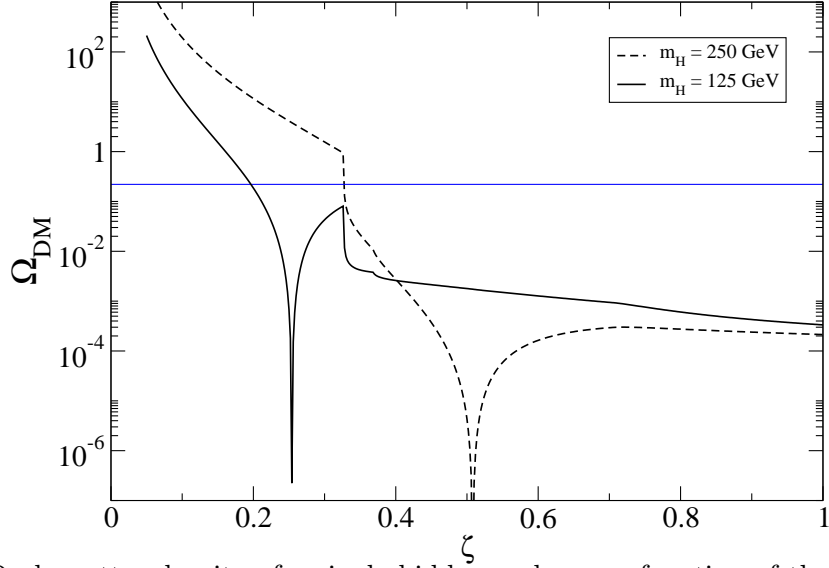


Figure 3.3: Dark matter density of a single hidden scalar as a function of the coupling ζ in the conformal case and two different values for the Higgs mass.

by the bottom-quark Yukawa coupling. This leads to an increase of the dark matter density below the W-boson threshold. Notice also that taking temperature effects into account, one expects that the annihilation cross-section changes less drastically when the scalar mass is varied. In particular the enhancement close to the Higgs mass is expected to be less prominent. Likewise, the drop below the W-boson threshold proceeds in an interval of width $\Delta M_S \approx T$.

Therefore, we see that there are two regimes in which we can reproduce the required value $\Omega_{DM} = 0.228 \pm 0.013$ [45]. The first option is to increase the scalar mass term m_S , while keeping the coupling ζ fixed. However, even in the case of a rather large number of scalars $N_S = 12$, this requires scalar masses of order TeV and such scalars cannot be responsible for a strong phase transition. Alternatively, the scalar could be rather light, with $M_S \leq M_W$, and weakly coupled, such that its annihilation is suppressed. Also in this case, the impact of the scalars on the phase transition is small.

In fig. 3.3 the dark matter density in the conformal case ($m_S = 0$) is plotted as a function of ζ for two different values of the Higgs mass. The predicted dark matter density typically surpasses the observed one below the W-boson threshold. Besides, in the case that the Higgs boson is lighter than two W-bosons, the resonant enhancement in the decay channel can lead to two additional viable values for the parameter ζ that reproduce the observed dark matter density.

In conclusion, if extra scalar degrees of freedom are responsible for a strong electroweak first-order phase transition, as well as for dark matter, it seems that either the coupling constants ζ_i or the mass terms $m_{S,i}$ are non-universal. Scalar dark matter requires either a scalar with a rather large mass $M_S \approx \text{TeV}$, or a rather weak coupling $\zeta \approx M_W/v$. However both types of scalars cannot contribute significantly to the strength of the phase transition. Hence, the existence of both features in a universal scalar framework would require a very large number of scalars, which we estimate to be $N_S \geq 50$.

Part II

Phenomenology of Conformal Hidden Sectors: Unparticles.

Chapter 4

Introduction

4.1 The Unparticle Idea.

About two years ago, Howard Georgi published two seminal papers [8, 9] in which he looked into the possibility of having a conformal sector with a nontrivial infrared fixed point coupled to the SM; he argued that if such a conformal sector would exist and would couple to our ordinary world of particles, the features it would exhibit would be very peculiar, since it would behave unlike a common particle sector.

Field theories with nontrivial scale invariance in the infrared (see for example [46]) would give rise to stuff very different from anything we are used to seeing in our world, which seems to be well-described in terms of particles, with definite masses. Scale invariant stuff cannot have a definite mass unless that mass is zero (since a scale transformation multiplies all dimensional quantities by a rescaling factor raised to the mass dimension, a nonzero mass is not scale invariant). A free massless particle is a simple example of scale invariant stuff because the zero mass is unaffected by rescaling (but in this case the scale invariance is trivial). However, there are more complicated, interacting, field theories¹⁶ which have the property of scale invariance. The Standard Model does not have this property, but there could be a sector of the theory, as yet unseen, that is scale invariant and very weakly interacting with the rest of the Standard Model (so as to approximately preserve the scale invariance of the new sector). In such an interacting scale invariant sector there are no particles (because there can be no particle states with a definite nonzero mass). Georgi then called the scale invariant stuff Unparticles.

The scheme envisaged by Georgi is the following:

- At very high energy (UV regime), the theory contains the Standard Model, a hidden sector with a nontrivial IR fixed point, and the two sectors interact via a third, very massive sector, which we will call “mediator sector” and whose mass scale is \mathcal{M}_U (see fig. 4.1).

¹⁶In these theories there are fields that get multiplied by fractional powers of the rescaling parameter (they scale with fractional dimensions).

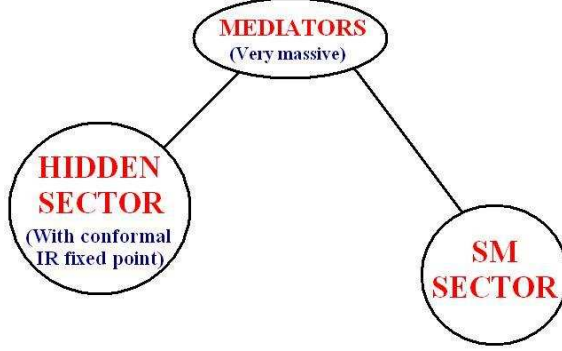


Figure 4.1: Georgi's Scheme.

- Below the scale $\mathcal{M}_{\mathcal{U}}$, the mediator sector is integrated out and that results in nonrenormalizable couplings between the SM fields and the hidden sector fields, suppressed by powers of $\mathcal{M}_{\mathcal{U}}$, of the generic form:

$$\frac{1}{\mathcal{M}_{\mathcal{U}}^{d_{SM}+d_{UV}-4}} \mathcal{O}_{SM} \mathcal{O}_{UV} \quad (4.1)$$

where \mathcal{O}_{SM} is a Standard Model operator of mass dimension d_{SM} and \mathcal{O}_{UV} is a hidden sector operator with mass dimension d_{UV} .

- The hidden sector reaches its conformal IR fixed point at a scale $\Lambda_{\mathcal{U}}$ (becoming scale invariant below $\Lambda_{\mathcal{U}}$); in the effective theory below the scale $\Lambda_{\mathcal{U}}$ the operators \mathcal{O}_{UV} match onto Unparticle operators $\mathcal{O}_{\mathcal{U}}$, and the interactions of (4.1) match onto interactions of the form:

$$\mathcal{C}_{\mathcal{U}} \frac{\Lambda_{\mathcal{U}}^{d_{UV}-d_{\mathcal{U}}}}{\mathcal{M}_{\mathcal{U}}^{d_{SM}+d_{UV}-4}} \mathcal{O}_{SM} \mathcal{O}_{\mathcal{U}} = \mathcal{C}_{\mathcal{U}} \left(\frac{\Lambda_{\mathcal{U}}}{\mathcal{M}_{\mathcal{U}}} \right)^{d_{SM}+d_{UV}-4} \Lambda_{\mathcal{U}}^{4-d_{SM}-d_{\mathcal{U}}} \mathcal{O}_{SM} \mathcal{O}_{\mathcal{U}} \quad (4.2)$$

where $d_{\mathcal{U}}$ is the scaling dimension¹⁷ of the Unparticle operator $\mathcal{O}_{\mathcal{U}}$, and $\mathcal{C}_{\mathcal{U}}$ is a dimensionless constant.

The key idea of this scheme is the fact that, as the hidden sector decouples from the SM sector at low energies (it is then a necessary condition for the scheme to work that the couplings from (4.1) are irrelevant, $d_{SM} + d_{UV} - 4 > 0$), the hidden sector still reaches its conformal IR fixed point despite being coupled to a non conformal sector; so, the interaction from (4.1) does not affect the IR scale invariance of the Unparticles, and this makes the low energy effective theory below $\Lambda_{\mathcal{U}}$ very simple.

¹⁷It corresponds to the sum of the canonical dimension and the anomalous dimension, and will typically be a noninteger number. If the IR fixed point is weakly coupled (as in [46]) the anomalous dimensions are small and the operators have dimensions close to their classical values; however, for strongly coupled fixed points (see [11] for a brief discussion) the anomalous dimensions can be large.

As an example, consider a scalar Unparticle operator $\mathcal{O}_{\mathcal{U}}$, with dimension $d_{\mathcal{U}}$ (for the moment we assume that $1 < d_{\mathcal{U}} < 2$, although $d_{\mathcal{U}}$ could be greater than 2 [47]). Conformal invariance completely fixes the two-point function for $\mathcal{O}_{\mathcal{U}}$:

$$P_{\mathcal{U}}(p^2) = \frac{A_{d_{\mathcal{U}}}}{2 \sin(\pi d_{\mathcal{U}})} \frac{i}{(-p^2 - i\epsilon)^{2-d_{\mathcal{U}}}} \quad A_{d_{\mathcal{U}}} \equiv \frac{16\pi^{5/2}}{(2\pi)^{2d_{\mathcal{U}}}} \frac{\Gamma(d_{\mathcal{U}} + 1/2)}{\Gamma(d_{\mathcal{U}} - 1)\Gamma(2d_{\mathcal{U}})} \quad (4.3)$$

The coefficient $A_{d_{\mathcal{U}}}$ is taken so that the phase space for Unparticles matches the one for n massless scalar particles when $d_{\mathcal{U}} \rightarrow n$. We also recover the usual scalar propagator for $d_{\mathcal{U}} \rightarrow 1$. The spectral function representation for this propagator is:

$$-iP_{\mathcal{U}}(p^2) = \int_0^\infty \frac{\rho_{\mathcal{U}}(s)}{p^2 - s + i\epsilon} ds \quad \longrightarrow \quad \rho_{\mathcal{U}}(s) = \frac{A_{d_{\mathcal{U}}}}{2\pi} s^{d_{\mathcal{U}}-2} \quad (4.4)$$

with no poles and an essential singularity at $s = 0$.

Before continuing, a few comments are in order:

1. Here we are considering the Unparticles as a certain type of Hidden sector, meaning that Unparticles are not charged under the Standard Model gauge group; however, one can think of scenarios where the unparticles do carry Standard Model gauge quantum numbers, as in [48].
2. Apart from scalar Unparticle operators $\mathcal{O}_{\mathcal{U}}$, Unparticle operators in other representations of the Lorentz group exist, such as $\mathcal{O}_{\mathcal{U}}^\mu$.
3. There are constraints of the possible values of $d_{\mathcal{U}}$. Unitarity of the conformal algebra imposes lower bounds¹⁸ on the scaling dimension of the various types of operators [49]:
 - Scalar operators: $d_{\mathcal{U}} \geq 1$
 - Fermion operators: $d_{\mathcal{U}} \geq 3/2$
 - Gauge invariant vector operators: $d_{\mathcal{U}} \geq 3$
4. Conformal invariance not only fixes the two-point function for the unparticle operator $\mathcal{O}_{\mathcal{U}}$, but also higher order point functions as the three-point function [50], responsible for Unparticle self-interactions.

4.2 Stephanov Deconstruction.

Shortly after the birth of the Unparticle idea, M. A. Stephanov developed an alternative view of Unparticles based on the fact that, since the definition of the spectral function for $\mathcal{O}_{\mathcal{U}}$ is:

$$\rho_{\mathcal{U}}(s) = 2\pi \sum_{\lambda} \delta(s - M_{\lambda}^2) \langle 0 | \mathcal{O}_{\mathcal{U}}(0) | \lambda \rangle \quad (4.5)$$

¹⁸These bounds can nevertheless be avoided if the Unparticle sector is scale invariant but not conformal.

The sum is performed over all relativistically normalized states $|\lambda\rangle$ at fixed spatial momentum. The definition (4.5) together with (4.4) implies that the Unparticle spectrum is continuous [51, 52]. Stephanov proposed to break the scale invariance in a controllable way, in a process he called “Deconstruction of Unparticles” [51]:

1. Instead of a continuous spectrum of states, an infinite tower of discrete states is taken, with the mass spacing controlled by a parameter Δ (in the limit $\Delta \rightarrow 0$ a continuous mass spectrum is recovered).
2. We take a certain mass spectrum for the tower of states, as $M_n^2 = \Delta^2 n$.
3. We define the deconstructed form of the Unparticle operator $\mathcal{O}_{\mathcal{U}}$ in terms of the discrete tower of fields:

$$\mathcal{O} \equiv \sum_n F_n \varphi_n \quad (4.6)$$

The constants F_n are fixed by the condition that the two-point function for \mathcal{O} matches that of $\mathcal{O}_{\mathcal{U}}$ in the continuum limit:

$$\begin{aligned} \lim_{\Delta \rightarrow 0} \sum_n \frac{i F_n^2}{p^2 - M_n^2 + i\epsilon} &= \frac{A_{d_{\mathcal{U}}}}{2 \sin(\pi d_{\mathcal{U}})} \frac{i}{(-p^2 - i\epsilon)^{2-d_{\mathcal{U}}}} \\ &\Downarrow \\ F_n^2 &= \frac{A_{d_{\mathcal{U}}}}{2\pi} \Delta^2 \left(M_n^2\right)^{d_{\mathcal{U}}-2} \end{aligned} \quad (4.7)$$

However, it is important to stress that although Stephanov Deconstruction provides a familiar way to deal with Unparticles, and makes it possible to study easily certain issues, conformal invariance fixes not only the two-point function for the Unparticles (which Stephanov Deconstruction reproduces in the continuum limit), but also the higher order point functions (which Stephanov Deconstruction would not reproduce). So, Stephanov Deconstruction can be viewed as an approximate description of Unparticles.

Chapter 5

Higgs-Unparticle Interplay.

5.1 Higgs Portal to Unparticles.

Let us begin by recalling the generic coupling between the Standard Model sector and the Unparticle sector, introduced in the previous chapter:

$$\mathcal{C}_{\mathcal{U}} \left(\frac{\Lambda_{\mathcal{U}}}{\mathcal{M}_{\mathcal{U}}} \right)^{d_{SM}+d_{UV}-4} \Lambda_{\mathcal{U}}^{4-d_{SM}-d_{\mathcal{U}}} \mathcal{O}_{SM} \mathcal{O}_{\mathcal{U}} \quad (5.1)$$

The value of $\mathcal{C}_{\mathcal{U}}$ can be absorbed in the definition of the scales $\Lambda_{\mathcal{U}}$ and $\mathcal{M}_{\mathcal{U}}$, so we will set $\mathcal{C}_{\mathcal{U}} = 1$. Depending on the particular SM operator the Unparticles couple to, the phenomenology of Unparticles can vary enormously. Since the birth of the Unparticle idea, a lot of effort has been devoted to the study of the phenomenological implications (see [10, 53] for a review, and references therein) of the different couplings that can be considered, such as [54]:

$$\left(\frac{\Lambda_{\mathcal{U}}}{\mathcal{M}_{\mathcal{U}}} \right)^{d_{UV}-2} \Lambda_{\mathcal{U}}^{2-d_{\mathcal{U}}} |H|^2 \mathcal{O}_{\mathcal{U}} \quad \left(\frac{\Lambda_{\mathcal{U}}}{\mathcal{M}_{\mathcal{U}}} \right)^{d_{UV}-1} \Lambda_{\mathcal{U}}^{1-d_{\mathcal{U}}} \bar{\Psi} \gamma_{\mu} \Psi \mathcal{O}_{\mathcal{U}}^{\mu} \quad (5.2)$$

$$\left(\frac{\Lambda_{\mathcal{U}}}{\mathcal{M}_{\mathcal{U}}} \right)^{d_{UV}} \Lambda_{\mathcal{U}}^{-d_{\mathcal{U}}} H \bar{\Psi} \Psi \mathcal{O}_{\mathcal{U}} \quad \left(\frac{\Lambda_{\mathcal{U}}}{\mathcal{M}_{\mathcal{U}}} \right)^{d_{UV}} \Lambda_{\mathcal{U}}^{-d_{\mathcal{U}}} F_{\mu\nu} F^{\mu\nu} \mathcal{O}_{\mathcal{U}} \quad \dots \quad (5.3)$$

In each case d_{UV} is such that $d_{UV} + d_{SM} - 4 > 0$. The first coupling is special for various reasons: $|H|^2$ is the only (scalar) gauge invariant operator in the Standard Model with $d_{SM} < 3$; so, whereas all the other possible Unparticle couplings are irrelevant (notice that $d_{\mathcal{U}} > 1$), $|H|^2 \mathcal{O}_{\mathcal{U}}$ is a relevant coupling for $1 < d_{\mathcal{U}} < 2$, which makes it the potentially most important coupling for the low energy physics of the Unparticle sector¹⁹; notice that an Unparticle scenario where this coupling is present is just a particular example of the “Higgs Portal” or “Hidden Valley” scenario [5, 6, 55], with the Unparticles being just a special type of hidden sector (a conformally invariant one). Also, when the Electroweak Symmetry is broken and the Higgs field acquires a vacuum expectation value (VEV), the coupling $|H|^2 \mathcal{O}_{\mathcal{U}}$ will introduce a scale into the Conformal Sector, and hence the conformal invariance of the Unparticles will be broken [11, 12], in a way that will be described shortly.

¹⁹Specially when either $\mathcal{M}_{\mathcal{U}} \gg \Lambda_{\mathcal{U}}$ or $\Lambda_{\mathcal{U}} \gg v$, since then all the other couplings decouple at low energy.

Moreover, the phenomenological importance of this coupling goes both ways: not only electroweak Symmetry breaking affects the low energy phenomenology of Unparticles in a crucial way, but also the coupling between the Higgs and the unparticles may affect the breaking of the electroweak symmetry and the nature of the Higgs sector [12, 56, 57]; we will study both sides of the same coupling in the next sections.

We will then consider the ultraviolet (UV) coupling of a scalar operator of dimension $d_{UV} \geq 3$ in the hidden sector to the SM dimension-two operator $|H|^2$ as:

$$V = \frac{1}{\mathcal{M}_{\mathcal{U}}^{d_{UV}-2}} |H|^2 \mathcal{O}_{UV} \quad (5.4)$$

which flows in the infrared (IR) to the Unparticle coupling

$$V = \left(\frac{\Lambda_{\mathcal{U}}}{\mathcal{M}_{\mathcal{U}}} \right)^{d_{UV}-2} \Lambda_{\mathcal{U}}^{2-d_{\mathcal{U}}} |H|^2 \mathcal{O}_{\mathcal{U}} \equiv \kappa_{\mathcal{U}} |H|^2 \mathcal{O}_{\mathcal{U}} \quad (5.5)$$

where $\kappa_{\mathcal{U}}$ has mass dimension $2 - d_{\mathcal{U}}$. The scalar Unparticle operator $\mathcal{O}_{\mathcal{U}}$ has scaling dimension in the range $1 \leq d_{\mathcal{U}} < 2$ and its two-point function is given by (4.3). We take then the tree-level scalar potential as:

$$V_0 = m^2 |H|^2 + \lambda |H|^4 + \kappa_{\mathcal{U}} |H|^2 \mathcal{O}_{\mathcal{U}} \quad (5.6)$$

The first two terms are the usual SM Higgs potential; as usual, the quartic coupling λ would be related in the SM to the Higgs mass at tree level by $m_{h^0}^2 = 2\lambda v^2$. We write the Higgs real direction as $Re(H^0) = (h^0 + v)/\sqrt{2}$, with $v = 246$ GeV.

5.1.1 Electroweak Symmetry Breaking and the IR Problem.

Let us begin by analyzing the consequences of Electroweak Symmetry breaking in the Unparticle sector. In the presence of a non-zero Higgs background the physical Higgs field mixes with the unparticle operator $\mathcal{O}_{\mathcal{U}}$ and also a tadpole appears for $\mathcal{O}_{\mathcal{U}}$ itself which will therefore develop a non-zero VEV.

As done in [12], it is very convenient to use the deconstructed version of the Unparticle sector proposed by Stephanov and introduced in section 4.2: One considers an infinite tower of scalars φ_n ($n = 1, \dots, \infty$) with masses squared $M_n^2 = \Delta^2 n$; the mass parameter Δ is small and eventually taken to zero, limit in which one recovers a (scale-invariant) continuous mass spectrum. The deconstructed form of the scalar operator $\mathcal{O}_{\mathcal{U}}$ is given by (4.6). In the deconstructed theory the scalar potential (5.6) transforms into:

$$V_0 = m^2 |H|^2 + \lambda |H|^4 + \frac{1}{2} \sum_n M_n^2 \varphi_n^2 + \kappa_{\mathcal{U}} |H|^2 \sum_n F_n \varphi_n \quad (5.7)$$

Here F_n is chosen as in (4.7), so that the two-point correlator of \mathcal{O} matches that of \mathcal{O}_U in the $\Delta \rightarrow 0$ limit. A non-zero VEV, $\langle |H|^2 \rangle = v^2/2$, triggers a VEV for the fields φ_n , which results in a tadpole for \mathcal{O} :

$$v_n \equiv \langle \varphi_n \rangle = -\frac{\kappa_U v^2}{2M_n^2} F_n \quad \langle \mathcal{O} \rangle = -\frac{\kappa_U v^2}{2} \sum_{n=0}^{\infty} \frac{F_n^2}{M_n^2} \quad (5.8)$$

In the continuum limit it reads:

$$\langle \mathcal{O}_U \rangle = -\frac{\kappa_U v^2}{2} \int_0^\infty \frac{F^2(M^2)}{M^2} dM^2 \quad F^2(M^2) = \frac{A_{d_U}}{2\pi} (M^2)^{d_U-2} \quad (5.9)$$

The quantity $F^2(M^2)$ is the continuum version of (4.7). We see that $\langle \mathcal{O}_U \rangle$ has an IR divergence for $d_U < 2$, due to the fact that for $M \rightarrow 0$ the tadpole diverges while the mass itself, that should stabilize the unparticle VEV, goes to zero. This IR divergence, that should be cured before trying to continue any analysis, is referred to as the IR problem in [12], and it should be noted that it is not an artifact of the Deconstruction.

5.1.2 Solving the IR Problem.

In order to cure the IR problem within the Stephanov Deconstruction formalism [12, 56], we need to add new terms to the deconstructed scalar potential in order to achieve a finite $\langle \mathcal{O}_U \rangle$; these terms have to be also scale invariant in the continuum limit (since otherwise they would break the scale invariance explicitly). Two possible terms involving H and φ_n that fulfill both conditions are:

$$\delta V = \frac{1}{4} \xi \left(\sum_{n=1}^{\infty} \varphi_n^2 \right)^2 \quad \delta V = \zeta |H|^2 \sum_{n=1}^{\infty} \varphi_n^2 \quad (5.10)$$

Other possible choices, like $\delta V = \lambda_U \sum_{n=1}^{\infty} \varphi_n^4$ fail in this respect. It can be easily shown that both couplings from (5.10) have a finite and scale-invariant continuum limit; we take the following scale transformations for the deconstructed fields φ_n and the Higgs field H :

$$\varphi_n(x) \rightarrow a \varphi_n(xa) \quad H(x) \rightarrow a H(xa) \quad (5.11)$$

At the same time we leave the space-time coordinates unscaled ($x \rightarrow xa$). Under such scale transformation the kinetic part of the (deconstructed) action is invariant while the mass terms are not, as usual. However, taking $\Delta \cdot u(M^2, x)$ as the continuum limit of $\varphi_n(x)$, and using the scale transformation in the continuum limit

$$u(M^2, x) \rightarrow u(M^2/a^2, xa) \quad (5.12)$$

The continuum action (including the kinetic and mass terms for the continuum field $u(M^2, x)$, as well as the continuum limit of the couplings from (5.10)) is well defined and scale invariant, being explicitly given by:

$$S = \int d^4x \left\{ \int_0^\infty dM^2 \left[\frac{1}{2} \partial_\mu u(M^2, x) \partial^\mu u(M^2, x) - \left(M^2 + \zeta |H|^2 \right) u^2(M^2, x) \right] \right. \\ \left. - \int_0^\infty dM_1^2 \int_0^\infty dM_2^2 \frac{1}{4} \xi u^2(M_1^2, x) u^2(M_2^2, x) \right\} \quad (5.13)$$

As we shall see later, the inclusion of any of the couplings from (5.10) in the scalar potential (5.7) solves the IR problem through the generation of a mass gap m_g .

There is also a simple way of obtaining an estimate for the conformal breaking scale [11] without using the Stephanov Deconstruction formalism. Electroweak symmetry breaking introduces a scale in the Unparticle sector, effectively breaking the conformal invariance at that scale, which is approximately given by $\Lambda_{\mathcal{U}}$:

$$\kappa_{\mathcal{U}} |H|^2 \mathcal{O}_{\mathcal{U}} \rightarrow \kappa_{\mathcal{U}} v^2 \mathcal{O}_{\mathcal{U}} = \Lambda_{\mathcal{U}}^{4-d_{\mathcal{U}}} \mathcal{O}_{\mathcal{U}} \quad \Lambda_{\mathcal{U}}^{4-d_{\mathcal{U}}} \equiv \left(\frac{\Lambda_{\mathcal{U}}}{\mathcal{M}_{\mathcal{U}}} \right)^{d_{UV}-2} \Lambda_{\mathcal{U}}^{2-d_{\mathcal{U}}} v^2 \quad (5.14)$$

In either case, we see that in the presence of a coupling $|H|^2 \mathcal{O}_{\mathcal{U}}$, Electroweak Symmetry breaking implies the breaking of the scale invariance of the Unparticle sector through the appearance of a mass gap (which is called either m_g or $\Lambda_{\mathcal{U}}$).

5.1.3 Constrains on $\mathcal{M}_{\mathcal{U}}$ and $\Lambda_{\mathcal{U}}$.

Once the scale invariance of the Unparticle sector is broken at a certain energy scale²⁰, we are left with a range of energies (that we call the ‘‘Conformal window’’) in which the hidden sector is approximately scale invariant. For consistency, it is required that $\Lambda_{\mathcal{U}} > \Lambda_{\mathcal{U}}$; we can write $\Lambda_{\mathcal{U}}$ as:

$$\Lambda_{\mathcal{U}}^{4-d_{\mathcal{U}}} = \left(\frac{\Lambda_{\mathcal{U}}}{\mathcal{M}_{\mathcal{U}}} \right)^{d_{UV}-2} \left(\frac{v}{\Lambda_{\mathcal{U}}} \right)^2 \Lambda_{\mathcal{U}}^{4-d_{\mathcal{U}}} \quad (5.15)$$

Then this condition is automatically satisfied for $\mathcal{M}_{\mathcal{U}} > \Lambda_{\mathcal{U}}$ and $\Lambda_{\mathcal{U}} > v$. However it is not sufficient; if there is any sense in which the Unparticle sector is approximately scale invariant in the conformal window, this conformal window has to be large, implying:

$$\Lambda_{\mathcal{U}} \gg \Lambda_{\mathcal{U}} \quad (\Lambda_{\mathcal{U}} = R \Lambda_{\mathcal{U}} \quad R \gg 1) \quad (5.16)$$

Furthermore, since the coupling $\kappa_{\mathcal{U}} |H|^2 \mathcal{O}_{\mathcal{U}}$ connects the Unparticle sector with the Standard Model (which is non-conformal) and it is a relevant coupling (implying that it need not

²⁰In this section we will follow [11] and call this scale $\Lambda_{\mathcal{U}}$.

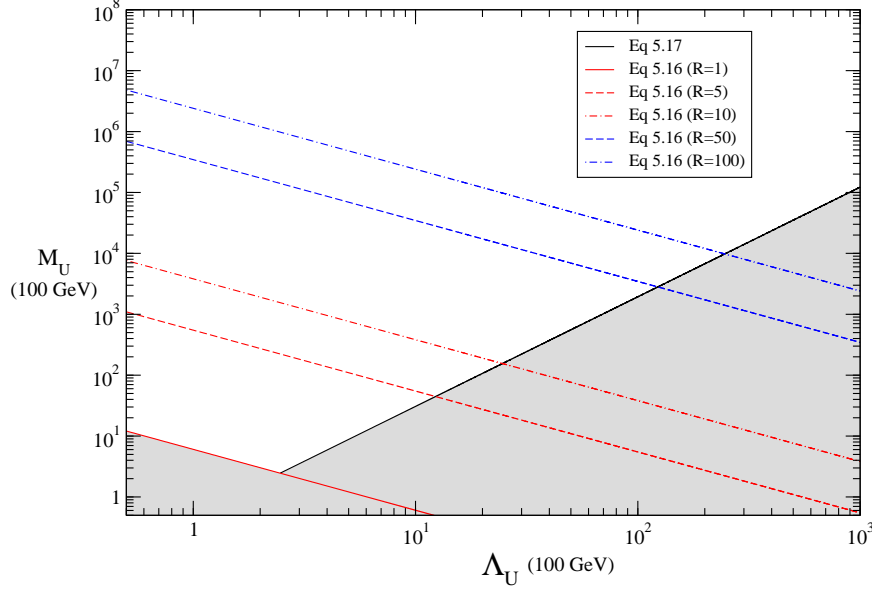


Figure 5.1: Allowed values of $\Lambda_{\mathcal{U}}$ and $\mathcal{M}_{\mathcal{U}}$ for $d_{UV} = 3$ and $d_{\mathcal{U}} = 1.2$. The shaded region is excluded by (5.16) and (5.17).

be suppressed at low energies, as opposed to the rest of the possible couplings between the Standard Model and the Unparticles) it breaks the scale invariance of the Unparticle sector even in the absence of a VEV for the Higgs. For self-consistency in our analysis this breaking scale μ has to be $\mu < \Lambda_{\mathcal{U}}$. A naive estimate of the breaking scale μ would be $\mu^{2-d_{\mathcal{U}}} \simeq \kappa_{\mathcal{U}}$. So in this case the bound is

$$\frac{1}{\kappa_{\mathcal{U}}^{2-d_{\mathcal{U}}}} < \Lambda_{\mathcal{U}} \quad (5.17)$$

Both conditions (5.16) and (5.17) constrain the possible values of $\Lambda_{\mathcal{U}}$ and $\mathcal{M}_{\mathcal{U}}$, depending also on the values of d_{UV} and $d_{\mathcal{U}}$, as shown in figs. (5.1) and (5.2). Notice that (5.17) is just a rough estimate, and the actual breaking scale μ in () could significantly differ from $\mu^{2-d_{\mathcal{U}}} \simeq \kappa_{\mathcal{U}}$, meaning that the bounds shown in figs. (5.1) and (5.2) are just qualitatively correct. However, in any case there will be a constrain analogous to (5.17).

5.2 Plasmon Scenario.

5.2.1 Curing the IR Problem (Deconstructed Unparticle Self-interactions).

It is natural to attempt to solve the IR problem by introducing a quartic coupling term for the deconstructed scalar fields φ_n so that the VEVs v_n are under control. We will now show explicitly that the first term from (5.10) is successful in providing a finite value for $\langle \mathcal{O}_{\mathcal{U}} \rangle$. We write for the deconstructed form of the scalar potential:

$$V = m^2 |H|^2 + \lambda |H|^4 + \frac{1}{2} \sum_n M_n^2 \varphi_n^2 + \kappa_{\mathcal{U}} |H|^2 \sum_n F_n \varphi_n + \frac{1}{4} \xi \left(\sum_{n=1}^{\infty} \varphi_n^2 \right)^2 \quad (5.18)$$

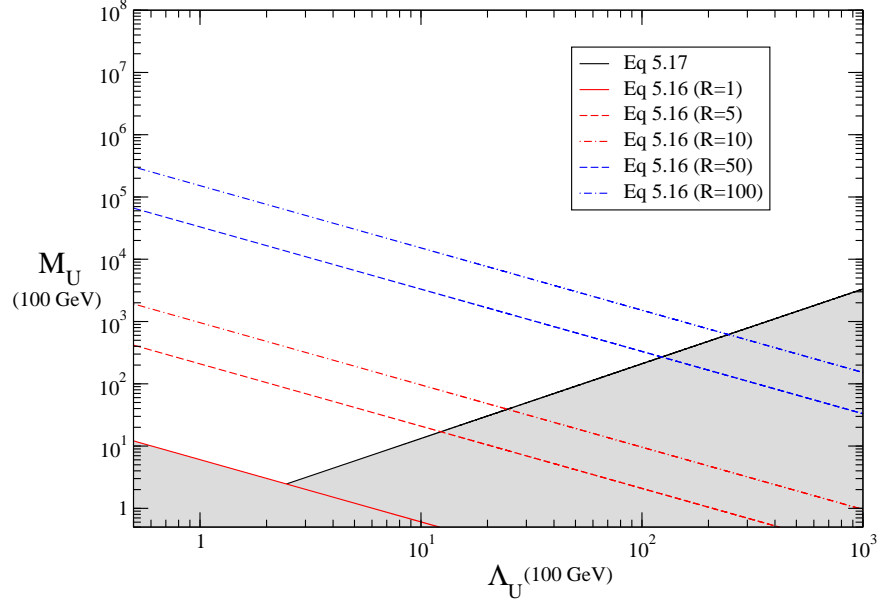


Figure 5.2: Same as in fig. 5.1, but for $d_{\mathcal{U}} = 1.8$.

The minimization equation for the Higgs field is not affected by the coupling ξ , while that for $v_n \equiv \langle \varphi_n \rangle$ can be put in the following form:

$$v_n = \frac{-\frac{1}{2}\kappa_{\mathcal{U}}v^2F_n}{M_n^2 + \xi \sum_{m=1}^{\infty} v_m^2} \quad \sum_{m=1}^{\infty} v_m^2 \equiv \sigma^2 \quad (5.19)$$

Then, the value of $\langle \mathcal{O} \rangle$ is:

$$\langle \mathcal{O} \rangle = \sum_{n=1}^{\infty} F_n v_n = -\frac{1}{2}\kappa_{\mathcal{U}}v^2 \sum_{n=1}^{\infty} \frac{F_n^2}{M_n^2 + \xi\sigma^2} \quad (5.20)$$

In the continuum limit we obtain:

$$\begin{aligned} \langle \mathcal{O}_{\mathcal{U}} \rangle &= -\frac{A_{d_{\mathcal{U}}}}{4\pi} \kappa_{\mathcal{U}} v^2 \int_0^{\infty} \frac{(M^2)^{d_{\mathcal{U}}-2}}{M^2 + \xi\sigma^2} dM^2 = \\ &= -\frac{A_{d_{\mathcal{U}}}}{4\pi} \kappa_{\mathcal{U}} v^2 \Gamma(2 - d_{\mathcal{U}}) \Gamma(d_{\mathcal{U}} - 1) (m_g^2)^{d_{\mathcal{U}}-2} \end{aligned} \quad (5.21)$$

Here we have defined $m_g^2 \equiv \xi\sigma^2$. We see that the generation of this mass gap m_g^2 cuts-off the IR divergence of $\langle \mathcal{O}_{\mathcal{U}} \rangle$, solving therefore the IR problem; and in the limit $m_g^2 \rightarrow 0$ the divergence in $\langle \mathcal{O}_{\mathcal{U}} \rangle$ is recovered.

In order to actually compute the value of m_g^2 we start from (5.19); squaring the equation and summing in n one gets an implicit equation for σ^2 , which in the continuum limit reads:

$$\begin{aligned}\sigma^2 &= \frac{1}{4}(\mu_{\mathcal{U}}^2)^{2-d_{\mathcal{U}}}v^4 \int_0^\infty dM^2 \frac{(M^2)^{d_{\mathcal{U}}-2}}{(M^2 + \xi\sigma^2)^2} = \\ &= \frac{1}{4}\Gamma(d_{\mathcal{U}} - 1)\Gamma(3 - d_{\mathcal{U}})(\mu_{\mathcal{U}}^2)^{2-d_{\mathcal{U}}}v^4(\xi\sigma^2)^{d_{\mathcal{U}}-3}\end{aligned}\quad (5.22)$$

where we have defined

$$(\mu_{\mathcal{U}}^2)^{2-d_{\mathcal{U}}} \equiv \kappa_{\mathcal{U}}^2 \frac{A_{d_{\mathcal{U}}}}{2\pi} \quad (5.23)$$

Then, (5.22) can be analytically solved for σ^2 . Note that $\sigma \neq 0$ only if $v \neq 0$ so that the appearance of a mass gap m_g^2 is in any case associated with EWSB.

5.2.2 Higgs-Unparticle Mixing and Plasmon Resonances from Unparticles.

Once Electroweak symmetry is broken, the (real) neutral component h^0 of the Higgs mixes with the Unparticle continuum [12, 56, 57] (see also [58] for the description of mixing of an isolated state with a continuum in the context of condensed matter physics). In order to study this issue using the deconstructed theory, we begin by writing down explicitly the infinite mass matrix that mixes h^0 with the deconstructed tower of Unparticle scalars φ_n ; the different matrix elements are:

$$M_{hh}^2 = 2\lambda v^2 \equiv m_{h^0}^2 \quad (5.24)$$

$$M_{hn}^2 = \kappa_{\mathcal{U}} v F_n \equiv A_n \quad (5.25)$$

$$\begin{aligned}M_{nm}^2 &= (M_n^2 + m_g^2)\delta_{nm} + \frac{1}{2}\kappa_{\mathcal{U}}^2 \xi v^4 \frac{F_n F_m}{(M_n^2 + m_g^2)(M_m^2 + m_g^2)} \\ &\equiv (M_n^2 + m_g^2)\delta_{nm} + a_n a_m\end{aligned}\quad (5.26)$$

The inverse matrix propagator for the system is simply given by:

$$i(P^{-1})_{ij}(p^2) = p^2 \delta_{ij} - M_{ij}^2 \quad (5.27)$$

Inverting (5.27) to obtain $-iP_{ij}(p^2)$ and taking its hh -entry we obtain (already in the continuum limit):

$$i(P_{hh}(p^2))^{-1} = p^2 - m_{h^0}^2 + J_2(p^2) - \frac{1}{2}\xi v^2 \frac{[J_1(p^2)]^2}{1 + \frac{1}{2}\xi v^2 J_0(p^2)} \quad (5.28)$$

Here we have used the integrals

$$\begin{aligned}
J_k(p^2) &\equiv \int_0^\infty G_{\mathcal{U}}(M^2, p^2) (M^2 + m_g^2)^{k-2} dM^2 \\
&= \frac{v^2}{p^4} \left(\frac{\mu_{\mathcal{U}}^2}{m_g^2} \right)^{2-d_{\mathcal{U}}} \Gamma(d_{\mathcal{U}} - 1) \Gamma(2 - d_{\mathcal{U}}) \left\{ \left(1 - \frac{p^2}{m_g^2} \right)^{d_{\mathcal{U}}-2} (p^2)^k \right. \\
&\quad \left. - \left[1 + (2 - d_{\mathcal{U}}) \frac{p^2}{m_g^2} \right] \delta_{k0} - p^2 \delta_{k1} \right\}
\end{aligned} \tag{5.29}$$

with integer k and where $G_{\mathcal{U}}(M^2, p^2)$ is:

$$G_{\mathcal{U}}(M^2, p^2) \equiv v^2 (\mu_{\mathcal{U}}^2)^{2-d_{\mathcal{U}}} \frac{(M^2)^{d_{\mathcal{U}}-2}}{(M^2 + m_g^2 - p^2)} \tag{5.30}$$

These integrals are real for $p^2 < m_g^2$ but they develop an imaginary part for $p^2 > m_g^2$, due to the term

$$\left(1 - \frac{p^2}{m_g^2} \right)^{d_{\mathcal{U}}-2} \tag{5.31}$$

We can see that this term generates an imaginary part for noninteger $d_{\mathcal{U}}$. Although the integrals in (5.28) diverge for $p^2 \rightarrow m_g^2$, the combination entering (5.28) is finite in this limit.

As stated in [12], the mass of the eigenstates after the mixing are given by the solutions to the pole equation

$$i \left(P_{hh}(\tilde{m}_h^2) \right)^{-1} = 0 \tag{5.32}$$

If $p^2 < m_g^2$ the pole equation is real, and happens to admit a real solution $m_h^2 < m_g^2$. However, for $p^2 > m_g^2$ the pole equation is complex, and the solution to the equation \tilde{m}_h^2 is also found to be complex, $\tilde{m}_h^2 \equiv m_h^2 - i\Gamma_h m_h$, with m_h being the corresponding mass (for consistency, $m_h^2 > m_g^2$) and Γ_h the tree-level width. For the moment we will suppose that the widths of the poles are small, so that the solution is approximately given by

$$\text{Re} \left[i \left(P_{hh}(m_{hR}^2) \right)^{-1} \right] = 0 \tag{5.33}$$

Here the subscript R indicates that m_{hR}^2 is the (real) pole of the real part of the propagator. The quantity m_{hR}^2 is of course the exact solution when $m_{hR}^2 < m_g^2$, and is a first order approximation to the real part of the solution, m_h^2 , when $m_{hR}^2 > m_g^2$ (the smaller Γ_h , the

better the approximation). Turning to the evaluation of (5.33), we find that in general $P_{hh}(p^2)$ has two poles and one zero; in a matrix propagator $P_{ij}(p^2)$, this is precisely the expected behaviour when two isolated states mix:

$$\begin{aligned}
i(P^{-1})_{ij}(p^2) &= \begin{pmatrix} p^2 - m_{11} & -m_{12} \\ -m_{12} & p^2 - m_{22} \end{pmatrix} \\
&\Downarrow \\
-iP_{ij}(p^2) &= \frac{1}{\text{Det}[i(P^{-1})_{ij}(p^2)]} \begin{pmatrix} p^2 - m_{22} & m_{12} \\ m_{12} & p^2 - m_{11} \end{pmatrix} \\
&\Downarrow \\
-iP_{11}(p^2) &= \frac{p^2 - m_{22}}{\text{Det}[i(P^{-1})_{ij}(p^2)]} \tag{5.34}
\end{aligned}$$

Here the two poles correspond to the eigenmasses after the mixing and the zero corresponds to the mass of the other state before the mixing. The fact that $P_{hh}(p^2)$ has precisely the same features as (5.34), with an additional pole (apart from the expected one associated with the Higgs eigenstate after the mixing) and a zero is a signal that the Higgs is effectively mixing with another state coming from the Unparticle continuum. In order to understand the origin of this additional pole we consider the unparticle submatrix (5.26); it has a simple form that allows us to find a particularly interesting eigenvalue $\omega_{p^0}^2$ (and eigenvector $\{r_n\}$) that satisfy

$$1 + \sum_n \frac{a_n^2}{M_n^2 + m_g^2 - \omega_{p^0}^2} = 0 \quad r_n = \frac{a_n}{N_p(\omega_{p^0}^2 - M_n^2 - m_g^2)} \tag{5.35}$$

The quantity N_p is a normalization constant that ensures $\sum_{n=1}^{\infty} r_n^2 = 1$. For sufficiently large values of the a_n 's (5.35) has a solution, with $\omega_{p^0}^2 > m_g^2$ necessarily²¹. In the continuum limit the eigenvalue condition (5.35) takes the form

$$1 + \frac{1}{2}\xi v^2 J_0(\tilde{\omega}_{p^0}^2) = 0 \quad \longrightarrow \quad 1 + \frac{1}{2}\xi v^2 \text{Re}[J_0(\omega_{p^0}^2)] = 0 \tag{5.36}$$

Taking a look at (5.28) we see that indeed $\omega_{p^0}^2$ is a zero of $P_{hh}(p^2)$ (notice that $\omega_{p^0}^2$ being above m_g^2 , the true zero $\tilde{\omega}_{p^0}^2$ of $P_{hh}(p^2)$ will be complex; however, we use again the approximation that Γ_ω is small and we can take $\omega_{p^0}^2$ as the solution to the righthand side of (5.36)).

The appearance of this collective state associated with the Unparticle continuum is reminiscent of the appearance of plasmon excitations in condensed matter physics. In fact, the

²¹Note that this pole can exist due to the presence of the new quartic coupling ξ and only after EWSB, which gives $a_n \neq 0$

structure of the unparticle submatrix is similar to the Hamiltonian that describes the residual long-range Coulomb interactions induced in a plasma by a probe electromagnetic wave; such structure lies at the root of different collective phenomena in different fields of physics [59]. Therefore, we will call this new state “the Plasmon”. Then, in general we expect two poles in (5.28), one Higgs-like at m_h^2 coming from the unmixed m_{h0}^2 , and one plasmon-like at ω_p^2 coming from the unmixed ω_{p0}^2 , both of them somewhat displaced by the mixing.

5.2.3 Spectral Function Analysis.

In order to study in more detail this interplay between the Higgs and the unparticle sector it is instructive to examine the spectral representation of the mixed propagator (5.28), which is given by

$$\rho_{hh}(s) = -\frac{1}{\pi} \text{Im}[P_{hh}(s + i\epsilon)] \quad (5.37)$$

Here the limit $\epsilon \rightarrow 0$ is understood. We can easily calculate this spectral function by using $1/(x + i\epsilon) \rightarrow \text{P.V.}[1/x] - i\pi\delta(x)$ directly in the integrals J_k of (5.29) to obtain for $s > m_g^2$

$$J_k(s + i\epsilon) = R_k(s) + iI_k(s) \quad (5.38)$$

with

$$\begin{aligned} R_k(s) &= \frac{v^2}{s^2} \left(\frac{\mu_{\mathcal{U}}^2}{m_g^2} \right)^{2-d_{\mathcal{U}}} \Gamma(d_{\mathcal{U}} - 1) \Gamma(2 - d_{\mathcal{U}}) \left\{ \left(\frac{s}{m_g^2} - 1 \right)^{d_{\mathcal{U}}-2} s^k \cos(d_{\mathcal{U}}\pi) \right. \\ &\quad \left. - \left[1 + (2 - d_{\mathcal{U}}) \frac{s}{m_g^2} \right] \delta_{k0} - s \delta_{k1} \right\} \\ I_k(s) &= \pi \frac{v^2}{s^{2-k}} \left(\frac{\mu_{\mathcal{U}}^2}{s - m_g^2} \right)^{2-d_{\mathcal{U}}} \end{aligned} \quad (5.39)$$

There are two qualitatively different cases, depending on whether the Higgs mass m_h is larger or smaller than m_g . For $m_h < m_g$, the spectral function is explicitly given by

$$\rho_{hh}(s) = \frac{1}{K^2(m_h^2)} \delta(s - m_h^2) + \theta(s - m_g^2) \frac{T_{\mathcal{U}}(s)}{\mathcal{D}^2(s) + \pi^2 T_{\mathcal{U}}^2(s)} \quad (5.40)$$

Here $\mathcal{D}(s)$ and $T_{\mathcal{U}}(s)$ are the real and imaginary parts of $iP_{hh}(s + i\epsilon)^{-1}$ when $s > m_g^2$:

$$iP_{hh}(s + i\epsilon)^{-1} = \mathcal{D}(s) + i \pi T_{\mathcal{U}}(s) \quad (5.41)$$

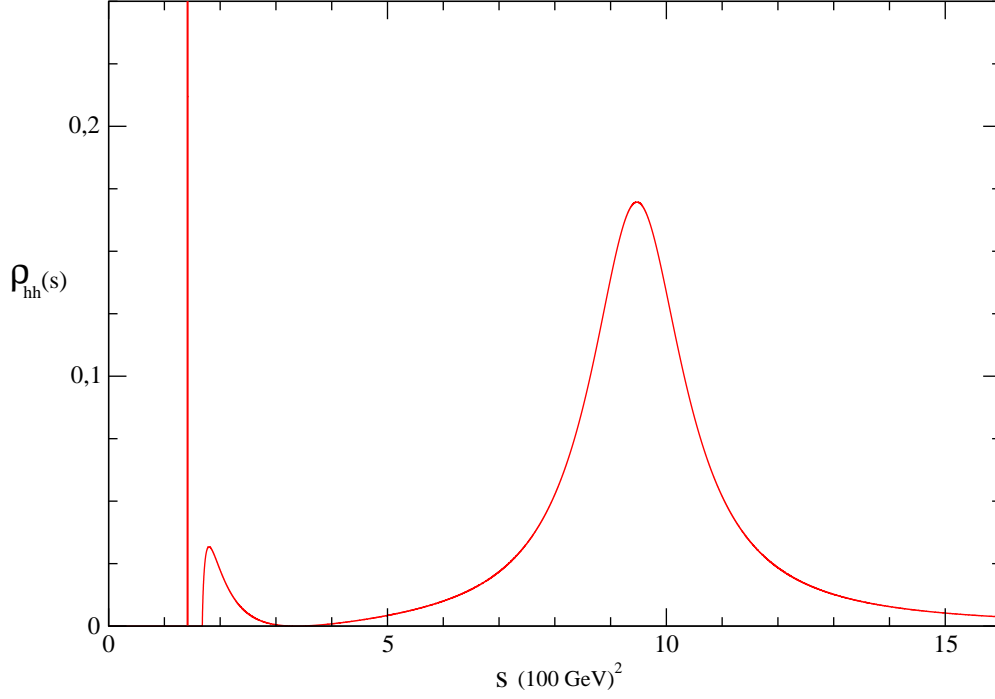


Figure 5.3: Spectral function with a Higgs below m_g , obtained for the case $\xi = 0.3$, $m^2 = 1$, $\kappa_{\mathcal{U}} = v^{2-d_{\mathcal{U}}}$ and $d_{\mathcal{U}} = 1.2$ (these give $m_g = 129$ GeV, $m_{h^0} = 240$ GeV, $\omega_{p^0} = 229$ GeV, $m_h = 119$ GeV and $\omega_p = 306$ GeV).

The quantity $K^2(m_h^2)$ is defined as:

$$K^2(s_0) \equiv \left. \frac{d}{ds} \mathcal{D}(s) \right|_{s=s_0} \quad (5.42)$$

More explicitly, one finds

$$\begin{aligned} \mathcal{D}(s) = & s - m_{h^0}^2 + R_2(s) - \frac{1}{2N(s)} \xi v^2 \left\{ \xi v^2 I_0(s) R_1(s) I_1(s) + \right. \\ & \left. + \left[1 + \frac{1}{2} \xi v^2 R_0(s) \right] \left[R_1(s)^2 - I_1(s)^2 \right] \right\} \end{aligned} \quad (5.43)$$

$$T_{\mathcal{U}}(s) = \frac{v^2}{s^2 N(s)} (s - 2m_g^2)^2 \left(\frac{\mu_{\mathcal{U}}^2}{s - m_g^2} \right)^{2-d_{\mathcal{U}}} \quad (5.44)$$

with

$$N(s) \equiv \left[1 + \frac{1}{2} \xi v^2 R_0(s) \right]^2 + \left[\frac{1}{2} \xi v^2 I_0(s) \right]^2 \quad (5.45)$$

An explicit expression for $K^2(s_0)$ can be obtained directly from (5.42) and (5.43) above, but we do not reproduce it here.

For $m_h > m_g$, there is no isolated pole (the Higgs mass eigenstate merges with the Unparticle continuum), and the spectral function is given by

$$\rho_{hh}(s) = \theta(s - m_g^2) \frac{T_{\mathcal{U}}(s)}{\mathcal{D}^2(s) + \pi^2 T_{\mathcal{U}}^2(s)} \quad (5.46)$$

The quantities $\mathcal{D}(s)$ and $T_{\mathcal{U}}(s)$ as defined above. One can check that the spectral functions (5.40) and (5.46) are properly normalized²²:

$$\int_0^\infty \rho_{hh}(s) ds = 1 \quad (5.47)$$

The physical interpretation of this spectral function is the following: let us call $|h\rangle$ the Higgs interaction eigenstate and $|u, M\rangle$ the Unparticle interaction eigenstates (a continuous function of M) and $|H\rangle, |U, M\rangle$ the respective mass eigenstates after EWSB. Then one has

$$|\langle H|h\rangle|^2 = \frac{1}{K^2(m_h^2)} \quad (5.48)$$

$$|\langle U, M|h\rangle|^2 = \frac{T_{\mathcal{U}}(M^2)}{\mathcal{D}^2(M^2) + \pi^2 T_{\mathcal{U}}^2(M^2)} \quad (5.49)$$

So, ρ_{hh} describes in fact the Higgs composition of the isolated pole and the Unparticle continuum²³:

$$\rho_{hh}(s) \equiv \langle h|s\rangle\langle s|h\rangle = |\langle H|h\rangle|^2 \delta(s - m_h^2) + \theta(s - m_g^2) |\langle U, M|h\rangle|^2 \quad (5.50)$$

The proper normalization (5.47) is simply a consequence of the proper normalization of $|h\rangle$, *i.e.* $|\langle h|h\rangle|^2 = 1$. From the simple form of $T_{\mathcal{U}}(s)$ in (5.44) we can see directly that for $M_0^2 = 2m_g^2$ the spectral function is zero, corresponding to an Unparticle state $|U, M_0\rangle$ which has $\langle h|U, M_0\rangle = 0$. The amount of $|h\rangle$ admixture in any state is very important because it will determine key properties of that state, like its coupling to gauge bosons and fermions, that are crucial for its production and decay.

Fig. (5.3) shows the spectral function for a case with $m_h < m_g$. The parameters have been chosen as follows: $d_U = 1.2$, $\kappa_U = v^{2-d_U}$, $m^2 = 1(100 \text{ GeV})^2$ and $\xi = 0.3$. We see a Dirac delta at $m_h^2 = (119 \text{ GeV})^2$, a mass gap for the Unparticle continuum at $m_g^2 = (129 \text{ GeV})^2$, and a zero at $M_0^2 = (183 \text{ GeV})^2$. There is also a plasmon-like resonance at $\omega_p^2 = (306 \text{ GeV})^2$; in this case the Higgs-plasmon mixing is rather strong (the values of m_{h^0} and ω_{p^0} before the mixing are close to each other), so both mass eigenstates share approximately the same amount of Higgs composition. In other cases one of the mass eigenstates carries most of the Higgs composition and is therefore identified with the higgs mass eigenstate, as in fig. (5.4),

²² Appendix C shows that $\rho_{hh}(s)$, as defined by (5.37), is normalized in this way.

²³ For $m_h > m_g$, the spectral function is given by (5.49) only, without a Dirac delta-function representing an isolated pole, and there is no separate $|H\rangle$ state (it is merged into the continuum of states $|U, M\rangle$).

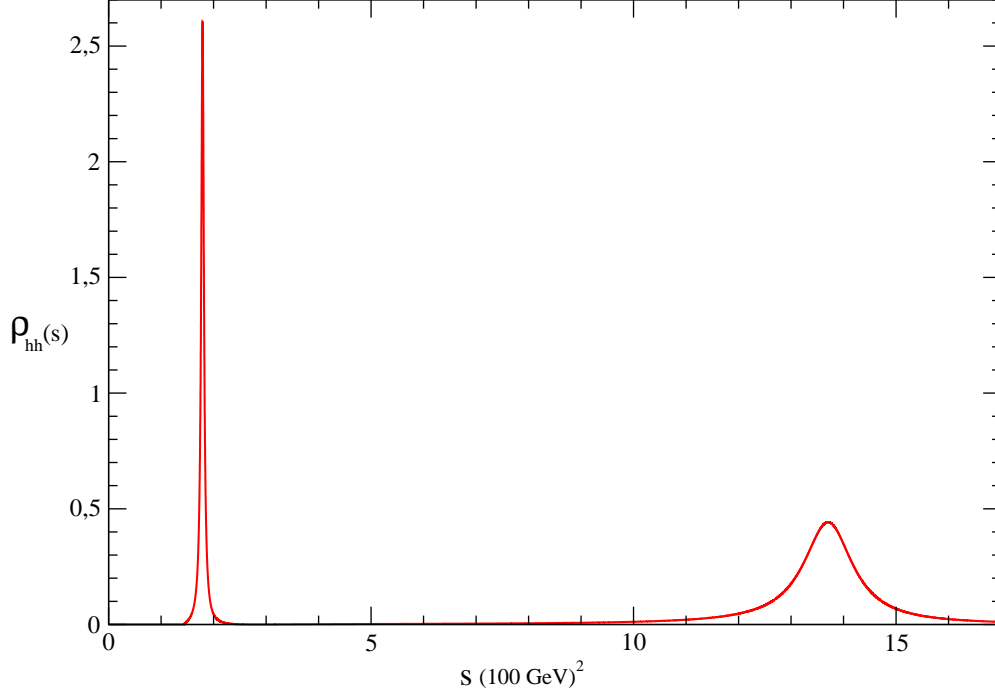


Figure 5.4: Spectral function with a Higgs below m_g , obtained for the case $\xi = 0.1$, $m^2 = 2$, $\kappa_U = v^{2-d_U}$ and $d_U = 1.1$ (these give $m_g = 119$ GeV, $m_{h^0} = 332$ GeV, $\omega_{p^0} = 209$ GeV, $m_h = 370$ GeV and $\omega_p = 133$ GeV).

with $m_h > m_g$. This case corresponds to $d_U = 1.1$, $\kappa_U = v^{2-d_U}$, $m^2 = 2(100 \text{ GeV})^2$, and $\xi = 0.1$ and has a mass gap at $m_g^2 = (119 \text{ GeV})^2$, a Higgs resonance at $m_h^2 = (370 \text{ GeV})^2$ and a plasmon-like spike at $\omega_p^2 = (133 \text{ GeV})^2$. There is also a zero at $M_0^2 = (169 \text{ GeV})^2$ right above the plasmon resonance.

The shape of the continuum around the resonances above m_g^2 at $s_r = \{m_h^2, \omega_p^2\}$ can be obtained directly from the spectral density (5.49) expanding $\mathcal{D}(s)$ to first order around s_r :

$$\mathcal{D}(s) \simeq (s - s_r)K^2(s_r) \quad (5.51)$$

where $K^2(s_r)$ is defined²⁴ in (5.42). Substituting (5.51) in the spectral function (5.49), we see that the resonances have an approximate Breit-Wigner shape:

$$\rho_{hh}(s) = \frac{1}{\pi K^2(s_r)} \frac{\frac{\pi T_U(s)}{K^2(s_r)}}{(s - s_r)^2 + \left(\frac{\pi T_U(s)}{K^2(s_r)}\right)^2} = C \frac{\Gamma_r s_r}{(s - s_r)^2 + (\Gamma_r s_r)^2}$$

where the width Γ_r is given by

$$\frac{\Gamma_r}{\sqrt{s_r}} = \frac{\pi T_U(s_r)}{s_r K^2(s_r)} \quad (5.52)$$

²⁴In the case with $s_r > m_g^2$ one should be careful about using the principal value definition of the integrals entering $\mathcal{D}(s)$ to properly calculate its derivative at s_r .

It turns out that Γ_r given by (5.52) is precisely the first order approximation to the decay width given by the complex pole $\tilde{s}_r = s_r - i \Gamma_r \sqrt{s_r}$.

5.3 Phantom Higgs Scenario.

5.3.1 Curing the IR Problem.

Another way (apart from the one resulting in the Plasmon scenario) to solve the IR problem consists in adding to the scalar potential the second term from (5.10) as an IR regulator:

$$\delta V = \zeta |H|^2 \sum_{n=1}^{\infty} \varphi_n^2 \quad (5.53)$$

The scalar potential is now:

$$V = m^2 |H|^2 + \lambda |H|^4 + \frac{1}{2} \sum_n M_n^2 \varphi_n^2 + \kappa_{\mathcal{U}} |H|^2 \sum_n F_n \varphi_n + \zeta |H|^2 \sum_{n=1}^{\infty} \varphi_n^2 \quad (5.54)$$

The effect that the inclusion of (5.53) has on Electroweak symmetry breaking will be analyzed in the next section. In its presence, the minimization condition that $v_n \equiv \langle \varphi_n \rangle$ reads:

$$v_n = \frac{-\frac{1}{2} \kappa_{\mathcal{U}} v^2 F_n}{M_n^2 + \zeta v^2} \quad \zeta v^2 = m_g^2 \quad (5.55)$$

We see again that the IR problem will be solved through the appearance of a mass gap $m_g^2 = \zeta v^2$. In the continuum limit we obtain for $\langle \mathcal{O}_{\mathcal{U}} \rangle$:

$$\begin{aligned} \langle \mathcal{O}_{\mathcal{U}} \rangle &= -\frac{A_{d_{\mathcal{U}}}}{4\pi} \kappa_{\mathcal{U}} v^2 \int_0^{\infty} \frac{(M^2)^{d_{\mathcal{U}}-2}}{M^2 + m_g^2} dM^2 = \\ &= -\frac{A_{d_{\mathcal{U}}}}{4\pi} \kappa_{\mathcal{U}} v^2 \Gamma(2 - d_{\mathcal{U}}) \Gamma(d_{\mathcal{U}} - 1) (m_g^2)^{d_{\mathcal{U}}-2} \end{aligned} \quad (5.56)$$

This is just the same result as (5.21). There is however an important difference between the expressions for the mass gap in the plasmon and the present case: whereas in the plasmon scenario the mass gap has a dependence on $\kappa_{\mathcal{U}}$, which in turn means a dependence on the various scales $\mathcal{M}_{\mathcal{U}}$, $\Lambda_{\mathcal{U}}$ (in analogy with the breaking scale $\Lambda_{\mathcal{U}}$ from [11]), in the present case the mass gap depends only on the phenomenological coupling ζ (notice however that depending on the origin of (5.53), the coupling ζ could indeed depend on $\kappa_{\mathcal{U}}$, but here we just treat it as a phenomenological parameter).

5.3.2 Effect of Unparticles on Electroweak Symmetry Breaking.

In the presence of (5.53) the minimization condition for the Higgs VEV v is:

$$m^2 + \lambda v^2 + \kappa_{\mathcal{U}} \sum_n F_n v_n + \zeta \sum_n v_n^2 = 0 \quad (5.57)$$

Using the VEV (5.55), taking the continuum limit and performing the integral in M^2 , this translates into:

$$m^2 + \lambda v^2 - \lambda_{\mathcal{U}} (\mu_{\mathcal{U}}^2)^{2-d_{\mathcal{U}}} v^{2(d_{\mathcal{U}}-1)} = 0 \quad (5.58)$$

Here we have defined $\lambda_{\mathcal{U}}$ as:

$$\lambda_{\mathcal{U}} \equiv \frac{d_{\mathcal{U}}}{4} \zeta^{d_{\mathcal{U}}-2} \Gamma(d_{\mathcal{U}} - 1) \Gamma(2 - d_{\mathcal{U}}) \quad (5.59)$$

We see that the effect of the unparticles in the minimization equation (5.58) is similar to having a Higgs term $h^{2d_{\mathcal{U}}}$ in the potential (so for $1 < d_{\mathcal{U}} < 2$, a term somewhere between h^2 and h^4). Also, since the term induced by the Unparticles is negative, the condition (5.58) can be easily satisfied. In particular, for $m^2 = 0$ the Higgs VEV is induced by its coupling to Unparticles as:

$$(v^2)^{2-d_{\mathcal{U}}} = (\lambda_{\mathcal{U}}/\lambda) (\mu_{\mathcal{U}}^2)^{2-d_{\mathcal{U}}} \quad (5.60)$$

It is therefore determined by the mass parameter $\mu_{\mathcal{U}}$. Electroweak symmetry breaking at tree level requires the condition

$$m^2 \leq \lambda_{\mathcal{U}} (\mu_{\mathcal{U}}^2)^{2-d_{\mathcal{U}}} v^{2(d_{\mathcal{U}}-1)} \quad (5.61)$$

In this case the Higgs potential has a Mexican-hat shape. In the particular case of $m^2 = 0$, condition (5.61) is automatically satisfied. Of course one has to adjust the parameters in (5.58) to have the minimum at the correct value. This requires the Higgs quartic coupling to be chosen as

$$\lambda = -\frac{m^2}{v^2} + \lambda_{\mathcal{U}} (\mu_{\mathcal{U}}^2)^{2-d_{\mathcal{U}}} v^{2(d_{\mathcal{U}}-2)} \quad (5.62)$$

This relation clearly shows how Unparticles modify the usual Standard Model relation in this case.

5.3.3 Phantom Higgs from Higgs-Unparticle Mixing.

Just as in the Plasmon scenario, the real neutral component of the Higgs field h^0 mixes with the Unparticle continuum after Electroweak symmetry breaking. The infinite squared mass matrix that mixes h^0 with the deconstructed tower of Unparticle scalars φ_n is given by:

$$M_{hh}^2 = 2\lambda v^2 \equiv m_{h^0}^2, \quad (5.63)$$

$$M_{hn}^2 = \kappa_{\mathcal{U}} v F_n \frac{M_n^2}{M_n^2 + m_g^2} \equiv A_n, \quad (5.64)$$

$$M_{nm}^2 = (M_n^2 + m_g^2) \delta_{nm}. \quad (5.65)$$

It is a simple matter to obtain the hh -entry of the propagator $-iP_{ij}(p^2)$ associated with this infinite mass matrix. In the continuum limit we obtain:

$$i \left(P_{hh}(p^2) \right)^{-1} = p^2 - m_{h^0}^2 + \tilde{J}(p^2), \quad (5.66)$$

Here

$$\begin{aligned} \tilde{J}(p^2) &\equiv \int_0^\infty G_{\mathcal{U}}(M^2, p^2) \frac{M^4}{(M^2 + m_g^2)^2} dM^2 = v^2 \left(\frac{m_g^2}{p^2} \right)^2 \left(\frac{\mu_{\mathcal{U}}^2}{m_g^2} \right)^{2-d_{\mathcal{U}}} \\ &\quad \Gamma(d_{\mathcal{U}} - 1) \Gamma(2 - d_{\mathcal{U}}) \left[\left(1 - \frac{p^2}{m_g^2} \right)^{d_{\mathcal{U}}} + d_{\mathcal{U}} \frac{p^2}{m_g^2} - 1 \right] \end{aligned} \quad (5.67)$$

The quantity $G_{\mathcal{U}}(M^2, p^2)$ is defined as in (5.30). Just like in the previous case, due to the extra Unparticle term $\tilde{J}(p^2)$ the Higgs pole will no longer be at its SM value $m_{h^0}^2$ but displaced from it. Whether this displacement is positive (towards higher masses) or negative will depend on the balance between two competing eigenvalue repulsion effects: the unparticle continuum above $m_{h^0}^2$ will tend to lower the Higgs mass while the continuum below will tend to increase it. Of course, when $m_{h^0}^2$ is below m_g^2 the shift is necessarily negative [12].

As in the Plasmon scenario, when the imaginary part of the pole (complex in general²⁵) is small, the final outcome for the Higgs mass m_h^2 is well approximated by the solution m_{hR}^2 to the real pole equation (5.33). However, in order to explore the possible qualitative behaviours of the solutions in the present case, we will solve (5.32) to find the complex poles of the propagator $\tilde{m}_h^2 \equiv m_h^2 - im_h \Gamma_h$.

It is convenient to rewrite (5.66) in terms of the following dimensionless quantities:

$$R_{\mathcal{U}} \equiv \frac{v^2}{m_g^2} \left(\frac{\mu_{\mathcal{U}}^2}{m_g^2} \right)^{2-d_{\mathcal{U}}} \quad \tilde{x} \equiv \frac{\tilde{m}_h^2}{m_g^2} \quad x_0 \equiv \frac{m_{h^0}^2}{m_g^2}, \quad (5.68)$$

²⁵Except when it lies below the mass gap m_g^2 , case in which it is a real pole.

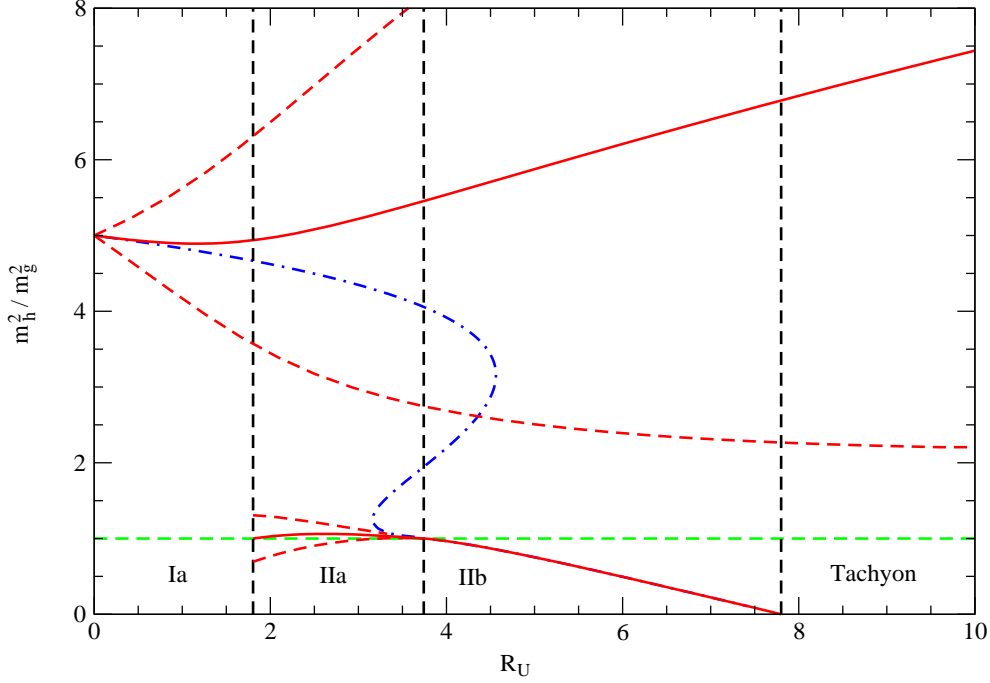


Figure 5.5: The solid red curves give the Higgs pole masses m_h^2 as a function of R_U for $m_{h0}^2 = 5m_g^2$ and $d_U = 1.2$ while the red-dashed curves give $m_h^2 \pm m_h \Gamma_h$. The dot-dashed blue line gives m_{hR} , the pole of the real part of the propagator. The horizontal dashed line gives m_g and the vertical dashed lines delimit the different zones as indicated by the labels.

The quantity R_U measures the strength of the Higgs-unparticle interaction. The pole equation takes then the simple form

$$\tilde{x} = x_0 - \frac{R_U}{\tilde{x}^2} f_U(\tilde{x}) , \quad (5.69)$$

with

$$f_U(\tilde{x}) \equiv \Gamma(d_U - 1)\Gamma(2 - d_U) \left[(1 - \tilde{x})^{d_U} + d_U \tilde{x} - 1 \right] . \quad (5.70)$$

In order to solve the pole equation (5.69) one should specify in what Riemann sheet z^{d_U} is taken in (5.70). If one sticks to the principal sheet, with angles defined from $-\pi$ to π , the only possible poles appear in the real axis and below the mass gap. If one goes to the second Riemann sheet (with angles between -3π and $-\pi$) one finds also complex poles²⁶; we refer to these poles in what follows. For small values of the unparticle effect, as measured by the parameter R_U (*i.e.* for $R_U \ll 1$), a perturbative solution gives

$$m_h^2 \simeq m_{h0}^2 - m_g^6 \frac{R_U}{m_{h0}^4} \mathcal{R}e[f_U(x_0)] \quad (5.71)$$

²⁶The absence of complex poles in the principal sheet will be used in appendix C to obtain the normalization of the spectral function $\rho_{hh}(s)$, given by (5.47).

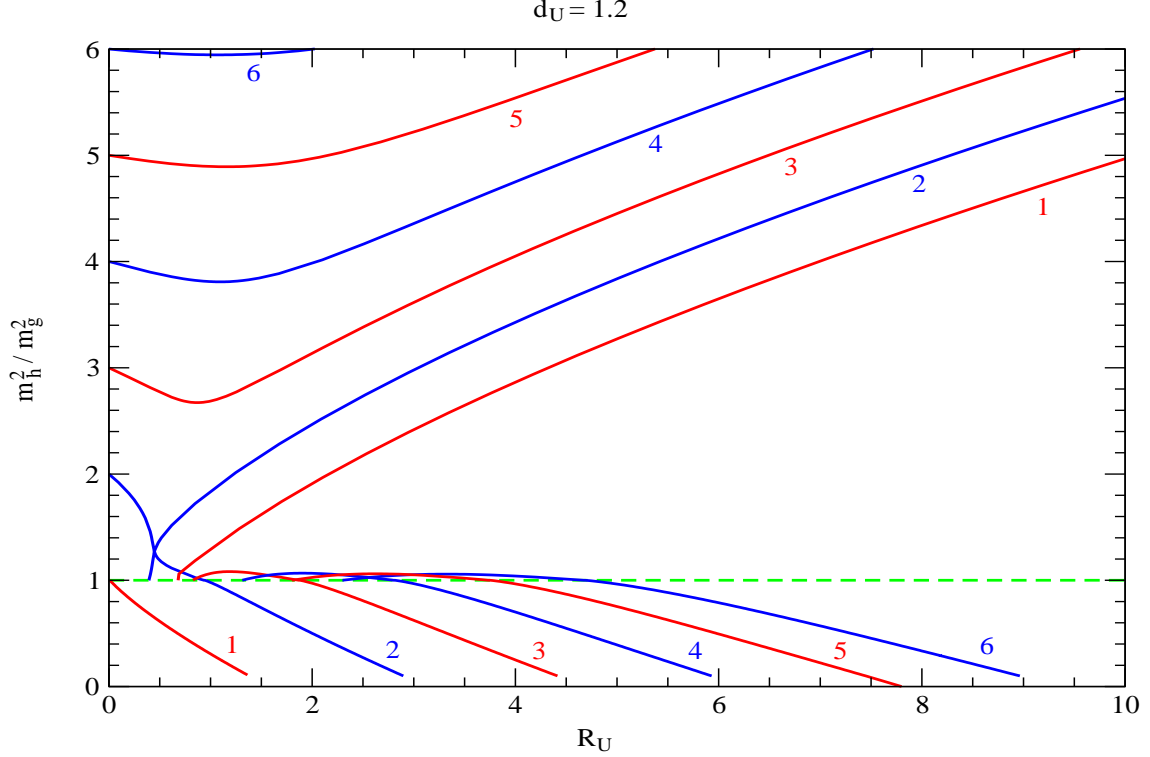


Figure 5.6: Same as fig. 5.5 for different values of $x_0 = m_{h^0}^2/m_g^2$ as indicated by the labels.

Here the sign of the shift determined by the sign of the function $f_{\mathcal{U}}$ and

$$\Gamma_h \simeq m_g^6 \frac{R_{\mathcal{U}}}{m_{h^0}^5} \mathcal{I}m[f_{\mathcal{U}}(x_0)] \theta(x_0 - 1) \quad (5.72)$$

New interesting effects occur for larger values of $R_{\mathcal{U}}$. Fig. 5.5 illustrates this for the particular case $d_{\mathcal{U}} = 1.2$ and $m_{h^0}^2/m_g^2 = 5$ by showing m_h^2 (solid lines) as a function of $R_{\mathcal{U}}$. For small $R_{\mathcal{U}}$ one simply gets a negative shift for m_h (zone labelled as Ia). However, for larger values of $R_{\mathcal{U}}$ (in this case $R_{\mathcal{U}} \geq 1.8$) the spectrum turns out to be much richer. In zone IIa one finds two Higgs poles above m_g , one of them very close to the mass gap and the other closer to the initial value m_{h^0} . In zone IIb the lighter of these poles goes below the mass gap while the other gets heavier. Eventually, for sufficiently large $R_{\mathcal{U}}$, the squared mass of the lighter pole gets negative and the state becomes tachyonic. We also show the width of these poles by giving (dashed lines) the curves for $m_h^2 \pm m_h \Gamma_h$. We see that the heavy pole gets wider and wider with increasing $R_{\mathcal{U}}$ while the lighter has always a small width (when the light Higgs pole gets below the mass gap its width (at tree-level) is zero). For comparison, we also show in the figure the value of m_{hR} (dot-dashed line), that approximates m_h when the Higgs width is small but can be very different from it when the width gets larger.

Zone II is particularly interesting: from the initial SM Higgs pole m_{h^0} , which was well above the mass gap, and through the mixing with the unparticle continuum, we get a very wide pole quite close to m_{h^0} and a much lighter pole below the mass gap (IIb) or just above it (IIa). We call this new state the “Phantom higgs” [57], because it is generated

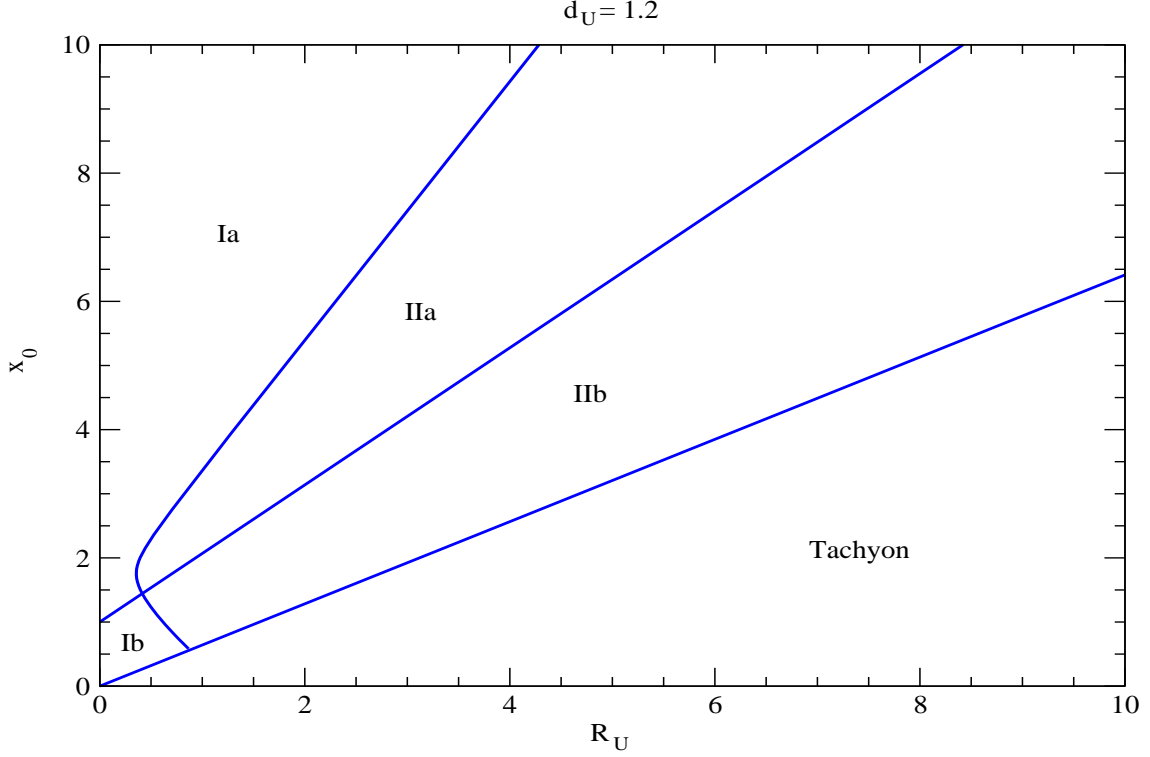


Figure 5.7: Different zones in the plane $(R_U, x_0 = m_{h_0}^2/m_g^2)$ with different number of Higgs poles: one in zone I (above m_g in zone Ia, below in zone Ib) and two in zone II (both above m_g in IIa, one above and one below in IIb). In the zone labeled “Tachyon” the lightest pole becomes tachyonic.

entirely through the Higgs-unparticle mixing and is much lighter than naively expected. This behaviour is generic and persists for other values of $x_0 = m_{h_0}^2/m_g^2$ and/or d_U ; fig. 5.6 shows m_h^2 vs. R_U for different values of the initial x_0 (notice that once the lighter phantom Higgs becomes tachyonic the parameter choice is not acceptable). Finally, fig. 5.7 shows the different zones, with the coding explained above, in the plane (x_0, R_U) for $d_U = 1.2$. In addition to the zones discussed above, there is also the possibility of having a single pole below the mass gap, corresponding to zone Ib in this plot. Between the lines delimiting zone Ib+IIb the mass of the pole below m_g tends to zero at the lower boundary (the border with the tachyonic zone) and to m_g in the upper boundary. In the boundary between zones Ia and IIa the mass of the light Higgs is also m_g .

It should be stressed that even though in the Phantom Higgs scenario there can be two poles (just as in the Plasmon scenario), none of them is associated with a collective state coming from the Unparticle continuum (as opposed to the Plasmon scenario); this can be easily inferred from the fact that $P_{hh}(p^2)$ does not have a zero. Therefore the emergence of the additional Phantom Higgs state is purely associated with a strong mixing between the original Higgs state and the Unparticle continuum.

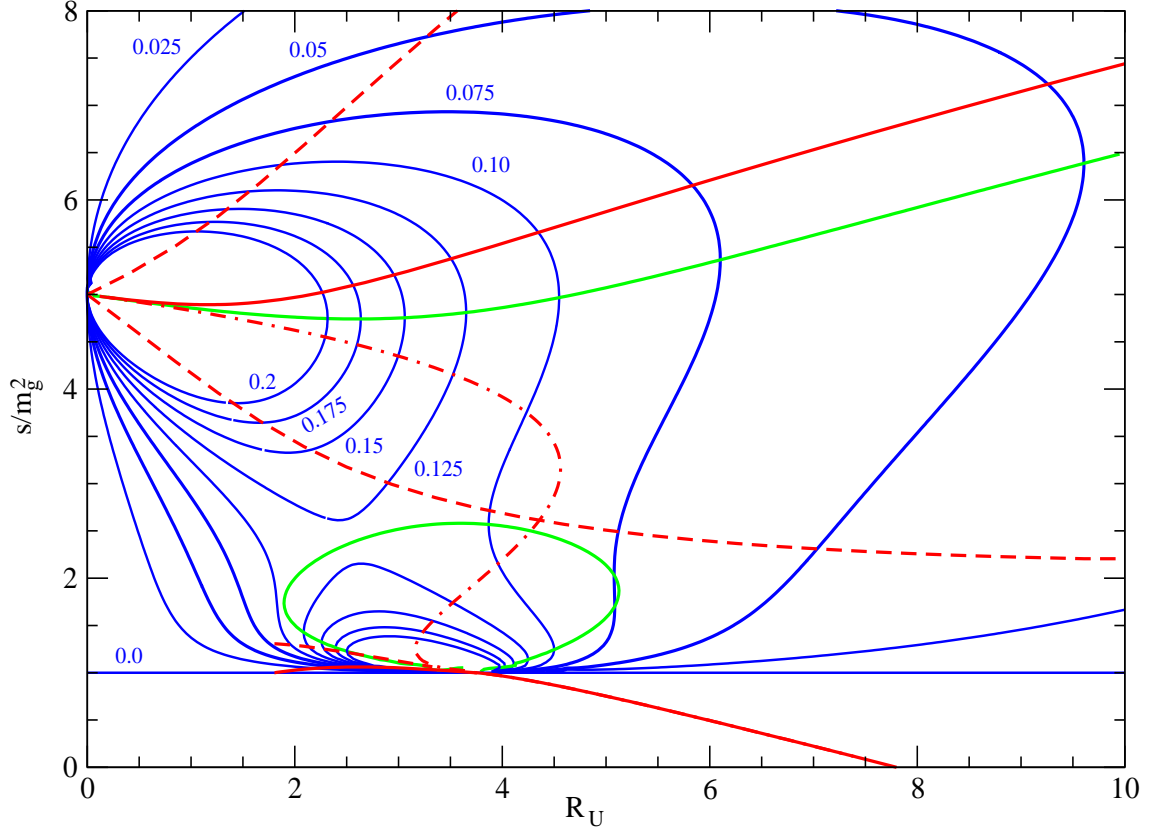


Figure 5.8: Contour lines of $\rho_{hh}(s)$ (we stop at 0.2) in the plane $(R_U, s/m_g^2)$ for $d_U = 1.2$, $x_0 = 5$ (blue lines). Information on the Higgs poles (both m_{hR} and m_h) is given by the same curves as in fig. 5.5. The green lines give the extrema of the spectral function at fixed R_U .

5.3.4 Spectral Function Analysis.

To clarify further the pole structure of the mixed Higgs-unparticle propagator we now turn to the study of its spectral function, given by (5.37). We have, for $s > m_g^2$,

$$\tilde{J}(s) = \tilde{J}_R(s) + i\tilde{J}_I(s) = \text{P.V.}[\tilde{J}(s)] + i\tilde{J}_I(s) , \quad (5.73)$$

with

$$\begin{aligned} \tilde{J}_R(s) &= \left(\frac{m_g^2}{s}\right)^2 \left(\frac{\mu_U^2}{m_g^2}\right)^{2-d_U} \frac{\pi v^2}{\text{Sen}(d_U \pi)} \left[1 - \left(\frac{s}{m_g^2} - 1\right)^{d_U} \text{Cos}(d_U \pi) - d_U \frac{s}{m_g^2} \right] \\ \tilde{J}_I(s) &= \pi v^2 \left(\frac{m_g^2}{s}\right)^2 \left(\frac{\mu_U^2}{m_g^2}\right)^{2-d_U} \left(\frac{s}{m_g^2} - 1\right)^{d_U} . \end{aligned} \quad (5.74)$$

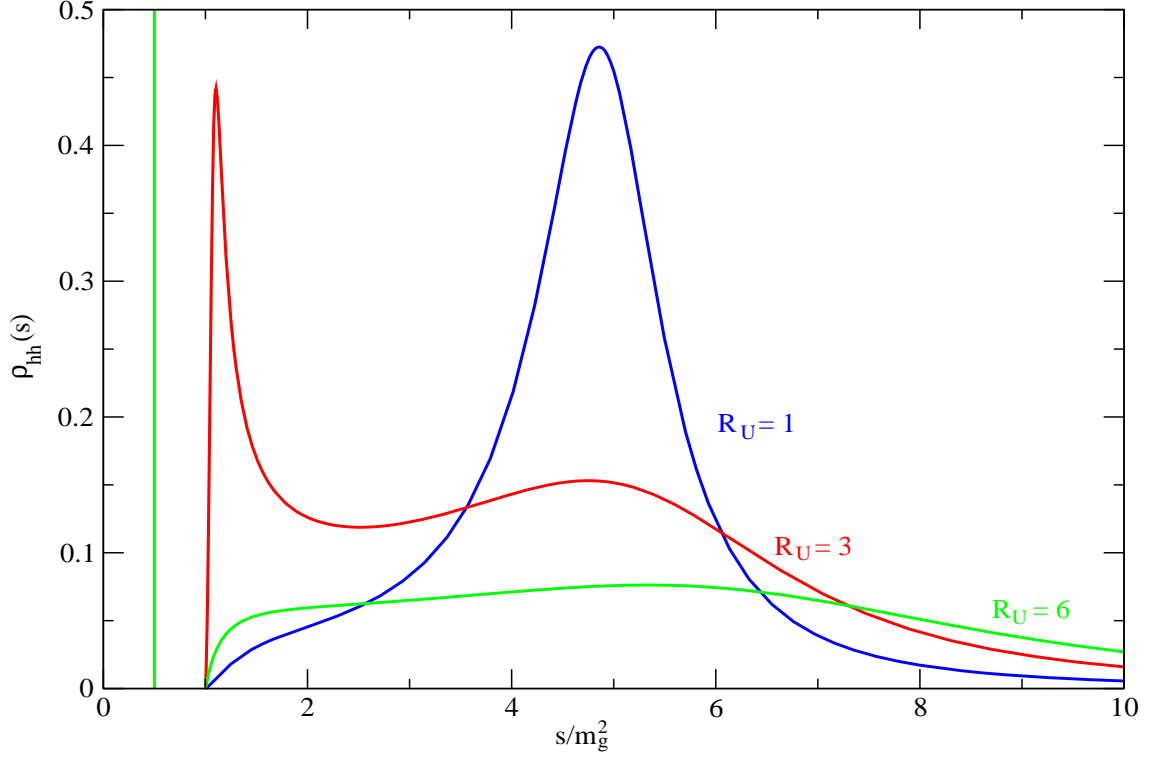


Figure 5.9: Spectral functions for $d_{\mathcal{U}} = 1.2$, $x_0 = 5$ and $R_{\mathcal{U}} = 1$, $R_{\mathcal{U}} = 3$ and $R_{\mathcal{U}} = 6$. One can see the different pole structure in each case: just one pole m_g^2 (Blue); two poles above m_g^2 , being the lightest the “Phantom Higgs” (Red); one pole (Phantom Higgs) below m_g^2 and the other (very wide) above m_g^2 (Green).

Just as in the Plasmon scenario, when there is one pole below the mass gap, and irrespective of whether there is another pole above it or not, the spectral function takes the form²⁷

$$\rho_{hh}(s) = \frac{1}{K^2(m_h^2)} \delta(s - m_h^2) + \theta(s - m_g^2) \frac{T_{\mathcal{U}}(s)}{\mathcal{D}^2(s) + \pi^2 T_{\mathcal{U}}^2(s)} \quad (5.75)$$

where $K^2(s_0)$ is given by (5.42) and $\mathcal{D}(s)$ and $\pi T_{\mathcal{U}}(s)$ are the real and imaginary parts of $iP_{hh}(s + i\epsilon)^{-1}$ when $s > m_g^2$:

$$iP_{hh}(s + i\epsilon)^{-1} = \mathcal{D}(s) + i\pi T_{\mathcal{U}}(s) = \left[s - m_{h^0}^2 + \tilde{J}_R(s) \right] + i\tilde{J}_I(s) \quad (5.76)$$

In fig. 5.8 we give contour lines of $\rho_{hh}(s)$ for the case $d_{\mathcal{U}} = 1.2$, $x_0 = 5$ (we stop the contours at 0.2) in the plane $(R_{\mathcal{U}}, s/m_g^2)$. For $R_{\mathcal{U}} \geq 3.5$ we see how the Phantom Higgs drops below the mass gap giving rise to a delta pole in the spectral function. We show by the solid red lines the Higgs poles in this particular case. The green solid lines give the extrema of the spectral function for fixed $R_{\mathcal{U}}$. We see that the pole lines offer reliable information

²⁷ Again, when all the poles are above m_g the Dirac-delta term is absent.

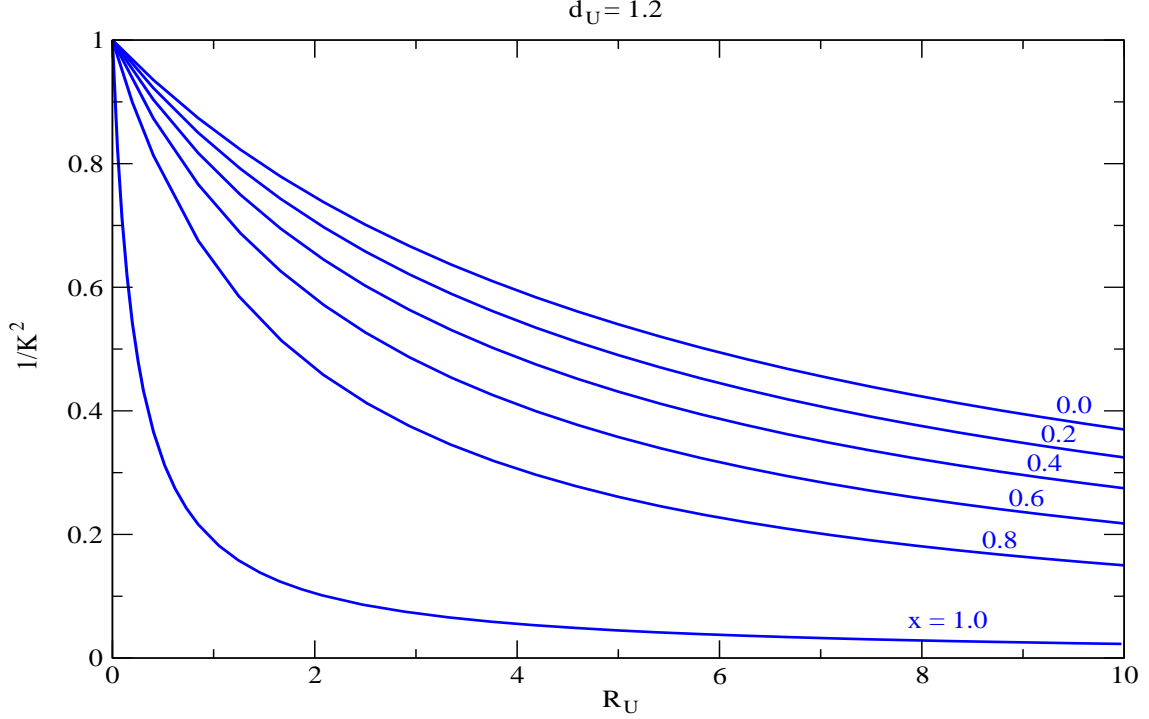


Figure 5.10: Pure Higgs composition of the isolated pole below m_g as a function of R_U for different values of $x = m_h^2/m_g^2$ and for $d_U = 1.2$.

about the location of the maxima of the spectral function (however, the correspondence is not perfect [60]) and their widths. In any case, it is clear that the spectral function carries more information concerning the structure of the Higgs propagator than simply giving the location and width of its poles and it is therefore much more useful to deal directly with it.

To clarify further the structure of the spectral function, fig. 5.9 gives $\rho_{hh}(s)$ at fixed values of R_U for the same parameters as before ($d_U = 1.2$ and $x_0 = 5$). For $R_U = 1$ there is only one pole, it is above m_g and corresponds to the somewhat wide resonance of the spectral function (zone Ia). One can directly relate the width of this resonance (as measured by the width across it at half the peak maximum) to the width as given by the dashed lines in fig. 5.5. For $R_U = 3$, the pole above m_g has become wider and less pronounced while a sharper resonance (corresponding to the Phantom Higgs state) has appeared right above the mass gap (zone IIa). For $R_U = 6$ this resonance has detached from the continuum giving a delta function below m_g ; the pole above m_g is very broad and shallow (zone IIb) and could hardly be called a resonance.

From the previous figures one cannot obtain information on the prefactor $1/K^2$ which weights the Dirac delta contribution to $\rho_{hh}(s)$ when there is a pole below m_g and gives information of the pure Higgs composition of that pole, as explained above. This information is given by fig. 5.10 (for $d_U = 1.2$), where the different lines correspond to different values of $x = m_h^2/m_g^2$ from $x = 0$ to $x \rightarrow 1$. When the influence of unparticles is small (small R_U) $1/K^2 \rightarrow 1$ as it should be for a Higgs with SM properties. The departure of $1/K^2$ from 1 is larger for larger R_U (larger unparticle mixing) or when m_h gets closer to m_g (smaller mass difference between the states that mix).

Chapter 6

Unparticle Decays.

6.1 Introduction.

In the previous chapter we have analyzed the phenomenology of Unparticles coupled to the Higgs, and the consequences this scenario would have both for Electroweak symmetry breaking and for the breaking of the conformal symmetry in the Unparticle sector. In this chapter we will analyze the issue of the stability of Unparticles coupled to the Standard Model (or, in other words, their possible decay into SM particles [61, 62]). This issue is very important since it should have a great impact for unparticles in their influence on early Universe cosmology, in their capability as Dark Matter candidates and in their possible detection at high-energy colliders through its production and subsequent decay into SM particles. However, in order to study Unparticle decays, one has to go beyond the tree-level studies from the previous chapter through the inclusion of 1-loop corrections.

We will consider the possible decay of unparticles into SM particles via the Lagrangian coupling $\mathcal{L} = -\kappa_{\mathcal{U}} \mathcal{O}_{SM} \mathcal{O}_{\mathcal{U}}$ where \mathcal{O}_{SM} is a SM operator which can provide a channel for unparticle decay, such as $F_{\mu\nu}^2$, $\bar{f}f$ or the previously studied $|H|^2$.

Before focusing on a particular SM operator, we will start by simply considering a toy model with a real scalar φ , with bare mass m_0 and zero VEV, coupled to the unparticle scalar operator $\mathcal{O}_{\mathcal{U}}$ with scaling dimension $d_{\mathcal{U}}$ through the effective Lagrangian

$$\mathcal{L}_{eff} = \frac{1}{2}(\partial_{\mu}\varphi)^2 - \frac{1}{2}m_0^2\varphi^2 - \frac{1}{2}\kappa_{\mathcal{U}}\varphi^2\mathcal{O}_{\mathcal{U}} . \quad (6.1)$$

This toy model should capture the main features of realistic channels, involving SM operators like $\bar{f}f$ or $|H|^2$.

It is important to notice that the last term in (6.1) induces a tadpole term for the Unparticle operator at 1-loop, which will trigger an Unparticle VEV. This is similar to what happens when $\mathcal{O}_{SM} = |H|^2$ and the Higgs field H acquires a VEV, although there the tadpole for $\mathcal{O}_{\mathcal{U}}$ is a tree-level effect; in that case it has proven necessary to introduce a mass gap m_g in order to cure the IR divergence associated with the tadpole. For the case of the toy model (6.1), we will simply assume that a mass gap m_g is provided by the theory, without specifying how it is generated. Also, the VEV of $\mathcal{O}_{\mathcal{U}}$ in turn generates a 1-loop correction to the mass m_0

of the field φ . We assume that this 1-loop corrected mass squared is positive²⁸, $m^2 > 0$, so as to keep $\langle\varphi\rangle = 0$.

6.2 Simple Model of Unparticle Decays.

For the case of the toy model, since we have introduced the mass gap m_g by hand, and $\langle\varphi\rangle = 0$ (there is no mixing between φ and the Unparticle continuum), it will not be necessary to use the deconstructed theory. In the presence of m_g , the scalar Unparticle propagator for $\mathcal{O}_{\mathcal{U}}$ reads [11]:

$$-iP_{\mathcal{U}}^{(0)}(s) = \frac{1}{D_{\mathcal{U}}^{(0)}(s)} \equiv \frac{A_{d_{\mathcal{U}}}}{2 \sin(\pi d_{\mathcal{U}})} \frac{1}{(-s + m_g^2 - i\epsilon)^{2-d_{\mathcal{U}}}} , \quad (6.2)$$

with $A_{d_{\mathcal{U}}}$ given by

$$A_{d_{\mathcal{U}}} \equiv \frac{16\pi^{5/2}}{(2\pi)^{2d_{\mathcal{U}}}} \frac{\Gamma(d_{\mathcal{U}} + 1/2)}{\Gamma(d_{\mathcal{U}} - 1)\Gamma(2d_{\mathcal{U}})} \quad (6.3)$$

The polarization $\Sigma(s)$ induced in the unparticle propagator by the 1-loop diagram exchanging φ -fields can be simply added by Dyson resummation to give

$$-iP_{\mathcal{U}}^{(1)}(s) = \frac{1}{D_{\mathcal{U}}^{(1)}(s)} = \frac{1}{D_{\mathcal{U}}^{(0)}(s) + \Sigma(s)} \quad (6.4)$$

The polarization $\Sigma(s)$ is given in the \overline{MS} -renormalization scheme by [63]

$$\Sigma(s) = \frac{\kappa_{\mathcal{U}}^2}{32\pi^2} \left\{ \log \left(\frac{\Lambda_{\mathcal{U}}^2}{m^2} \right) + 2 - 2\lambda(s) \log \left[\frac{1 + \lambda(s)}{\sqrt{\lambda^2(s) - 1}} \right] \right\} \quad (6.5)$$

Here $\lambda(s) = \sqrt{1 - 4m^2/s}$ and we have set the renormalization scale equal to the Unparticle cutoff scale $\Lambda_{\mathcal{U}}$.

6.2.1 Pole Analysis.

The location of the unparticle resonances will be determined by the propagator poles $s = m_p^2 - im_p\Gamma_p$ in the complex s -plane; the polarization $\Sigma(s)$ has a branch cut that we take from the threshold at $s = 4m^2$ to $+\infty$ along the real axis with the principal Riemann sheet corresponding to $0 \leq \theta \leq 2\pi$, where θ is defined as $s - 4m^2 = |s - 4m^2|e^{i\theta}$; the second Riemann sheet is reached by shifting $\theta \rightarrow \theta + 2\pi$. A change in the Riemann sheet is equivalent to the replacement $\lambda(s) \rightarrow -\lambda(s)$.

²⁸An alternative possibility is to impose the renormalization condition of zero unparticle tadpole at 1-loop so that $\langle\mathcal{O}_{\mathcal{U}}\rangle = 0$.

The complete propagator is a function of $\lambda(s)$

$$D^{(1)}(s) \equiv \mathcal{D}[s, \lambda(s)] \quad (6.6)$$

So, the pole equations read

$$\mathcal{D}[s, \epsilon_R \lambda(s)] = 0 \quad (6.7)$$

where $\epsilon_R = 1(-1)$ correspond to solutions in the first (second) Riemann sheet [64].

For numerical work we fix $\Lambda_{\mathcal{U}} = 100m$. A numerical analysis of the pole equation (6.7) shows that, besides the Unparticle continuum, an isolated pole appears. Since the tree-level propagator had no pole (m_g^2 is not a pole but a branch point) the pole appearance is purely a 1-loop effect. Due to the sign of the polarization we find that this pole m_p^2 is always²⁹ below m_g^2 , but quite close to it as the polarization is a radiative effect: $m_p^2 \simeq m_g^2$.

For $m_p \leq 2m$ this isolated pole is real ($\Gamma_p = 0$) and located in the first Riemann sheet. Such pole does not correspond to any decaying unparticle, but it is entirely due to the fact that $\Sigma \neq 0$ below the threshold and could be interpreted as an unparticle bound state. We show in fig. 6.1 [left panel] a plot of m_p vs. $d_{\mathcal{U}}$ for $m = m_g$ (in this plot one can see that indeed $m_p \rightarrow m_g$ for $d_{\mathcal{U}} \rightarrow 2$).

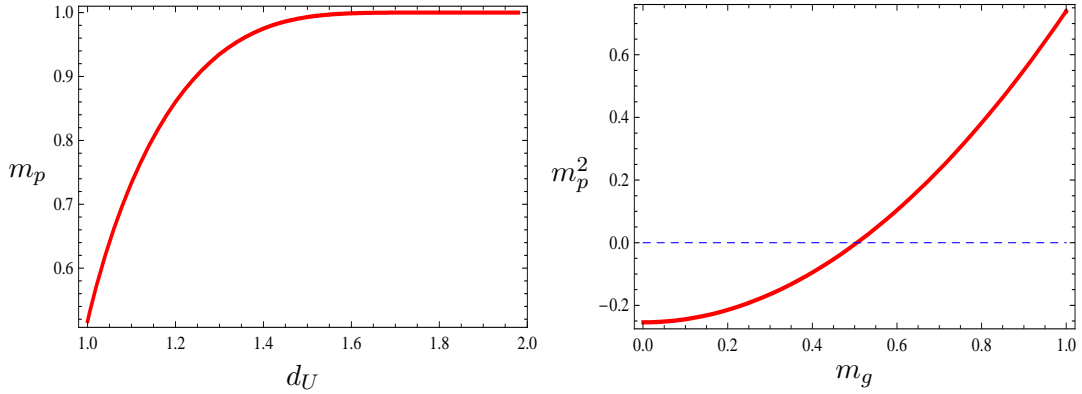


Figure 6.1: Left panel: Plot of m_p as a function of $d_{\mathcal{U}}$ for $\kappa_{\mathcal{U}} = 5$, $m_g = m$ and $\mu = \Lambda_{\mathcal{U}} = 100m$. Right panel: Plot of m_p^2 vs. m_g for $\kappa_{\mathcal{U}} = 5$ and $d_{\mathcal{U}} = 1.2$. All masses are in units of m .

For $m_g > 2m$ the isolated unparticle pole is complex ($\Gamma_p > 0$) and appears in the second Riemann sheet, and this now corresponds to the decay of a resonance. This case is exhibited in fig. 6.2, where m_p and Γ_p are plotted vs. $d_{\mathcal{U}}$ for the case $m_g = 4m$ (thick solid lines). Contrary to the claim from [62], it is found that there are complex pole solutions for all values of $d_{\mathcal{U}}$ in the considered range $1 \leq d_{\mathcal{U}} < 2$, and nothing special happens for $d_{\mathcal{U}} > 3/2$ (m_p^2 and Γ_p smoothly approach m_g^2 and zero respectively when $d_{\mathcal{U}} \rightarrow 2$).

²⁹For $d_{\mathcal{U}}$ very close to 2 one can also have $m_p > m_g$, but in such cases the mass difference between the pole and the mass gap is infinitesimal.

An important consequence of the negative mass shift responsible for $m_p^2 < m_g^2$ is that it yields a lower bound on the scale of conformal breaking m_g ; the bound is in turn related to the masses of the SM particles the Unparticle operator couples to (m in our case). This fact is shown by fig. 6.1 [right panel], where the pole squared mass m_p^2 is plotted vs. m_g for $d_U = 1.2$. We can see that the isolated unparticle pole becomes tachyonic for small values of m_g ($m_g < 0.5 m$). Moreover, this shows that in the particular limit $m_g \rightarrow 0$ the theory becomes unstable, implying that the mass gap m_g is necessary for the theory to be well defined.

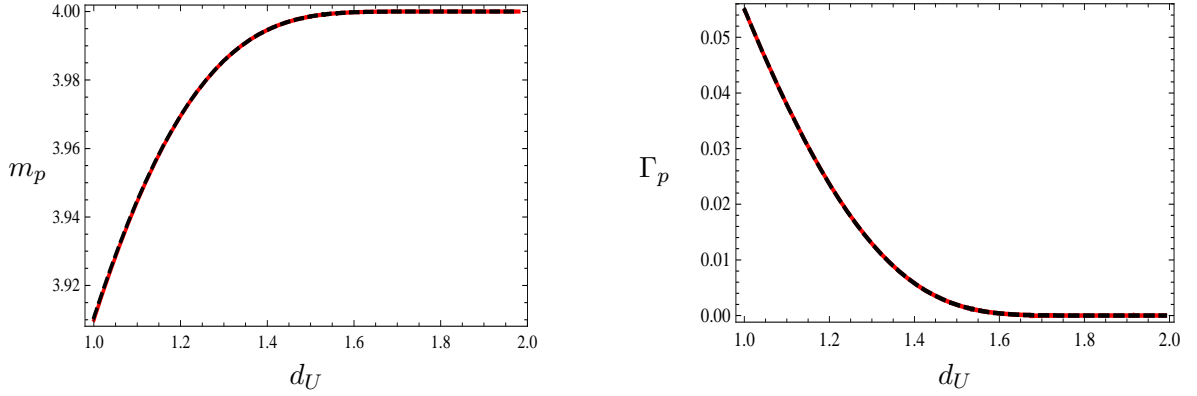


Figure 6.2: Left [right] panel: Plot of m_p [Γ_p] as a function of d_U for $\kappa_U = 5$ and $m_g = 4m$ (thick solid). Corresponding results based on the analytical approximation of (6.9) are plotted in thick dashed lines. All masses are in units of m .

It is easy to understand analytically our results for the case $m_g > 2m$. For values of s close to the resonance region one can approximate the complex polarization by the constant $\Sigma(m_g^2)$:

$$\Sigma(s) \simeq \Sigma(m_g^2) = \frac{\kappa_U^2}{32\pi^2} \left\{ \log \left(\frac{\Lambda_U^2}{m^2} \right) + 2 - \lambda(m_g^2) \left[\log \frac{1 + \lambda(m_g^2)}{1 - \lambda(m_g^2)} - i\pi \right] \right\} \quad (6.8)$$

So, since $m_p^2 \simeq m_g^2$, we obtain an analytic approximation for the pole mass and width as

$$\begin{aligned} m_p^2 &\simeq m_g^2 - \delta m^2 \cos \alpha, \\ m_p \Gamma_p &\simeq \lambda(m_g^2) \delta m^2 |\sin \alpha| \end{aligned} \quad (6.9)$$

Here we have

$$\delta m^2 \equiv \left[\frac{|\Sigma(m_g^2)| A_{d_U}}{2 |\sin(\pi d_U)|} \right]^{\frac{1}{2-d_U}} \quad \alpha = \frac{1}{(2-d_U)} \arctan \frac{\text{Im}[\Sigma(m_g^2)]}{\text{Re}[\Sigma(m_g^2)]}. \quad (6.10)$$

Fig. 6.2 compares the values for m_p and Γ_p obtained using the analytic approximation in (6.9) (dashed thick lines) with the full numerical results (thick solid lines) showing that

the analytical approximation is excellent. We can use this approximation to write down analytically the lower bound on m_g^2 to avoid a tachyon. It is given by

$$m_g^2 > \left[\frac{\Sigma(0)A_{d_U}}{2|\sin(\pi d_U)|} \right]^{\frac{1}{2-d_U}} \quad \Sigma(0) = \frac{\kappa_U^2}{16\pi^2} \log(\Lambda_U/m) \quad (6.11)$$

6.2.2 Spectral Function Analysis.

We may gain further insight on the unparticle spectrum using the spectral function for the 1-loop corrected propagator

$$\rho_U(s) = -\frac{1}{\pi} \text{Im}[-iP_U^{(1)}(s+i\epsilon)] \quad (6.12)$$

This spectral function reproduces faithfully the main features of the pole structure discussed previously, giving also information on the Unparticle continuum above the mass gap. The expression for this spectral function is the following:

$$\begin{aligned} \rho_U(s) = & \frac{1}{\pi} \frac{\text{Im}[\Sigma(s)]}{|D_U^{(1)}(s)|^2} + \theta(4m^2 - m_p^2) \frac{\delta(s - m_p^2)}{K^2(s, d_U)} + \\ & + \theta(s - m_g^2) \frac{2 \sin^2(\pi d_U)}{\pi A_{d_U}} \frac{(s - m_g^2)^{2-d_U}}{|D_U^{(1)}(s)|^2} . \end{aligned} \quad (6.13)$$

where

$$\frac{1}{K^2(s, d_U)} \equiv \frac{dD_U^{(1)}(s)}{ds} \quad (6.14)$$

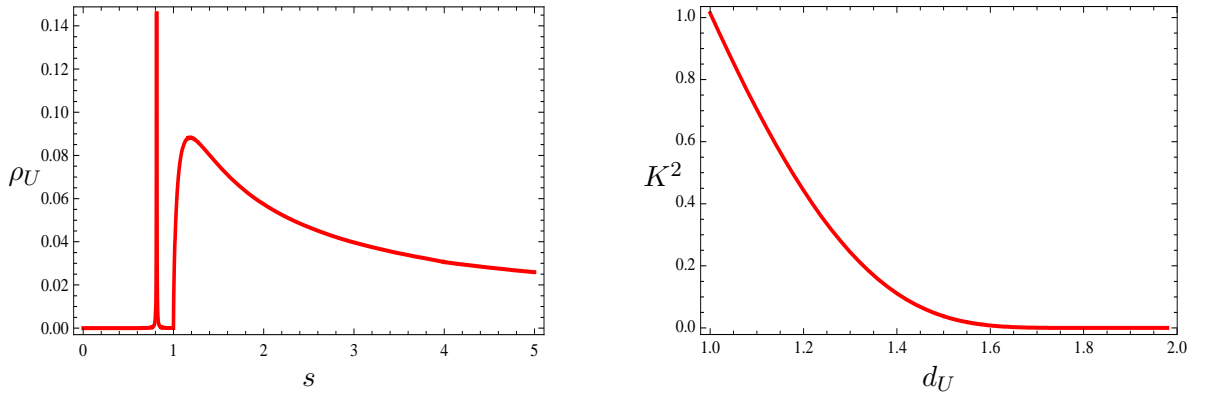


Figure 6.3: Left panel: Plot of $\rho_U(s)$ for $m_g = m$, $d_U = 1.25$, $\kappa_U = 5$ and $\mu = \Lambda_U = 100m$. Right panel: Plot of $K^2(m_p^2, d_U)$ for the same values of mass parameters. All masses are in units of m .

The first term of $\rho_{\mathcal{U}}(s)$ is proportional to the imaginary part of $\Sigma(s)$ (which contains a factor $\theta(s - 4m^2)$) and thus for $m_p^2 > 4m^2$ it corresponds (through the Cutkosky rules) to a width for the unparticles, which decay beyond the threshold. The second term corresponds to a real pole in the first Riemann sheet (for $m_p^2 < 4m^2$), and should be interpreted as a stable (un)particle of mass m_p . Finally, the third term is proportional to the imaginary part of $D_{\mathcal{U}}^{(0)}(s)$ (which contains a factor $\theta(s - m_g^2)$) and does not signal unparticle decay, but corresponds to the familiar continuous contribution to the spectral function above the mass gap. For $m_p > 2m$, the term proportional to $\text{Im}[\Sigma(s)]$ gives rise to a resonant structure in the spectral function $\rho_{\mathcal{U}}(s)$, with an approximate Breit-Wigner distribution centered around m_p^2 of width Γ_p . This should be in correspondence with the structure of the poles of the propagator $P^{(1)}(s)$ in the complex s -plane, *i.e.* to the zeroes of the function $D^{(1)}(s)$ which we have previously studied.

In the left panel of fig. 6.3 we have plotted the spectral function for the case $m_p < 2m$ (that of fig. 6.1) in which a real pole appears. We see a delta function corresponding to that pole and a continuous component for $s > m_g^2$. In the right panel of fig. 6.3 we have plotted the strength of the isolated pole as measured by $K^2(m_p^2, d_{\mathcal{U}})$

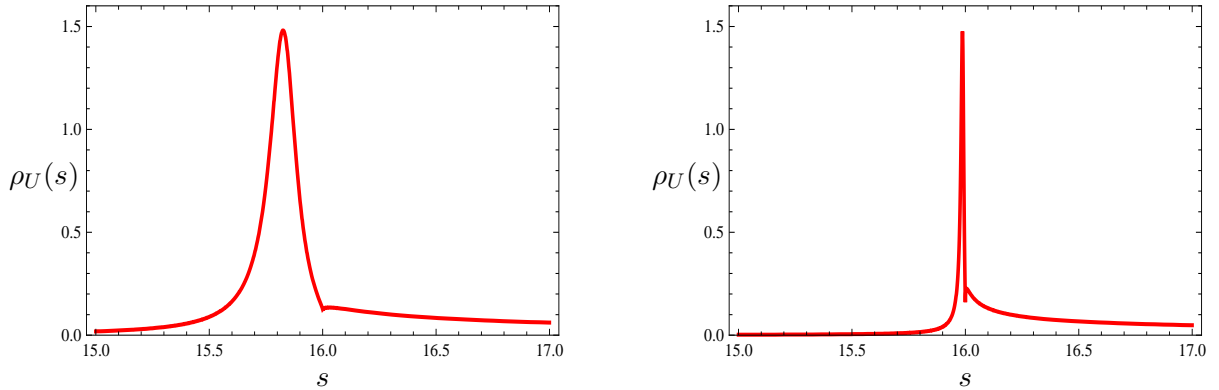


Figure 6.4: Left [right] panel: Plot of $\rho_{\mathcal{U}}(s)$ for $d_{\mathcal{U}} = 1.25$ [$d_{\mathcal{U}} = 1.5$], $m_g = 4m$, $\kappa_{\mathcal{U}} = 5$ and $\mu = \Lambda_{\mathcal{U}} = 100m$. All masses are in units of m .

In fig. 6.4 we show the spectral function for the case $m_g > 2m$, where the resonant structure leading to unparticle decay can be clearly distinguished; the fact that for $m_g > 2m$ the pole width is sharpening for increasing values of $d_{\mathcal{U}}$ (as shown by the right plot in fig. 6.2) is also shown in fig. 6.4. Both for $d_{\mathcal{U}} = 1.25$ and $d_{\mathcal{U}} = 1.5$ we see a clear resonant contribution that overwhelms the continuous one; in this region and for values of s close to the value of m_p^2 the unparticle behaves as a resonance. The height of the peak can be approximately calculated, and turns out to be independent of $d_{\mathcal{U}}$ ³⁰ and given by:

$$\rho_{\mathcal{U}}^{max} \simeq \frac{32}{\kappa_{\mathcal{U}}^2 \lambda(m_g^2)}. \quad (6.15)$$

³⁰This statement is true up to values of $d_{\mathcal{U}}$ very close to 2, for which the width of the resonance is zero and $m_p = m_g$ for all practical purposes.

Therefore, as the width goes to zero we do not recover a Dirac delta function at m_p and the resonance cannot be distinguished over the continuous background starting at m_g .

Notice that for $m_g^2 > 4m^2$ the resonant (“on-shell”) production of unparticles would dominate the amplitude $\varphi\varphi \rightarrow \varphi\varphi$ as it happens with ordinary exchange of particles in the s-channel. Here the presence of unparticles should be detected through a peak in the invariant mass distribution of the final state similar to the case of a new particle resonance (e.g. the production of a Z'). For the case $m_p^2 < 4m^2$ the resonance is located below the production threshold and the spectral function is dominated by the continuous contribution, which does not provide any decay; In that case there is no resonant production and the production of the final state $\varphi\varphi$ will be as if induced “off-shell”; the presence of unparticles in the intermediate state would then be detected by the continuous enhancement of the corresponding cross-section.

The formalism to be used for any realistic Standard Model channel as e.g. $A_\mu A_\nu, \bar{f}f$ or $|H|^2$, is similar to the one used in the simple model previously considered. In any case, for the decay channel $\mathcal{O}_U \rightarrow AB$, if $m_p^2 > (m_A + m_B)^2$ the Unparticle should be detected in the corresponding cross-section through a peak in the invariant mass distribution of the final state which should reconstruct the resonant pole (much like the reconstruction of a Z' resonance). On the contrary if $m_p^2 < (m_A + m_B)^2$ then the only indirect detection of the unparticle should be by means of an excess of events with respect to the corresponding Standard Model cross-section.

Summary and Conclusions.

We have studied some issues concerning hidden sectors coupled to the Standard Model through the Higgs portal. In the first part of the Thesis we have explored the cosmological implications of hidden sectors, focusing on the study of the dynamics of the Electroweak Phase Transition in these scenarios, and also on dark matter from the hidden sector. In the second part, we have considered a scenario in which the hidden sector coupled to the Standard Model through the Higgs portal is conformally invariant; this kind of scenarios in which a conformal hidden sector is coupled to the SM were recently put forward by Georgi as a possible extension of the Standard Model with very unusual features, and were given the name “Unparticle Scenarios”. Here we have analyzed the effects that a coupling between the conformal hidden sector and the Standard Model through the Higgs portal will have both for the Higgs sector and for the hidden conformal sector.

Cosmological Aspects of Hidden Sectors.

We have explored several cosmological implications of Standard Model extensions through hidden sector scalars, using a very simple hidden sector extension of the Standard Model, which consists in adding a set of N real scalar singlets S_i coupled to the SM Higgs doublet H .

We first performed a study of the Electroweak phase transition in this models. In Electroweak Baryogenesis scenarios, the Electroweak phase transition plays a crucial role since it can provide the necessary departure from thermal equilibrium; for Baryogenesis to occur a 1st order phase transition is needed, and it also has to be strong enough to suppress sphaleron processes in the broken phase after the phase transition, namely $v(T)/T > 1$. In the Standard Model, the Electroweak phase transition is of second order or a crossover for Higgs masses above the LEP experimental limit, preventing Electroweak Baryogenesis from being realized in the Standard Model. Here we find that in models with a moderate number of hidden sector scalars ($N_S \sim 12$) the phase transition is of first order for Higgs masses of the order of the electroweak scale (or lighter) and sizable Higgs couplings to the hidden sector, $\zeta \geq 0.9$. We also find that this persists in the case of classical conformal invariance, in which the electroweak scale is generated by dimensional transmutation.

The study of the first order phase transition is performed identifying and computing the relevant parameters for describing the dynamics of the transition: critical temperature T_c , nucleation temperature T_n , duration of the transition Δt (or, equivalently, temperature at which the transition ends T_f), strength of the transition $R \equiv v(T)/T$ and latent heat liberated (normalized to the energy in the plasma) α . In this respect we improve most previous studies of the transition and clarify the proper definition of T_n and Δt , which are defined in several,

inequivalent ways in the literature; we also find that the definition of these two parameters can be related to values of the tunneling action at finite temperature $S_3(T)/T$ in a model independent way, obtaining $S_3(T_n)/T_n \simeq 142 - 148$ and $S_3(T_f)/T_f \simeq 110 - 115$ (this last one is true except for very strong phase transitions).

As a result of this study, we find that in a large portion of parameter space the 1st order phase transition is strong enough to avoid the erasure of the baryon asymmetry through sphaleron processes after the transition, $v(T_f)/T_f > 1$.

Also, we consider the possibility that the hidden sector scalars account for the dark matter of the universe. We compute the relic mass density of scalar particles Ω_S and find that the required dark matter abundance $\Omega_{DM} = 0.228 \pm 0.013$ can be provided by hidden-sector scalars in two different regimes. In the first, the hidden-sector scalars have moderate couplings but large masses $M_S \sim 1$ TeV. In the second, the hidden-sector scalars are rather light, $M_S \leq M_W$; in this case, the scalars cannot annihilate into W-bosons, and this fact greatly enhances the dark matter abundance.

Nevertheless, neither type of scalar can contribute significantly to the previously discussed strength of the phase transition. Hence, a simultaneous solution of the dark matter and baryogenesis problems of the Standard Model in this kind of hidden sector extensions either requires a large number of scalars (in which case we found $N_S \sim 50$), or several types of scalars in the hidden sector with non-uniform masses and/or couplings to the Higgs sector.

Unparticles Coupled to the Higgs.

Unparticle models have been regarded lately as hidden sector extensions of the Standard Model with very interesting and unusual features. After giving a brief introduction on the Unparticle idea and describing Stephanov deconstructed version Unparticles, we have investigated the possibility of coupling the Higgs to the conformally invariant hidden sector (Unparticle sector), through a ‘‘Higgs portal’’ type of coupling $|H|^2 \mathcal{O}_U$. The study of this scenario is important for Unparticle physics since, being $|H|^2$ the only gauge invariant scalar operator with dimension $d < 3$, its coupling to Unparticles can be relevant at low energies, therefore strongly affecting the low energy phenomenology of Unparticles.

A first consequence of this coupling is that Electroweak symmetry breaking introduces a divergent tadpole for the Unparticle operator \mathcal{O}_U ; once this divergence is cured (we have achieved this by introducing new interactions in a deconstructed model for Unparticles, that keep the VEV for the Unparticle operator finite) a mass gap m_g is generated for the Unparticle sector, implying the breaking of the conformal symmetry of the Unparticles.

Within the Stephanov deconstruction formalism, We have analyzed two different ways of curing the divergent tadpole for \mathcal{O}_U , giving rise to two different types of spectra for the Higgs-Unparticles system once the Higgs and the scalar Unparticles mix. In the first scenario, the Higgs mixes with a collective state coming from the Unparticle continuum of states, giving rise to two different eigenstates in the spectrum, plus a continuum above the mass gap; the eigenstates can be embedded in the continuum or be isolated depending on if their mass lies above or below the mass gap; we call this type of scenario, ‘‘Plasmon scenario’’ (because the collective Unparticle state is similar to plasmon excitations in condensed matter physics). In

the second scenario, the mixing between the Higgs field and the Unparticles is rather strong, resulting in the appearance of a second eigenstate (apart from the one associated with the Higgs state before the mixing) not associated with a collective Unparticle state; we call this eigenstate the “Phantom Higgs” since both its mass and couplings to gauge bosons and fermions can be much lower than naively expected. In both cases, we analyze both the pole structure of the system and perform a spectral function analysis.

Finally, we have investigated the issue of Unparticle decays, using a toy model that captures the main aspects of more realistic SM-Unparticle couplings.

Resumen y Conclusiones.

Hemos estudiado algunos aspectos relativos a sectores ocultos acoplados al Modelo Estandar por medio del “Higgs portal”. En la primera parte de la tesis hemos explorado las implicaciones cosmológicas de los sectores ocultos, centrándonos en el estudio de la dinámica de la transición de fase electrodébil en estos escenarios, y también en la posibilidad de que el sector oculto proporcione un candidato a materia oscura. En la segunda parte, hemos considerado un escenario en el cual el sector oculto acoplado al Modelo Estandar a través del “Higgs portal” es invariante conforme; este tipo de escenarios en los que un sector invariante conforme se acopla al Modelo Estandar han sido descritos recientemente por Georgi como una posible extensión del Modelo Estandar con características muy inusuales, y se les bautizó como “Escenarios de Unpartículas”. Aquí hemos analizado los efectos que un acoplo entre el sector conforme y el Modelo Estandar a través del Higgs tendría tanto para el sector de Higgs como para el sector oculto invariante conforme.

Cosmología y Sectores Ocultos.

Hemos explorado varias implicaciones cosmológicas de extensiones del Modelo Estandar a través de escalares pertenecientes a sectores ocultos, usando para ello una extensión del Modelo Estandar muy simple, consistente en añadir un conjunto de N escalares reales (singletes) S_i acoplados al doblete de Higgs del Modelo Estandar H .

En primer lugar hemos llevado a cabo un estudio de la transición de fase electrodébil en estos modelos. En escenarios de Bariogénesis electrodébil, la transición de fase electrodébil juega un papel crucial ya que puede aportar la desviación del equilibrio térmico que se necesita; para que sea posible tener Bariogénesis en estos escenarios, la transición ha de ser de primer orden, y además ha de ser lo suficientemente fuerte para que los procesos de esfalerones en la fase rota después de la transición estén suprimidos, lo que se traduce en $v(T)/T > 1$. En el Modelo Estandar, la transición de fase es de segundo orden o un crossover para masas del Higgs por encima de la cota experimental de LEP, por lo que no se puede tener Bariogénesis electrodébil en el Modelo Estandar. En nuestro caso encontramos que en modelos con un número moderado de escalares ($N_S \sim 12$) la transición de fase es de primer orden para masas del Higgs del orden de la escala electrodébil (o mas ligeros) y acoplos entre el Higgs y el sector oculto de orden $\zeta \geq 0.9$. También encontramos que esto ocurre incluso en el caso de invariancia conforme a nivel clásico, en el cual la escala electrodébil es generada por transmutación dimensional.

El estudio de la transición de fase de primer orden se lleva a cabo identificando y calculando las cantidades relevantes para describir la dinámica de la transición: temperatura crítica T_c , temperatura de nucleación T_n , duración de la transición Δt (o en su lugar la tem-

peratura a la que la transición termina T_f), fuerza de la transición $R \equiv v(T)/T$ y calor latente liberado (normalizado a la energía del plasma) α . En este sentido mejoramos la mayoría de los estudios de la transición hechos anteriormente, y clarificamos las definiciones de T_n y Δt , que en la literatura se definen de varias maneras no equivalentes; también encontramos que la definición de estos dos parámetros se puede relacionar con valores de la acción $S_3(T)/T$, obteniendo $S_3(T_n)/T_n \simeq 142 - 148$ y $S_3(T_f)/T_f \simeq 110 - 115$ (esta última relación falla para transiciones muy fuertes).

Como resultado de este estudio, encontramos que en una gran parte del espacio de parámetros la transición de fase de primer orden es suficientemente fuerte para impedir que los procesos de esfalerones después de la transición eliminen la asimetría bariónica, $v(T_f)/T_f > 1$.

También consideramos la posibilidad de que los escalares del sector oculto constituyan la materia oscura del universo. Calculamos la densidad de energía de partículas escalares Ω_S y encontramos que la abundancia de materia oscura requerida $\Omega_{DM} = 0.228 \pm 0.013$ puede ser explicada por medio de los escalares en dos regimenes distintos. En el primero, los escalares del sector oculto tienen acoplos moderados pero son pesados, $M_S \sim 1$ TeV. En el segundo, los escalares son bastante ligeros, $M_S \leq M_W$; en este caso, los escalares no pueden aniquilarse en bosones W, y esto hace que la abundancia de materia oscura sea mayor.

Sin embargo, en ninguno de los dos límites los escalares contribuyen de forma apreciable a la fuerza de la transición de fase. Por tanto, una solución conjunta a los problemas de la materia oscura y de Bariogénesis del Modelo Estandar en este tipo de extensiones por medio de sectores ocultos requiere o bien un número muy grande de escalares $N_S \sim 50$ o bien varios tipos de escalares en el sector oculto con diferentes masas y/o acoplos al sector de Higgs.

Unpartículas Acopladas al Higgs.

Los modelos de Unpartículas han aparecido recientemente como extensiones del Modelo Estandar por medio de sectores ocultos con propiedades muy interesantes e inusuales. Después de dar un breve intrducción a la idea de Unpartículas y describir la versión deconstruida de Stephanov, hemos investigado la posibilidad de acoplar el Higgs al sector invariante conforme (sector de Unpartículas) a través de un acoplo de tipo “Higgs portal” $|H|^2 \mathcal{O}_U$. El estudio de este escenario es importante ya que $|H|^2$ es el único operador escalar invariante gauge con dimensión $d < 3$, y por tanto su acoplo a las Unpartículas puede ser relevante a bajas energías, jugando un papel decisivo en la fenomenología de baja energía de las Unpartículas

Una primera consecuencia de este acoplo es que la rotura de la simetría electrodébil induce un tadpolo divergente IR para el operador de Unpartículas \mathcal{O}_U ; una vez que esta divergencia se elimina (esto se consigue añadiendo nuevas interacciones en un modelo deconstruido de Unpartículas, que hacen finito el VEV para \mathcal{O}_U), se genera un “mass gap” m_g en el sector de Unpartículas, lo que implica la ruptura de la simetría conforme del sector oculto.

Usando el formalismo deconstruido de Stephanov, hemos analizado dos formas diferentes de solucionar el problema del tadpolo divergente para \mathcal{O}_U , dando lugar a dos tipos difenretes de espectro para el sistema Higgs-Unpartículas una vez que el Higgs y el continuo de Unpartículas se mezclan. En el primer escenario, el Higgs se mezcla con estado colectivo proveniente del continuo de Unpartículas dando lugar a dos autoestados diferentes en el es-

pectro, además de un continuo por encima del mass gap; los autoestados pueden estar dentro del continuo o aislados dependiendo de si su masa está por encima o por debajo del mass gap; llamamos a este escenario “Plasmon scenario” (porque el estado colectivo de Unpartículas es similar a las excitaciones plasmónicas que aparecen en Física de la materia condensada). En el segundo escenario, la mezcla entre el Higgs y las Unpartículas es bastante grande, dando como resultado la aparición de un segundo autoestado (aparte del asociado con el Higgs antes de la mezcla) no asociado a un estado colectivo de Unpartículas; llamamos a este autoestado el “Phantom Higgs” ya que tanto su masa como sus acoplos a bosones gauge y fermiones pueden ser mucho mas pequeños de los que se esperaría. En ambos escenarios analizamos tanto la estructura de polos como la función espectral del sistema.

Finalmente, hemos investigado los decays de Unpartículas, usando un modelo de juguete que contiene los aspectos importantes de acoplos mas realistas entre el SM y las Unpartículas.

Part III

Appendices.

A Effective Potential Formalism.

A.1 The Effective Potential in Field Theory.

The effective potential for a scalar field in Quantum Field Theory corresponds to the scalar potential of the theory once quantum effects (*i.e.* radiative corrections) are taken into account. It is a specially useful tool when discussing theories with spontaneously broken symmetries, since it allows to include radiative corrections in the analysis of spontaneous symmetry breaking.

Our starting point is the “Effective Action” $\Gamma[\phi_c]$, defined as the Legendre transform of the generating functional of connected Green functions $W[J]$:

$$\Gamma[\phi_c] = W[J] - \int J(x) \frac{\delta W[J]}{\delta J(x)} d^4x = W[J] - \int J(x) \phi_c(x) d^4x \quad (\text{A.1})$$

Here $\phi_c(x)$ corresponds to one-point function for the scalar field $\phi(x)$ in the presence of a source $J(x)$. The Effective Action turns out to be the generating functional of 1PI Green functions $\Gamma^{(n)}(x_1, \dots, x_n)$:

$$\Gamma[\phi_c] = \sum_{n=1}^{\infty} \frac{1}{n!} \int d^4x_1 d^4x_2 \dots d^4x_n \Gamma^{(n)}(x_1, \dots, x_n) \phi_c(x_1) \dots \phi_c(x_n) \quad (\text{A.2})$$

Apart from this expansion for $\Gamma[\phi_c]$ in powers of the field $\phi_c(x)$, there exists another expansion for the Effective Action in derivatives of the field around a constant field configuration (in momentum space, this corresponds to an expansion in powers of the momentum of the field around the point where all external momenta vanish):

$$\Gamma[\phi_c] = \int d^4x \left[-V_{eff}(\phi_c) + \frac{1}{2} Z(\phi_c) \partial_\mu \phi_c \partial^\mu \phi_c + \dots (\text{higher derivative terms}) \right] \quad (\text{A.3})$$

The zeroth-order term in the expansion, $V_{eff}(\phi_c)$ is known as the **Effective Potential**, and as it will be shown, it is the generalization of the scalar lagrangian potential $V(\phi)$ to the inclusion of radiative corrections.

In the case of a constant (static and homogeneous) field configuration, from (A.3) one gets:

$$\Gamma[\phi_c] = -V_{eff}(\phi_c) \int d^4x \quad (\text{A.4})$$

Now recalling (A.1), performing a functional variation of the Effective Action with respect to $\phi_c(x)$ one gets:

$$\begin{aligned} \frac{\delta\Gamma[\phi_c]}{\delta\phi_c(x)} &= \frac{\delta W[J]}{\delta\phi_c(x)} - J(x) - \int \phi_c(y) \frac{\delta J(y)}{\delta\phi_c(y)} d^4y = \\ &= \int \frac{\delta W[J]}{\delta J(y)} \frac{\delta J(y)}{\delta\phi_c(y)} d^4y - J(x) - \int \phi_c(y) \frac{\delta J(y)}{\delta\phi_c(y)} d^4y = -J(x) \\ &\Downarrow \\ \frac{\delta\Gamma[\phi_c]}{\delta\phi_c(x)} &= -J(x) \end{aligned} \quad (\text{A.5})$$

So, in the absence of sources $J(x)$, the Effective Action satisfies:

$$\frac{\delta\Gamma[\phi_c]}{\delta\phi_c(x)} = 0 \quad (\text{A.6})$$

As we are interested in field theories whose vacuum field configurations are invariant under the Poincare Group, we seek for solutions $\phi_c(x)$ to (A.6) which are independent of x ($\phi_c(x) \rightarrow v$), and recalling (A.4) we get:

$$\left. \frac{dV_{eff}(\phi_c)}{d\phi_c} \right|_{\phi_c=v} = 0 \quad (\text{A.7})$$

For the internal symmetry of the theory to be spontaneously broken, the vacuum field configuration v has to be nonzero (this is necessary, since otherwise the vacuum configuration is trivially invariant under the symmetry). This way, the study of spontaneous symmetry breaking in Quantum Field Theory including radiative corrections consists in minimizing the Effective Potential $V_{eff}(\phi)$, just in the same way as the study of spontaneous symmetry breaking at the semiclassical level consists in minimizing the lagrangian scalar potential $V(\phi)$. However, whereas we have an exact expression for the lagrangian scalar potential $V(\phi)$, it is not in principle obvious how to compute the Effective Potential³¹. There are several ways to compute it³². Here we will follow [23].

³¹In general it is not possible to obtain an exact expression for the Effective Potential, but only to do a perturbative expansion.

³²see for example [24] for an evaluation of $V_{eff}(\phi)$ from the functional integral definition of $\Gamma[\phi_c]$; for a recent review on the subject, see [30].

A.1.1 Computation of the Effective Potential.

1. Recalling (A.2), we expand the Effective Action $\Gamma[\phi_c]$ in powers of $\phi_c(x)$, around a constant field Φ :

$$\Gamma[\phi_c] = \sum_{n=1}^{\infty} \frac{1}{n!} \int d^4x_1 \dots d^4x_n \Gamma_{\Phi}^{(n)}(x_1, \dots, x_n) (\phi_c(x_1) - \Phi) \dots (\phi_c(x_n) - \Phi) \quad (\text{A.8})$$

2. Taking ϕ_c independent of x we will be able to find a formula for the Effective Potential equating (A.8) and (A.4). First, we take the 1PI Green functions $\Gamma_{\Phi}^{(n)}(x_1, \dots, x_n)$ in momentum space:

$$\begin{aligned} \tilde{\Gamma}_{\Phi}^{(n)}(p_1, \dots, p_n) \cdot (2\pi)^4 \cdot \delta^4(p_1 + \dots + p_n) &= \\ &= \int e^{i(p_1x_1 + \dots + p_nx_n)} \Gamma_{\Phi}^{(n)}(x_1, \dots, x_n) d^4x_1 \dots d^4x_n \end{aligned} \quad (\text{A.9})$$

So, in virtue of (A.9):

$$\begin{aligned} \int \Gamma_{\Phi}^{(n)}(x_1, \dots, x_n) d^4x_1 \dots d^4x_n &= \\ &= \tilde{\Gamma}_{\Phi}^{(n)}(0) \cdot (2\pi)^4 \cdot \delta^4(0) = \tilde{\Gamma}_{\Phi}^{(n)}(0) \cdot \int d^4x \end{aligned} \quad (\text{A.10})$$

3. Then:

$$\begin{aligned} \sum_{n=1}^{\infty} \frac{1}{n!} [\phi_c - \Phi] \dots [\phi_c - \Phi] \int d^4x_1 \dots d^4x_n \Gamma_{\Phi}^{(n)}(x_1, \dots, x_n) &= \\ \sum_{n=1}^{\infty} \frac{1}{n!} [\phi_c - \Phi] \dots [\phi_c - \Phi] \tilde{\Gamma}_{\Phi}^{(n)}(0) \cdot \int d^4x &= \\ &= -V_{eff}(\phi_c) \int d^4x \end{aligned} \quad (\text{A.11})$$

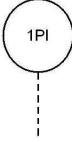
So finally the desired formula for the Effective Potential is:

$$V_{eff}(\phi_c) = - \sum \frac{1}{n!} [\phi_c - \Phi]^n \tilde{\Gamma}_{\Phi}^{(n)}(0) \quad (\text{A.12})$$

This is the formula originally used by Coleman and Weinberg [25] for the 1-loop computation of the Effective Potential in their study of spontaneous symmetry breaking through radiative corrections.

A.2 The Effective Potential at 1-Loop.

If we now take the derivative of (A.12) with respect to ϕ_c and set $\phi_c = \Phi$, we obtain:

$$\left. \frac{dV_{eff}(\phi_c)}{d\phi_c} \right|_{\phi_c=\Phi} = \frac{dV_{eff}(\Phi)}{d\Phi} = -\tilde{\Gamma}_{\Phi}^{(1)}(0) = i \text{ 1PI} \quad (\text{A.13})$$


Thus, in order to compute the Effective Potential all we need to do is to compute the 1PI “tadpole” of the shifted theory (in a background Φ) to the desired (n) loop order, and integrate once to obtain $V_{eff}^{n-loop}(\phi_c)$ ³³. It is instructive to compute explicitly the general formula for the 1-loop Effective Potential using (A.13). To do it, we have to obtain the Feynman rules for the shifted theory ($\phi_c \rightarrow \phi_c + \Phi$) and then compute the tree-level and 1-loop contributions to the 1PI tadpole.

1. In order to obtain the tree-level contribution we note that:

$$V(\phi_c + \Phi) = V(\Phi) + \phi_c \cdot \left. \frac{dV}{d\phi_c} \right|_{\phi_c=\Phi} + \dots \quad (\text{A.14})$$

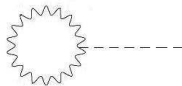
We then obtain a tree-level contribution to the tadpole due to the Feynman rule:

$$-i \frac{dV}{d\Phi} \quad \times \text{-----} \quad (\text{A.15})$$

The dashed line represents ϕ_c and $V(\Phi)$ is the classical potential.

Integrating, we obtain the expected tree-level result: $V_{eff}^{(0)}(\Phi) = V(\Phi)$

2. In turning to the computation of the 1-loop contribution to the Effective Potential, $V_{eff}^{(1)}(\phi_c)$, one has to consider the 1-loop tadpole diagrams (contributing to (A.13)) coming from possible couplings of $\phi(x)$ to other scalars (and itself), fermions and gauge bosons. As an example we will consider a spontaneously broken $SU(2)$ gauge theory, and calculate the contribution to $V_{eff}^{(1)}(\phi)$ (being ϕ the physical scalar degree of freedom after the breaking of the symmetry) from the gauge fields, through the Feynman diagram:



At this point one finds the problem that $V_{eff}(\phi)$ is gauge dependent beyond tree-level [24, 25, 65, 66]; the solution to this apparent problem relies on the so called “Nielsen

³³Note that if we take a background $\Phi = v$ (where v is the true vacuum of the theory), then the sum of all tadpoles must vanish, and we then regain the minimum condition for $V_{eff}(\phi_c)$.

identities” [67], which ensure that any physical quantity extracted from the Effective Potential is gauge invariant. In an actual full computation of $V_{eff}^{(1)}(\phi)$ the Landau gauge ($\xi = 0$ in the R_ξ gauge) is usually chosen for convenience, since in this gauge the Fadeev-Popov ghosts decouple from the scalar and we don’t have to take them into account in the calculation (however, in the Landau gauge the Goldstone degrees of freedom are not decoupled from ϕ , and one has to calculate their contribution to the 1-loop tadpole).


We need to determine the $\phi A_\mu A^\mu$ coupling in the shifted theory ($\phi \rightarrow \phi + \Phi$). From the scalar kinetic term the vector bosons acquire a field dependent mass matrix $M_{ab}^2(\phi)$:

$$\frac{1}{2}g^2 (0 \ \phi) \ T_a T_b \begin{pmatrix} 0 \\ \phi \end{pmatrix} A_\mu^a A^{\mu b} = \frac{1}{2}M_{ab}^2(\phi) A_\mu^a A^{\mu b} \quad (\text{A.16})$$

In the shifted lagrangian, the following trilinear coupling is generated:

$$\frac{1}{2} \left. \frac{dM_{ab}^2(\phi)}{d\phi} \right|_{\phi=\Phi} \phi A_\mu^a A^{\mu b} \quad (\text{A.17})$$

which results in the Feynman rule:



In this particular case the mass matrix $M_{ab}^2(\phi)$ is diagonal:

$$M_{ab}^2(\phi) = \frac{g^2 \phi^2}{4} \delta_{ab} \equiv M^2(\phi) \delta_{ab} \quad (\text{A.18})$$

Then the contribution from the gauge fields is:

$$\left. \frac{dV_{eff}^{(1)}(\phi)}{d\phi} \right|_{\phi=\Phi} = -\tilde{\Gamma}_\Phi^{(1)}(0) = i \sum_{a=1}^3 \frac{3}{2} \int \frac{d^4 k}{(2\pi)^4} \frac{1}{k^2 - M^2(\Phi)} \frac{dM^2(\Phi)}{d\Phi} \quad (\text{A.19})$$

Notice that the factor of 3 arises from $g_{\mu\nu} (g^{\mu\nu} - p^\mu p^\nu / p^2)$, which simply counts the number of degrees of freedom of a massive gauge boson. Integrating (A.19) we obtain:

$$V_{eff}^{(1)}(\Phi) = -\frac{9i}{2} \int \frac{d^4 k}{(2\pi)^4} \log(k^2 - M^2(\Phi)) \quad (\text{A.20})$$

This last result can be generalized to the case when arbitrary particles of spin J are allowed to run inside the loop of the tadpole:

$$V_{eff}^{(1)}(\Phi) = -\frac{i}{2} Str \int \frac{d^4 k}{(2\pi)^4} \log(k^2 - M_a^2(\Phi)) \quad (\text{A.21})$$

Here:

$$Str \{....\} = \sum_a (-1)^{2J_a} \cdot (2J_a + 1) \cdot C_a \{....\} \quad (\text{A.22})$$

(C_a counts the electric charge and colour degrees of freedom of the particle)

Rotating to Euclidean space in the $V_{eff}^{(1)}(\Phi)$ momentum integral and recalling the result for $V_{eff}^{(0)}(\Phi)$, the Effective Potential at 1-loop is:

$$V_{eff}^{1-loop}(\Phi) = V(\Phi) + \sum_a \frac{N_a}{2} \int \frac{d^4 k_E}{(2\pi)^4} \log(k_E^2 + M_a^2(\Phi)) \quad (\text{A.23})$$

Here N_a corresponds to the number of degrees of freedom (computed from the $Str \{....\}$) of each particle running in the tadpole loop, and is positive (negative) for bosons (fermions).

The 1-loop part of the effective potential is UV divergent, and so $V_{eff}^{1-loop}(\Phi)$ has to be regularized and renormalized. Here we present the result for \overline{MS} scheme renormalization³⁴ (see [68]). We first regularize the integral from (A.23) using dimensional regularization in $4 - \epsilon$ dimensions:

$$V_{eff}^{1-loop}(\Phi) = V(\Phi) + \sum_a \frac{N_a M_a^4(\Phi)}{64\pi^2} \left[\log\left(\frac{M_a^2(\Phi)}{Q^2}\right) - C_a - C_{UV} \right] \quad (\text{A.24})$$

Here $C_a = 5/6$ ($3/2$) for gauge bosons (fermions and scalars) and C_{UV} is given by

$$C_{UV} = \frac{2}{\epsilon} - \gamma_E + \log(4\pi) + \mathcal{O}(\epsilon) \quad (\text{A.25})$$

After renormalization in the \overline{MS} scheme, the zero-temperature 1-loop effective potential is given by (taking also a definitive form for the lagrangian scalar potential $V(\Phi)$):

$$V_{eff}^{1-loop}(\Phi) = \frac{m^2}{2} \Phi^2 + \frac{\lambda}{4} \Phi^4 + \sum_a \frac{N_a M_a^4(\Phi)}{64\pi^2} \left[\log\left(\frac{M_a^2(\Phi)}{Q^2}\right) - C_a \right] \quad (\text{A.26})$$

³⁴For an sketch of the renormalization of the 1-loop Effective Potential in the On-Shell scheme, see [69].

A.3 Finite Temperature Effective Potential.

A.3.1 Thermal Field Theory and the Effective Potential.

So far, we have considered QFT at zero temperature. However, in order to describe certain physical situations (as for example in the QFT description of the very early universe) it is necessary to account for temperature effects. Thermal field theory is a huge subject, and a proper introduction to it would be too lengthy and completely out of our scope³⁵, so here we will just sketch the basic arguments leading to the results we need.

In the Imaginary Time Formalism, the correspondence between QFT at zero temperature and thermal QFT is obtained by compactification of the Euclidean time dimension on a circle of length $\beta = 1/T$. The basic idea behind this correspondence is the fact that the partition function $\mathcal{Z} = \text{Tr } e^{-\beta H}$ for the thermal QFT can be written as:

$$\mathcal{Z} = \int d\phi_a \langle \phi_a | e^{-\beta \mathcal{H}} | \phi_a \rangle = \int \mathcal{D}\phi \mathcal{D}\pi e^{\int_0^\beta d\tau \int d^3x (\pi \dot{\phi} - \mathcal{H}(\pi, \phi))} \quad (\text{A.27})$$

This certainly looks like a path integral in Euclidean (imaginary) time. The path integral (A.27) is performed for field configurations periodic in τ ($\phi(x, \tau) = \phi(x, \tau + \beta)$) for the case of bosons, and antiperiodic in τ ($\psi(x, \tau) = -\psi(x, \tau + \beta)$) for the case of fermions. These boundary conditions allow to expand both types of fields in a Fourier series:

$$\phi(x, \tau) = \sum_n e^{-i\omega_n^b \tau} \phi_n(x) \quad \psi(x, \tau) = \sum_n e^{-i\omega_n^f \tau} \psi_n(x) \quad (\text{A.28})$$

The quantities ω_n are the so-called Matsubara frequencies in the Imaginary Time Formalism: $\omega_n^b = 2n\pi T$ for bosons (periodic in Euclidean time) and $\omega_n^f = (2n + 1)\pi T$ for fermions (antiperiodic in Euclidean time). Because of this expansion, the Feynman rules get modified at finite temperature. For example:

$$\int \frac{d^4 k_E}{(2\pi)^4} f(k_E^2) \longrightarrow \beta \sum_n \int \frac{d^3 k}{(2\pi)^3} f(k^2 + \omega_n^2) \quad (\text{A.29})$$

Here $k_E = (\omega_n, k)$ is the euclidean 4-momentum, and $f(\dots)$ is a certain function. Taking this into account, the Effective Potential at 1-loop (A.23) gets modified at finite temperature [28]:

$$\begin{aligned} & \sum_a \frac{N_a}{2} \int \frac{d^4 k_E}{(2\pi)^4} \log(k_E^2 + M_a^2(\Phi)) \\ & \quad \downarrow \\ & \sum_a \frac{N_a T}{2} \sum_{n=-\infty}^{\infty} \int \frac{d^3 k}{(2\pi)^3} \log(k^2 + \omega_n^2 + M_a^2(\Phi)) \end{aligned} \quad (\text{A.30})$$

³⁵For an excellent introduction to the subject, see for example [34]

In order to evaluate the infinite sum we use a standard trick. We first define

$$E^2 = k^2 + M_a^2(\Phi)$$

$$K(E) = \sum_{n=-\infty}^{\infty} \log(\omega_n^2 + E^2)$$

For the case of bosons we have:

$$K_B(E) = \sum_{n=-\infty}^{\infty} \log(4n^2\pi^2T^2 + E^2) = 2 \log(E) + 2 \sum_{n=1}^{\infty} \log(4n^2\pi^2T^2 + E^2)$$

$$\frac{\partial K_B(E)}{\partial E} = \frac{2}{E} + 4 \sum_{n=1}^{\infty} \frac{E}{4n^2\pi^2T^2 + E^2} \quad (\text{A.31})$$

Then, from the fact that:

$$\sum_{n=1}^{\infty} \frac{y}{n^2 + y^2} = \frac{-1}{2y} + \frac{\pi}{2} \text{Coth}(\pi y)$$

We get from (A.31):

$$\begin{aligned} \frac{\partial K_B(E)}{\partial E} &= \frac{2}{E} + \frac{2}{\pi T} \left[\frac{-\pi T}{E} + \frac{\pi}{2} \text{Coth}\left(\frac{E}{2T}\right) \right] = \\ &= \frac{2}{T} \left(\frac{1}{2} + \frac{1}{e^{E/T} - 1} \right) \end{aligned}$$

Integrating we obtain:

$$K_B(E) = \frac{2}{T} \left(\frac{E}{2} + T \log(1 - e^{-E/T}) \right)$$

For the case of fermions we proceed in the same way:

$$K_F(E) = \sum_{n=-\infty}^{\infty} \log((2n+1)^2\pi^2T^2 + E^2) = 2 \sum_{n=0}^{\infty} \log((2n+1)^2\pi^2T^2 + E^2)$$

$$\frac{\partial K_F(E)}{\partial E} = 4 \sum_{n=0}^{\infty} \frac{E}{(2n+1)^2\pi^2T^2 + E^2} \quad (\text{A.32})$$

This time we use the following formula:

$$\sum_{n=0}^{\infty} \frac{y}{(2n+1)^2 + y^2} = \frac{\pi}{4} \tanh\left(\frac{\pi y}{2}\right)$$

Integrating (A.32) we obtain:

$$K_F(E) = \frac{2}{T} \left(\frac{E}{2} + T \log\left(1 + e^{-E/T}\right) \right)$$

Then the 1-loop Effective Potential at finite temperature splits into a zero temperature part and a temperature dependent part which vanishes when $T \rightarrow 0$:

$$\begin{aligned} V_{eff}^{1-loop}(\Phi, T) &= V(\Phi) + \sum_a \frac{N_a}{2} \int \frac{d^3 k}{(2\pi)^3} \left(\sqrt{k^2 + M_a^2(\Phi)} \right) + \\ &+ \sum_a \frac{N_a T}{2} \int \frac{d^3 k}{(2\pi)^3} \log\left(1 \pm e^{-\sqrt{k^2 + M_a^2(\Phi)}/T}\right) = V_0^{1-loop}(\Phi) + V_T^{1-loop}(\Phi, T) \end{aligned} \quad (\text{A.33})$$

We first focus on the zero-temperature part from (A.33), $V_0^{1-loop}(\Phi)$; we notice the fact that, apart from an infinite constant (independent of E), one can write:

$$\int \frac{dk_0}{(2\pi)} \log(k_0^2 + E^2) = E \quad (\text{A.34})$$

So, the zero temperature part from (A.33) can be written as:

$$\begin{aligned} V_0^{1-loop}(\Phi) &= V(\Phi) + \sum_a \frac{N_a}{2} \int \frac{d^3 k}{(2\pi)^3} \int \frac{dk_0}{(2\pi)} \log(k_0^2 + k^2 + M_a^2(\Phi)) = \\ &= V(\Phi) + \sum_a \frac{N_a}{2} \int \frac{d^4 k_E}{(2\pi)^4} \log(k_E^2 + M_a^2(\Phi)) \end{aligned} \quad (\text{A.35})$$

We then find that, as expected, $V_0^{1-loop}(\Phi)$ corresponds to the zero-temperature 1-loop Effective Potential computed in section A.2.

The T -dependent part from (A.33), $V_T^{1-loop}(\Phi, T)$, corresponds to the thermal 1-loop corrections to the zero temperature Effective Potential, and can be written as:

$$V_T^{1-loop}(\Phi, T) = \frac{T^4}{2\pi^2} \left\{ \sum_{a \in Bosons} N_a \int_0^\infty dk k^2 \log \left(1 - e^{-\sqrt{k^2 + M_a^2(\Phi)/T^2}} \right) - \sum_{a \in Fermions} N_a \int_0^\infty dk k^2 \log \left(1 + e^{-\sqrt{k^2 + M_a^2(\Phi)/T^2}} \right) \right\} \quad (A.36)$$

This is just the free energy of the Bose-Einstein and Fermi-Dirac distributions of particles getting a mass from Φ . Expanding the argument of the logarithm and integrating, we obtain:

$$\begin{aligned} V_T^{1-loop}(\Phi, T) &= \sum_{a \in Bosons} \frac{N_a T^4}{2\pi^2} \left[\left(\frac{M_a(\Phi)}{T} \right)^2 \sum_{n=1}^\infty \frac{-1}{n^2} K_2 \left(\frac{n M_a(\Phi)}{T} \right) \right] + \\ &+ \sum_{a \in Fermions} \frac{N_a T^4}{2\pi^2} \left[\left(\frac{M_a(\Phi)}{T} \right)^2 \sum_{n=1}^\infty \frac{(-1)^n}{n^2} K_2 \left(\frac{n M_a(\Phi)}{T} \right) \right] = \\ &= \sum_{a \in Bosons} \frac{N_a T^4}{2\pi^2} J_B \left(\frac{M_a^2(\Phi)}{T^2} \right) - \sum_{a \in Fermions} \frac{N_a T^4}{2\pi^2} J_F \left(\frac{M_a^2(\Phi)}{T^2} \right) \end{aligned} \quad (A.37)$$

Here K_2 is the modified Bessel function. Since K_2 falls off exponentially for large values of its argument, (A.37) is well suited for numerical computation when $M_a(\Phi) \gg T$ (in the non-relativistic/small- T regime). In the high- T regime ($M_a(\Phi) \ll T$) we can expand J_B and J_F [28]:

$$J_B(x)_{x \rightarrow 0} = -\frac{11\pi^4}{180} + \frac{\pi^2}{12}x - \frac{\pi}{6}x^{3/2} - \frac{x^2}{32} \log \left(\frac{x}{a_b} \right) + \dots \quad (A.38)$$

$$J_F(x)_{x \rightarrow 0} = -\frac{7\pi^4}{360} - \frac{\pi^2}{24}x - \frac{x^2}{32} \log \left(\frac{x}{a_f} \right) + \dots$$

We have $\log(a_b) \simeq 5.41$ and $\log(a_f) \simeq 2.64$. So the High temperature expansion of the effective potential is:

$$\begin{aligned} V_T^{1-loop}(\Phi, T) &= \sum_{a \in Bosons} N_a \left\{ \frac{M_a^2(\Phi)T^2}{24} - \frac{M_a^3(\Phi)T}{12\pi} - \frac{M_a^4(\Phi)}{64\pi^2} \log \left(\frac{M_a^2(\Phi)}{a_b T^2} \right) \right\} \\ &+ \sum_{a \in Fermions} N_a \left\{ \frac{M_a^2(\Phi)T^2}{48} + \frac{M_a^4(\Phi)}{64\pi^2} \log \left(\frac{M_a^2(\Phi)}{a_f T^2} \right) \right\} \end{aligned} \quad (A.39)$$

A.3.2 Ring Diagrams.

In thermal Quantum field theory, in the presence of massless fields, the traditional perturbative expansion in terms of small coupling constants break down due to IR-divergences generated by long range fluctuations appearing as soon as one moves to finite temperature [70]. In our case this can be seen from the fact that in the high- T /small mass regime, a subleading term of order $3/2$ appears in the thermal bosonic corrections.

The main consequence is that, as it stands, we cannot trust the completeness of the 1-loop result, since there are higher loop contributions of the same order, as if the effect of temperature is to “dilute” the 1-loop correction to some multi-loop order in the IR. The leading part of these multi-loop corrections is contained in the so called “Ring” or “Daisy” diagrams. They are N -loop diagrams where $N - 1$ loops are “attached” to a main one.

The Daisy diagrams only need to be resummed in the IR limit of vanishing momenta running in the petals. It is also known that they can be taken into account using propagators resummed in the IR [29]. By solving a Dyson-like equation, this turns out to simply shift the bosonic masses:

$$M_a^2(\Phi) \rightarrow M_a^2(\Phi) + \Pi_b(T) \quad (\text{A.40})$$

Here $\Pi_b(T)$ is the self-energy of the bosonic field b in the IR limit ($\omega = k = 0$), known as a “Debye mass”.

Notice that the 1-loop result is still trustworthy for small T and large values of Φ ($M_a(\Phi) \gg T$). Hence the Ring diagrams will only give a significant contribution in the high T regime, where the particles can be approximated as nearly massless. Also, the fact that only massless bosons (and not fermions) feel the breakdown of perturbation theory, since at finite temperature bosonic fields have a massless Matsubara frequency (which will behave as a massless mode and generate IR divergences at high T), whereas fermions do not.

The self-consistent approach would be to apply the shift (A.40) to (A.30), bearing in mind that the shift in the gauge boson masses only occurs for the longitudinal component, and fermion contributions doesn’t shift either. We obtain:

$$V_1^{shift}(\Phi, T) = \sum_a \frac{N_a T}{2} \sum_{n=-\infty}^{\infty} \int \frac{d^3 k}{(2\pi)^3} \log \left(k^2 + \omega_n^2 + M_a^2(\Phi) + \Pi_a(T) \right) \quad (\text{A.41})$$

However, this self-consistent procedure has certain technical difficulties, because the UV divergent part of the potential becomes T -dependent, and requires a T -dependent counterterm to be made finite.

One can do the shift in an alternative way, which consists in just shifting the Matsubara zero modes, since they are the ones that feel the IR divergence at high T . We then get:

$$\begin{aligned}
V_1^{shift}(\Phi, T) &= \sum_{a=h,G,W,Z,t,S} \frac{N_a T}{2} \left\{ \sum_{n=-\infty}^{\infty}{}' \int \frac{d^3 k}{(2\pi)^3} \log(k^2 + \omega_n^2 + M_a^2(\Phi)) + \right. \\
&\quad \left. + \int \frac{d^3 k}{(2\pi)^3} \log(k^2 + M_a^2(\Phi) + \Pi_a(T)) \right\} = \\
&= \sum_a \frac{N_a T}{2} \left\{ \sum_{n=-\infty}^{\infty}{}' \int \frac{d^3 k}{(2\pi)^3} \log(k^2 + \omega_n^2 + M_a^2(\Phi)) + \right. \\
&\quad \left. + \int \frac{d^3 k}{(2\pi)^3} \log(k^2 + M_a^2(\Phi)) + \int \frac{d^3 k}{(2\pi)^3} \log\left(1 + \frac{\Pi_a(T)}{k^2 + M_a^2(\Phi)}\right) \right\} = \\
&= \sum_a \frac{N_a T}{2} \sum_{n=-\infty}^{\infty} \int \frac{d^3 k}{(2\pi)^3} \log(k^2 + \omega_n^2 + M_a^2(\Phi)) + \\
&\quad + \sum_a \frac{\bar{N}_a T}{2} \int \frac{d^3 k}{(2\pi)^3} \log\left(1 + \frac{\Pi_a(T)}{k^2 + M_a^2(\Phi)}\right) = \\
&= V_1(\Phi, T) + V_{Ring}(\Phi, T)
\end{aligned}$$

Here the prime $'$ in the sum means that the zero modes are excluded, and \bar{N}_a are the bosonic degrees of freedom that suffer the mass shift. The Daisy diagrams contribution to the effective potential (A.30) is then:

$$\begin{aligned}
V_{Ring}(\Phi, T) &= \sum_a \frac{\bar{N}_a T}{2} \int \frac{d^3 k}{(2\pi)^3} \log\left(1 + \frac{\Pi_a(T)}{k^2 + M_a^2(\Phi)}\right) = \\
&= \frac{T}{12\pi} \sum_a \bar{N}_a \left\{ M_a^3(\Phi) - \left[M_a^2(\Phi) + \Pi_a(T^2) \right]^{\frac{3}{2}} \right\} \tag{A.42}
\end{aligned}$$

The Debye masses for the fields can be obtained applying the techniques from [29].

A.4 Main Two-Loop Contributions to the Zero Temperature Effective Potential of the Hidden Scalar Extension of the SM.

The main two-loop corrections to the Higgs potential for the hidden sector model analyzed in section 1.1 are those that depend on the top Yukawa coupling y_t^2 and on ζ^2 . In order to obtain them, we isolate the stops-R contribution in the MSSM result [31], turning off all their interactions except:

$$\delta V_{MSSM}^0 = y_t^2 |\tilde{t}_R|^2 |H_2|^2 \rightarrow 2 \zeta^2 \sum_{i=1}^N S_i^2 |H|^2 \tag{A.43}$$

We have $N_s = 2N$; in applying the MSSM results to the hidden sector case, there are a few things we have to be careful about:

- To distinguish between N_t (number of degrees of freedom) from \tilde{t}_R and from t, b (since in the MSSM they are the same), we will call the former \tilde{N}_t , and identify $\tilde{N}_t \rightarrow N_s/2$.
- We take the limit of large M_A in order to end up with just one Higgs doublet at low energy in the MSSM; that way we get:

$$H_2 \rightarrow s_\beta H \quad H_1 \rightarrow c_\beta H \quad (\text{A.44})$$

So, when coming from the stop-R sector, $y_t^2 s_\beta^2 \equiv y_{t,SM}^2$ should be identified with $2\zeta^2$

- The same applies for trilinear couplings. e.g

$$\lambda_{h^0 \tilde{t}_R \tilde{t}_R}^2 = \left[\sqrt{2} y_t m_t s_\beta^2 \right]^2 \longrightarrow \left[\sqrt{2} y_t \frac{1}{\sqrt{2}} y_t h^2 s_\beta^2 \right]^2 = \left[2\zeta^2 h^2 \right]^2 \quad (\text{A.45})$$

Finally, the two-loop contribution to the Effective Potential is (we revert to the usual notation $y_{t,SM}^2 \rightarrow y_t^2$):

$$\begin{aligned} V_2(h) = & \frac{1}{(16\pi^2)^2} \left\{ \frac{1}{2} N_t y_t^2 \left[L(m_h^2, m_t^2, m_t^2) + 2m_t^2 I(m_h^2, m_t^2, m_t^2) + \right. \right. \\ & \left. \left. + L(m_{G^0}^2, m_t^2, m_t^2) + 2L(m_{G^0}^2, m_t^2, m_b^2) - 2m_t^2 I(m_G^2, m_t^2, m_t^2) \right] \right. \\ & \left. + \frac{1}{2} N_s \zeta^2 \left[J(m_h^2, m_s^2) + 3J(m_G^2, m_s^2) - \zeta^2 h^2 I(m_h^2, m_s^2, m_s^2) \right] \right\} \quad (\text{A.46}) \end{aligned}$$

The masses m_i^2 are the field dependent masses $M_i^2(h)$ for the various fields. The functions $J(m_1^2, m_2^2)$, $I(m_1^2, m_2^2, m_3^2)$ and $L(m_1^2, m_2^2, m_3^2)$ are given by:

$$J(m_1^2, m_2^2) = m_1^2 m_2^2 \left(1 - \log \frac{m_1^2}{Q^2} \right) \left(1 - \log \frac{m_2^2}{Q^2} \right) \quad (\text{A.47})$$

$$\begin{aligned} I(m_1^2, m_2^2, m_3^2) = & \frac{1}{2} \left[4 \left(m_1^2 \log \frac{m_1^2}{Q^2} + m_2^2 \log \frac{m_2^2}{Q^2} + m_3^2 \log \frac{m_3^2}{Q^2} \right) - 5(m_1^2 + m_2^2 + m_3^2) - \right. \\ & \left. - (-m_1^2 + m_2^2 + m_3^2) \log \frac{m_2^2}{Q^2} \log \frac{m_3^2}{Q^2} - (m_1^2 - m_2^2 + m_3^2) \log \frac{m_1^2}{Q^2} \log \frac{m_3^2}{Q^2} \right. \\ & \left. - (m_1^2 + m_2^2 - m_3^2) \log \frac{m_1^2}{Q^2} \log \frac{m_2^2}{Q^2} - \xi(m_1^2, m_2^2, m_3^2) \right] \quad (\text{A.48}) \end{aligned}$$

$$L(m_1^2, m_2^2, m_3^2) = J(m_2^2, m_3^2) - J(m_1^2, m_3^2) - J(m_1^2, m_2^2) - (m_1^2 - m_2^2 - m_3^2) I(m_1^2, m_2^2, m_3^2) \quad (\text{A.49})$$

Notice that the functions $J(m_1^2, m_2^2)$ and $I(m_1^2, m_2^2, m_3^2)$ are well behaved when taking one of its arguments to zero (as the bottom quark mass m_b in our case):

$$J(m_1^2, 0) = J(0, m_2^2) = 0$$

$$\begin{aligned} I(m_1^2, m_2^2, 0) = & 2 \left(m_1^2 \log \frac{m_1^2}{Q^2} + m_2^2 \log \frac{m_2^2}{Q^2} \right) - \frac{5}{2} (m_1^2 + m_2^2) - m_1^2 \log \frac{m_1^2}{Q^2} \log \frac{m_2^2}{Q^2} + \\ & + \frac{1}{2} (m_1^2 - m_2^2) \log^2 \frac{m_1^2}{Q^2} - (m_1^2 - m_2^2) \log \frac{m_1^2 - m_2^2}{Q^2} \log \frac{m_1^2}{m_2^2} + (m_1^2 - m_2^2) \left[-\frac{\pi^2}{6} + Li_2 \left(\frac{m_2^2}{m_1^2} \right) \right] \end{aligned}$$

Finally, the dilogarithm function $Li_2(x)$ and the function $\xi(x, y, z)$ are defined as [31]:

$$Li_2(x) = - \int_0^1 \frac{\log(1 - xy)}{y} dy$$

$$\xi(x, y, z) = 8b \left[L_b \left(\arctan \frac{y+z-x}{2b} \right) + L_b \left(\arctan \frac{x+z-y}{2b} \right) L_b \left(\arctan \frac{x+y-z}{2b} \right) - \frac{\pi \log 2}{2} \right]$$

when $4b^2 = -(x^2 + y^2 + z^2 - 2xy - 2xz - 2yz) \geq 0$, and

$$\xi(x, y, z) = 8a \left[-M \left(-\operatorname{arccoth} \frac{y+z-x}{2a} \right) + M \left(\operatorname{arccoth} \frac{x+z-y}{2a} \right) M \left(\operatorname{arccoth} \frac{x+y-z}{2a} \right) \right]$$

when $4a^2 = (x^2 + y^2 + z^2 - 2xy - 2xz - 2yz) \geq 0$. The Lobachevsky function $L_b(t)$ and the function $M(t)$ are defined as:

$$L_b(t) = - \int_0^t \log [\cos(x)] \, dx \quad M(t) = - \int_0^t \log [\sinh(x)] \, dx$$

B Approximations for $S_3(T)/T$.

B.1 Derivation of the approximation for $S_3(T_n)/T_n$.

Our starting point is (2.31). We make an approximate phenomenological ansatz for $S_3(T)/T$, expanding it around the nucleation temperature T_n :

$$\frac{S_3(T)}{T} \simeq \frac{S_3(T_n)}{T_n}(1+x) \quad x = \frac{T - T_n}{T_c - T} \quad (\text{B.1})$$

This ansatz⁶ captures the behaviour of $S_3(T)/T$ as it approaches both T_n and T_c . Making the change of variables $T \rightarrow x$ in (2.31), we get:

$$\begin{aligned} & \frac{16\xi^4 M_{Pl}^4 (T_c - T_n)}{(2\pi)^{3/2}} \left(\frac{S_3(T_n)}{T_n} \right)^{\frac{3}{2}} e^{-S_3(T_n)/T_n} \int_0^\infty \frac{(1+x)^{9/2}}{(T_c x + T_n)^5} e^{\frac{-S_3(T_n)}{T_n} x} dx \simeq \\ & \simeq \frac{16\xi^4 M_{Pl}^4 (T_c - T_n)}{(2\pi)^{3/2}} \left(\frac{S_3(T_n)}{T_n} \right)^{\frac{3}{2}} \frac{e^{-S_3(T_n)/T_n}}{T_n^5} \int_0^\infty \frac{e^{\frac{-S_3(T_n)}{T_n} x}}{(1+x)^{1/2}} dx = 1 \end{aligned} \quad (\text{B.2})$$

The integral from this last equation is sharply peaked around $x = 0$ (this justifies the ansatz), giving:

$$I\left(\frac{S_3(T_n)}{T_n}\right) \equiv \int_0^\infty \frac{e^{\frac{-S_3(T_n)}{T_n} x}}{(1+x)^{1/2}} dx = \sqrt{\pi} e^{S_3(T_n)/T_n} \left(\frac{S_3(T_n)}{T_n} \right)^{-\frac{1}{2}} \text{Erfc}\left(\sqrt{S_3(T_n)/T_n}\right) \quad (\text{B.3})$$

$\text{Erfc}(\dots)$ is the complementary Gaussian error function; the function $f(a) = a^{3/2}I(a)$ is approximately constant in the range $100 < a < 200$ ($f(a) \simeq 12 = \eta$), so we can obtain $S_3(T_n)/T_n$ from (B.2):

$$\frac{S_3(T_n)}{T_n} \simeq \text{Log}\left(\frac{16\xi^4 M_{Pl}^4 \eta}{(2\pi)^{3/2} v^4}\right) + 4 \text{Log}\left(\frac{v}{T_c}\right) + \text{Log}\left(\frac{T_c^4}{T_n^4} \left(\frac{T_c}{T_n} - 1\right)\right) \quad (\text{B.4})$$

⁶The rigorous expansion is $\frac{S_3(T)}{T} = \frac{S_3(T_n)}{T_n}(1 + k_1 x + k_2 x^2 + \dots)$. Numerically we find that $k_1 \simeq 1 - 2$, and $x \ll 1$ for T close to T_n , so our ansatz is a pretty accurate approximation; for an alternative expansion for $\frac{S_3(T)}{T}$ see [37].

Then, being $k = \frac{T_c}{T_n}$, one finds:

$$\frac{S_3(T_n)}{T_n} \simeq 143 + 4 \text{Log} \left(\frac{v}{T_c} \right) + \text{Log} \left(k^4 (k - 1) \right) \simeq 140 - 148 \quad (\text{B.5})$$

Notice that the last two terms from (B.5) will slightly raise the value of $S_3(T_n)/T_n$ as the strenght of the 1st order phase transition grows (see fig. 2.9), since for stronger phase transitions T_c tends to be lower, and T_c/T_n gets larger (see fig. 2.9).

B.2 Derivation of the approximation for $S_3(T_f)/T_f$.

Similarly to $S_3(T_n)/T_n$, there is also a way to obtain an approximate value for $S_3(T)/T$ at the end of the transition, $S_3(T_f)/T_f$; using again the ansatz from (B.1) and making the change of variables $T \rightarrow x$ in (2.39), we get:

$$\frac{S_3(T)}{T} \simeq \frac{S_3(T_f)}{T_f} (1 + x) \quad x = \frac{T - T_f}{T_c - T} \quad (\text{B.6})$$

\Downarrow

$$\begin{aligned} & \frac{64\pi v_B^3 \xi^4 M_{Pl}^4 (T_c - T_f)}{3 (2\pi)^{3/2} T_f^5} \left(\frac{S_3(T_f)}{T_f} \right)^{\frac{3}{2}} e^{-S_3(T_f)/T_f} \times \\ & \times \int_0^{\frac{T_n - T_f}{T_c - T_n} \equiv r \ll 1} \frac{(x + 1)^3}{\left(\frac{T_c}{T_f} x + 1 \right)^{11}} e^{-\frac{S_3(T_f)}{T_f} x} \left[\left(\frac{T_c^2}{T_f^2} - 1 \right) x^2 + 2 \left(\frac{T_c}{T_f} - 1 \right) x \right]^3 dx = \\ & = \frac{64\pi v_B^3 \xi^4 M_{Pl}^4 (T_c - T_f)}{3 (2\pi)^{3/2} T_f^5} \left(\frac{S_3(T_f)}{T_f} \right)^{\frac{3}{2}} e^{-S_3(T_f)/T_f} \times I \left(b \equiv \frac{S_3(T_f)}{T_f}, r, \delta \equiv \frac{T_c}{T_f} \right) = 1 \quad (\text{B.7}) \end{aligned}$$

We now turn to the evaluation of $I(b, r, \delta)$; since $r \ll 1$, we can safely approximate $(1 + x) \simeq 1$ and $(\delta x + 1) \simeq 1$ in the integrand, and get:

$$\begin{aligned} I(b, r, \delta) \simeq \int_0^{r \ll 1} e^{-bx} & \left[(\delta^2 - 1)^3 x^7 + 6(\delta - 1)(\delta^2 - 1)^2 x^5 + \right. \\ & \left. + 12(\delta^2 - 1)(\delta - 1)^2 x^4 + 8(\delta - 1)^3 x^3 \right] dx \end{aligned}$$

In the regime $b \gg 1$, $br \gg 1$ (which is the one we are dealing with), we obtain:

$$I(b, r, \delta) \simeq \frac{1}{b^4} \left[72 (\delta^2 - 1) (\delta - 1)^2 + 144 \frac{(\delta - 1) (\delta^2 - 1)^2}{b} + 960 \frac{(\delta - 1)^3}{b^2} + 720 \frac{(\delta^2 - 1)^3}{b^3} + \mathcal{O}(e^{-br} br) \right] \simeq \frac{1}{b^4} 72 (\delta^2 - 1) (\delta - 1)^2 + \mathcal{O}(b^{-5}) \quad (\text{B.8})$$

So finally condition (2.39) transforms into:

$$\frac{4608\pi v_B^3 \xi^4 M_{Pl}^4 (\delta - 1)^3 (\delta^2 - 1) \delta^4}{3 (2\pi)^{3/2} T_c^4} \left(\frac{S_3(T_f)}{T_f} \right)^{\frac{-5}{2}} e^{-S_3(T_f)/T_f} = 1 \quad (\text{B.9})$$

\Downarrow

$$\begin{aligned} F \left(\frac{S_3(T_f)}{T_f} \right) &\equiv \frac{S_3(T_f)}{T_f} + \frac{5}{2} \text{Log} \left(\frac{S_3(T_f)}{T_f} \right) = \\ &= \text{Log} \left(\frac{4608\pi v_B^3 \xi^4 M_{Pl}^4}{3 (2\pi)^{3/2} v^4} \right) + 4 \text{Log} \left(\frac{v}{T_c} \right) + \text{Log} \left[(\delta - 1)^3 (\delta^2 - 1) \delta^4 \right] \simeq \\ &\simeq 148 + 3 \text{Log} (v_B) + 4 \text{Log} \left(\frac{v}{T_c} \right) + \text{Log} \left[(\delta - 1)^3 (\delta^2 - 1) \delta^4 \right] \end{aligned} \quad (\text{B.10})$$

This last equation can be numerically solved for $S_3(T_f)/T_f$ in an easy way⁹. Again, the last two terms will raise the value of $S_3(T_f)/T_f$ as the strenght of the 1st order phase transition grows (see fig. 2.9).

⁹Making use of the fact that $\frac{T_c}{T_n} \simeq \frac{T_c}{T_f} \equiv \delta$ (see for example fig. 2.9).

C Normalization of the Spectral Function.

In this appendix we give an analytical proof of the normalization condition (5.47) for the spectral function $\rho_{hh}(s)$. The proof uses complex integration methods very common in the literature of dispersion techniques. Take the hh -propagator of (5.66)-(5.67) to be defined in the complex plane, $P_{hh}(z)$, and integrate it along the contour of fig. 6.5, which shows the general case with a real pole below the mass gap and a branch cut from that mass gap to infinity. The absence of complex poles of $P_{hh}(z)$ in the principal branch tells us that

$$\oint_C P_{hh}(z) dz = 0 \quad (C.1)$$

Along the circle at infinity, with $z = Re^{i\theta}$, noting that $P_{hh} \sim 1/(Re^{i\theta})$ we get a constant contribution:

$$\oint_{C_\infty} P_{hh}(z) dz \simeq \int_0^{2\pi} \frac{iRe^{i\theta} d\theta}{Re^{i\theta}} = 2i\pi \quad (C.2)$$

The integral along the real axis is

$$\oint_{C_{pole}} P_{hh}(z) dz + \int_{m_g^2}^{\infty} ds [P_{hh}(s + i\epsilon) - P_{hh}(s - i\epsilon)] \quad (C.3)$$

Here C_{pole} is an infinitesimal contour encircling clockwise the real pole (at $z = m_h^2$). The integral around this pole is evaluated using the theorem of residues and gives

$$\oint_{C_{pole}} P_{hh}(z) dz = -2i\pi \left. \frac{1}{D'(s)} \right|_{s=m_h^2} = -2i\pi \frac{1}{K^2(m_h^2)} \quad (C.4)$$

One can then also write

$$\oint_{C_{pole}} P_{hh}(z) dz = -2i\pi \int_0^{m_g^2} \frac{1}{K^2(s)} \delta(s - m_h^2) ds = -2i\pi \int_0^{m_g^2} \rho_{hh}(s) ds \quad (C.5)$$

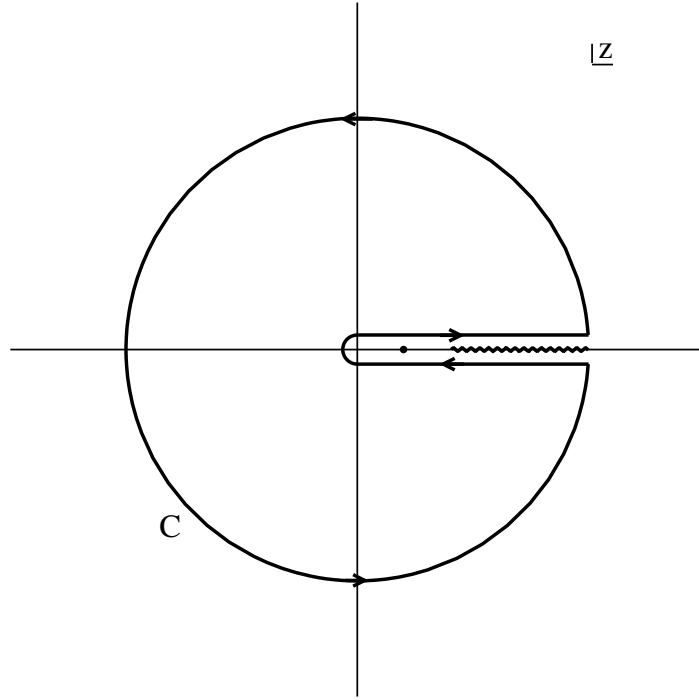


Figure 6.5: Integration contour for $P_{hh}(z)$ in the complex z -plane.

For the second piece in (C.3) we use (5.37) to write $P_{hh}(s+i\epsilon) = -i\pi\rho_{hh}(s)$. Then, notice that for this particular $P_{hh}(z)$ we also have (this is not always the case) $P_{hh}(s-i\epsilon) = i\pi\rho_{hh}(s)$. Putting all pieces together, (C.1) leads to

$$\int_0^\infty \rho_{hh}(s) ds = 1 \quad (\text{C.6})$$

This is the correct normalization of the spectral function for a stable state.

Bibliography

- [1] S. L. Glashow, Nucl. Phys. **22** (1961) 579; S. Weinberg, Phys. Rev. Lett. **19** (1967) 1264; A. Salam, in “Elementary Particle Theory”, ed. N. Svartholm, Almqvist and Wiksells, Stockholm (1969).
- [2] M. Gell-Mann, Phys. Lett. **8** (1964) 214; G. Zweig, CERN-TH-401; H. Fritzsch, M. Gell-Mann and H. Leutwyler, Phys. Lett. B **47** (1973) 365; D. J. Gross and F. Wilczek, Phys. Rev. Lett. **30** (1973) 1343; H. D. Politzer, Phys. Rev. Lett. **30** (1973) 1346.
- [3] P. W. Higgs, Phys. Lett. **12** (1964) 132; Phys. Rev. Lett. **13** (1964) 508; Phys. Rev. **145** (1966) 1156.
- [4] [LEP Collaboration], arXiv:hep-ex/0612034.
- [5] R. Schabinger and J. D. Wells, Phys. Rev. D **72** (2005) 093007 [hep-ph/0509209]. B. Patt and F. Wilczek, [hep-ph/0605188].
- [6] M. J. Strassler and K. M. Zurek, Phys. Lett. B **651** (2007) 374 [arXiv:hep-ph/0604261].
- [7] A. D. Sakharov, Pisma Zh. Eksp. Teor. Fiz. **5** (1967) 32 [JETP Lett. **5** (1967) 32] [SOPUA,34,392-393.1991 UFNAA,161,61-64.1991) 24].
- [8] H. Georgi, Phys. Rev. Lett. **98** (2007) 221601 [hep-ph/0703260].
- [9] H. Georgi, Phys. Lett. B **650** (2007) 275 [hep-ph/0704.2457].
- [10] K. Cheung, W. Y. Keung and T. C. Yuan, AIP Conf. Proc. **1078** (2009) 156 [arXiv:0809.0995 [hep-ph]].
- [11] P. J. Fox, A. Rajaraman and Y. Shirman, Phys. Rev. D **76** (2007) 075004 [hep-ph/0705.3092].
- [12] A. Delgado, J. R. Espinosa and M. Quirós, JHEP **0710** (2007) 094 [hep-ph/0707.4309].
- [13] D. Hooper, arXiv:0901.4090 [hep-ph].
- [14] O. Adriani *et al.* [PAMELA Collaboration], Nature **458** (2009) 607 [arXiv:0810.4995 [astro-ph]].
- [15] M. Boezio *et al.*, arXiv:0810.3508 [astro-ph].

- [16] N. Arkani-Hamed, D. P. Finkbeiner, T. Slatyer and N. Weiner, Phys. Rev. D **79** (2009) 015014; D. Feldman, Z. Liu and P. Nath, Phys. Rev. D **79** (2009) 063509; A. E. Nelson and C. Spitzer, arXiv:0810.5167 [hep-ph].
- [17] J. McDonald, Phys. Rev. D **50** (1994) 3637 [hep-ph/0702143].
- [18] C. P. Burgess, M. Pospelov and T. ter Veldhuis, Nucl. Phys. B **619** (2001) 709.
- [19] M. Yoshimura, Phys. Rev. Lett. **41** (1978) 281 [Erratum-ibid. **42** (1979) 746].
- [20] G. 't Hooft, Phys. Rev. Lett. **37** (1976) 8.
- [21] V. A. Kuzmin, V. A. Rubakov and M. E. Shaposhnikov, Phys. Lett. B **155** (1985) 36.
- [22] N. S. Manton, Phys. Rev. D **28** (1983) 2019; F. R. Klinkhamer and N. S. Manton, Phys. Rev. D **30** (1984) 2212.
- [23] G. Jona-Lasinio, Nuovo Cim. **34** (1964) 1790.
- [24] R. Jackiw, Phys. Rev. D **9** (1974) 1686.
- [25] S. R. Coleman and E. Weinberg, Phys. Rev. D **7** (1973) 1888.
- [26] J. R. Espinosa and M. Quirós, Phys. Rev. D **76** (2007) 076004.
- [27] J. R. Espinosa, T. Konstandin, J. M. No and M. Quiros, Phys. Rev. D **78** (2008) 123528.
- [28] L. Dolan and R. Jackiw, Phys. Rev. D **9** (1974) 3320.
- [29] M. E. Carrington, Phys. Rev. D **45** (1992) 2933.
- [30] M. Sher, Phys. Rept. **179** (1989) 273.
- [31] J. R. Espinosa and R. J. Zhang, Nucl. Phys. B **586** (2000) 3; J. R. Espinosa and R. J. Zhang, JHEP **0003** (2000) 026; R. J. Zhang, Phys. Lett. B **447** (1999) 89.
- [32] S. R. Coleman, Phys. Rev. D **15** (1977) 2929 [Erratum-ibid. D **16** (1977) 1248].
- [33] C. G. . Callan and S. R. Coleman, Phys. Rev. D **16** (1977) 1762.
- [34] M. Le Bellac, “Quantum And Statistical Field Theory,” *Oxford, UK: Clarendon (1991)*.
- [35] A. D. Linde, Nucl. Phys. B **216** (1983) 421 [Erratum-ibid. B **223** (1983) 544].
- [36] G. Isidori, G. Ridolfi and A. Strumia, Nucl. Phys. B **609** (2001) 387.
- [37] G. W. Anderson, L. J. Hall Phys. Rev. D **45** (1992) 2685.
- [38] A. H. Guth and S. H. H. Tye, Phys. Rev. Lett. **44** (1980) 631 [Erratum-ibid. **44** (1980) 963]; M. E. Carrington and J. I. Kapusta, Phys. Rev. D **47** (1993) 5304.

- [39] C. Grojean and G. Servant, Phys. Rev. D **75** (2007) 043507
- [40] A. Noble and M. Perelstein, arXiv:0711.3018 [hep-ph].
- [41] A. Ashoorioon and T. Konstandin, arXiv:0904.0353 [hep-ph].
- [42] E. W. Kolb and M. S. Turner, “The Early universe”, (1990)
- [43] M. Srednicki, R. Watkins and K. A. Olive, Nucl. Phys. B **310** (1988) 693.
- [44] B. W. Lee and S. Weinberg, Phys. Rev. Lett. **39** (1977) 165.
- [45] G. Hinshaw *et al.* [WMAP Collaboration], Astrophys. J. Suppl. **180** (2009) 225 [arXiv:0803.0732 [astro-ph]].
- [46] T. Banks and A. Zaks, Nucl. Phys. **B196** (1982) 189.
- [47] G. Cacciapaglia, G. Marandella and J. Terning, JHEP **0902** (2009) 049 [arXiv:0804.0424 [hep-ph]].
- [48] G. Cacciapaglia, G. Marandella and J. Terning, JHEP **0801** (2008) 070 [arXiv:0708.0005 [hep-ph]].
- [49] G. Mack, Commun. Math. Phys. **55** (1977) 1
- [50] J. L. Feng, A. Rajaraman and H. Tu, Phys. Rev. D **77** (2008) 075007 [arXiv:0801.1534 [hep-ph]].
- [51] M. A. Stephanov, Phys. Rev. D **76** (2007) 035008 [hep-ph/0705.3049];
- [52] N. V. Krasnikov, Int. J. Mod. Phys. A **22** (2007) 5117 [hep-ph/0707.1419].
- [53] A. Rajaraman, AIP Conf. Proc. **1078** (2009) 63 [arXiv:0809.5092 [hep-ph]].
- [54] M. Bander, J. L. Feng, A. Rajaraman and Y. Shirman, Phys. Rev. D **76** (2007) 115002 [hep-ph/0706.2677].
- [55] M. J. Strassler, [hep-ph/0801.0629].
- [56] A. Delgado, J. R. Espinosa, J. M. No and M. Quiros, JHEP **0804** (2008) 028 [arXiv:0802.2680 [hep-ph]].
- [57] A. Delgado, J. R. Espinosa, J. M. No and M. Quiros, JHEP **0811** (2008) 071 [arXiv:0804.4574 [hep-ph]].
- [58] P.W. Anderson, Phys. Rev. **124** (1961) 41; U. Fano, Phys. Rev. **124** (1961) 1866; G.D. Mahan, *Many-Particle Physics*, Plenum Press, New York, 1990.
- [59] U. Fano, Rev. Mod. Phys. **64** (1992) 313.
- [60] L. Jahnke and S. Leupold, Nucl. Phys. A **778** (2006) 53 [nucl-th/0601072].

- [61] A. Delgado, J. R. Espinosa, J. M. No and M. Quiros, Phys. Rev. D **79** (2009) 055011
- [62] A. Rajaraman, [hep-ph/0806.1533].
- [63] B. A. Kniehl, Phys. Rept. **240**, 211 (1994).
- [64] R. Escribano, A. Gallegos, J. L. Lucio M, G. Moreno and J. Pestieau, Eur. Phys. J. C **28**, 107 (2003) [hep-ph/0204338].
- [65] L. Dolan and R. Jackiw, Phys. Rev. D **9** (1974) 2904.
- [66] S. Weinberg, Phys. Rev. D **7** (1973) 2887.
- [67] N. K. Nielsen, Nucl. Phys. B **101** (1975) 173; R. Fukuda and T. Kugo, Phys. Rev. D **13** (1976) 3469.
- [68] M. Quiros, arXiv:hep-ph/9901312.
- [69] C. Delaunay, C. Grojean, J. D. Wells, JHEP **0804**, 029 (2008).
- [70] K. Takahashi Z. Phys. C **26** (1985) 601.